TRANSCRIPTOMIC ANALYSIS OF MAMMALIAN SPINAL NEURULATION

CAO SHOUFENG

NATIONAL UNIVERSITY OF SINGAPORE
2011

TRANSCRIPTOMIC ANALYSIS OF MAMMALIAN SPINAL NEURULATION

CAO SHOUFENG
(B.Med., M.Med.)

A THESIS SUBMITTED FOR THE DEGREE OF DOCTOR OF PHILOSOPHY

DEPARTMENT OF ANATOMY

YONG LOO LIN SCHOOL OF MEDCINE

NATIONAL UNIVERSITY OF SINGAPORE

2011

ACKNOWLEDGEMENTS

I would like to express my deepest gratitude to my supervisor, Associate Professor Yip Wai Cheong, George, Department of Anatomy, Yong Loo Lin School of Medicine, National University of Singapore (NUS), for his invaluable guidance and instruction， without which this work would not have been possible. He has guided me throughout the study with his original ideas, technical training, problem-solving, and countless discussions. His consistent encouragement and patience are also precious for me to have the right attitude to study, research, and life as well. It was a great honor to be supervised by him. The precious experience of working under him will benefit me in my future life.

I sincerely appreciate Professor Bay Boon Huat, Head of Department of Anatomy, Yong Loo Lin School of Medicine, National University of Singapore (NUS). He tries his best to create conditions for research and innovation, and always shows his kindness and encouragement during my study and research life in Anatomy. His expert advice and valuable suggestions regarding my PQE examination have enlightened me and inspired my independent thinking.

My deeply appreciation would be given to Professor Ling Eng Ang, the former Head of Department of Anatomy, Yong Loo Lin School of Medicine, National University of Singapore (NUS), for the opportunity to pursue my PhD candidature in the Department of Anatomy. His deep-thinking，great learning and great ability, rigorous and energetic attitude toward research as well as his gentlemanly manner impressed me and will surely influence me in my career.

I wish to express my sincerely appreciations to Associate Professors Teh Ming and Ong Wei Yi, for their kindly allowing me to use their laser capture microdissection machine, and colleagues in their lab for assisting me with operating the instruments. They generously share the particular things and experience which is much helpful in successfully obtaining the preliminary data.

I am grateful to Mrs. Ng Geok Lan, Mrs. Yong Eng Siang, Mrs. Pan Feng, and Mr. Poon Jun wei for their excellent technical assistance; I am also grateful to Mdm Teo Li Ching Violet, Mdm Ang Lye Gek Carolyne, and Mdm Singh for their secretarial assistance; Mr. Yick Tuck Yong for assistance in computer work.

I am also appreciate the friendship from my research group members, Ms. Leong Shu Xian Grace; Teng Hui Fang, Yvonne; Guo Chun Hua; Lo Soo Ling; Sim Wey Cheng; Sen Yin Ping; Omid Iravani; Koo Chuay Yeng; Low Jin Yih; Chua Pei Jou; Lai Yiyang; Yu Yingnan; Zin Mar Lwin Alice; and Shen Lan. We have spent time working together and making progress through frankly discussions. Their help in improving experimental skills and encouragement give me much strength and make my life much easier than if I am struggling alone.

I am also so grateful to have a special supporting fellowship, from where comes encouragement and strength. My sisters from the Department of Anatomy, Ms Li Jia'En, Jasmine, Ms Qiu Li Feng, Ms Du Xiao Li, and Ms Wu Ya Jun, as well as those not from our department or supporting me without letting me know, they come to my life not by chance, but by grace. They witness my weakness, share tears, joys and peace through each step I take. I am sure our friendship will be lasting forever.

I would like to express my heartiest thanks to all the staff members of the Department of Anatomy, Yong Loo Lin School of Medicine, National University of Singapore (NUS) for their generous help and friendship. I also give my thanks to the academic and technical staff of the BFIG lab (Clinical Research Center, Faculty of Medicine) for their help in my Affymetrix GeneChip analysis project.

I greatly acknowledge the Ministry of Education, Singapore and the National University of Singapore for supporting me with the Research Scholarship, with which I can finish my PhD study.

Last but not least, I am also grateful to be blessed with a family, my husband, my parents, my elder brother and sister-in-law, as well as my son and my nephew for their unfailing love and support.

TABLE OF CONTENTS

SUMMARY

Neurulation is a complex morphogenetic process of neural tube closure to form the central nervous system during embryonic development. Its driving forces originate from both the neuroepithelium and the surrounding mesoderm. Failure of neural tube closure leads to neural tube defects (NTDs), one of the most common birth defects.

Neurulation is a highly synchronic process with a highly-ordered regulation, but the exact molecular mechanism is still unclear. There are more than 200 genes that have been found related with neural tube closure. Mutation of these genes cause NTDs in mice by interrupting functions of cell proliferation, cell differentiation, cell migration, cell adhesion and the integrity of cytoskeleton. In addition, several signaling pathways have been identified to be involved in the neural tube closure process, such as the planner cell polarity (PCP) pathway, the sonic hedgehog (*Shh*) signaling pathway, the retinoid acid (*RA*) signaling, and the *BMP* signaling. A comprehensive molecular mechanism need to be provided in order to understand the neurulation process more clearly and target the critical genes that synchronize neural tube development.

Glycosaminoglycans (GAGs) have been found to participate in many cellular functions such as those mentioned above and regulate multiple signaling pathways that related with neurulation. They are the most abundant carbohydrate conjugates that exist ubiquitously at the cell surface or extracellular matrix. In addition, their distribution during neurulation is stage and tissue specific which makes it critical to explore their roles further.

This study intended to set up a framework for investigating the genetic mechanism of spinal neurulation. It was carried out using tissue of neuroepithelium and surrounding mesoderm separately selected by laser capture microdissection (LCM) in combination with Affymetrix microarray to provide a transcriptomic profile of neural tube, in particular the spinal region of mouse embryo.

By transcriptomic analysis, hundreds of median hinge point (MHP) - and dorsolateral hinge point (DLHP) - related genes have been screened out, most of them are novel genes that have been found involved in neurulation for the first time. These genes have multiple functions such as proliferation and adhesion. For the pathways such as BMP, Shh, or Wnt pathway, more genes related with these pathways have been found to be involved in neurulation for the first time. In addition, dozens of GAG genes have been found to be differentially expressed during this event, and their expressions are spatially and temporally specific. Most of these genes were first reported to be related with neurulation process, especially during the formation of hinge points and closure of neural tube.

B-1, 4-galactosyltransferase1 (B4galt1) is one of the biosynthesis enzymes of GAGs which is differentially expressed in the microarray datasets during the neurulation process in mouse embryo. It has been found to be critical for synthesizing different species of GAGs. Moreover, B4galt1 itself has been found to function in GAG distribution and as cell surface receptors with multiple functions. Knockdown of B4galt1 expression in mouse neuroepithelial (NE4C) cells by siRNA significantly inhibited cell proliferation and cell adhesion ability. This may account for its role in neurulation.

In summary, this study has generated a transcriptomic profile of neuroepithelium and the surrounding mesoderm separately during the critical stages of mouse neurulation using microarray in combination with LCM. It is the first time that the complex neurulation process was dissected in specific spatial and temporal way. By setting up a framework of neurulation-related genes, this study has allowed neurulation investigators to investigate the complex process in a new and comprehensive manner. The functional study of B4galt1 shed light on the importance of GAG genes, and held promise for further investigation.

LIST OF TABLES

CHAPTER 2

CHAPTER 3

LIST OF FIGURES

CHAPTER 1

CHAPTER 3

LIST OF ABBREVIATIONS

Ab	Antibody
ANOVA	Analysis of variance
β4GalT1	β1,4-galactosyltransferase1
BMP	Bone morphogenetic protein
bp	Base pair
BSA	Bovine serum albumin
cDNA	Complementary DNA
Col	Collagen
CS	Chondroitin sulphate
Ct	Circle tail
CX	Craniorachischisis
DEPC	Diethylpyrocarbonate
DF1	DharmaFECT transfection reagents
DLHPs	Dorsolateral hinge points
DMEM	Dulbecco's modified Eagle's medium
DMSO	Dimethyl sulfoxide
DNA	Deoxyribonucleic acid
DS	Dermatan suphate
dsRNA	Double-stranded RNA
ECL	Enhanced chemiluminescence
ECM	Extracellular matrix
EDTA	Ethylenediaminetetraacetic acid
EGF	Epidermal growth factor
EGFR	Epidermal growth factor receptor
ERK1/2	Extracellular signal-regulated kinase-1 or -2
ESCs	Embryonic stem cells
EX	Exencephaly
EXT	Hereditary multiple exostoses gene
EXTL	EXT-like gene
FAK	Focal adhesion kinase
FBS	Fetal bovine serum
FGF	Fibroblast growth factor
FGFR	Fibroblast growth factor receptor
FITC	Fluorescein isothiocyanate
FN	Fibronectin
GAGs	Glycosaminoglycans
Gal	Galactose
GalNAc	N-acetylgalactosamine
GalT	Galactosyltransferase
GAPDH	Glyceraldehyde-3-phosphate dehydrogenase
Glc	Glucose
GlcA	D-glucuronic acid
GlcAT	Glucuronyltransferase

GlcNAc	N-acetyl-D-glucosaminoglycan
GlcNS	N-sulphoglucosamine
Gsk3	Glycogen syntheses kinase 3
GPI	Glycosylphosphatidylinositol
HA	Hyaluronic acid
HME	Hereditary multiple exostoses
HS	Heparin sulphate
HSPG	Heparin sulphate proteoglycan
IdoA	L-Iduronic acid
Ig	Immunoglobulin
IgG	Immunoglobulin G
IgM	Immunoglobulin M
kDa	Kilo Dalton
KS	Keratin sulphate
LM	Laminin
Lp	Looptail
MAPK	Mitogen-activated protein kinase
MHP	Median hinge point
mRNA	Messenger RNA
NDST	N-deacetylase/N-sulphotransferase
NTC	Neural tube closure
NTDs	Neural tube defects
PAPS	3'-phosphoadenosine 5'-phosphosulphate
PBS	Phosphate buffered saline
PCR	Polymerase chain reaction
PG	Proteoglycan
PI	Propidium iodide
PI3K	Phosphoinositide 3-kinase
PKC	Protein kinase C
RNA	Ribonucleic acid
RNAi	RNA interference
RT	Room temperature
RT-PCR	Reverse transcription polymerase chain reaction
SB	Spina bifida
siRNA	Small interfering RNA
TGF-β	Transforming growth factor beta
Tris	2-amino-2-(hydroxymethyl)-1,3-propanediol
TSG	Twisted gastrulation
VEGF	Vascular endothelial growth factor
VEGFR	VEGF receptor
WB	Western blotting
Xnr3	Xenopus nodal-related 3
Xyl	Xylose

List of Publications

Article

Cao S, Bay BH, Yip GW. Transcriptome profiling of murine spinal neurulation using laser capture microdissection and high-density oligonucleotide microarrays. Methods Mol Biol. 2011; 755:375-84

Meeting Proceedings

SF Cao, AJ Copp, GW Yip. Transcriptomic analysis of mammalian spinal neurulation. In Proceedings of the Society for Developmental Biology 68th Annual Meeting. 23-27 July 2009, San Francisco, CA.

SF Cao, AJ Copp, GW Yip. A transcriptomic analysis of the closing mouse neural tube using laser capture microdissection. In proceedings of the International Anatomical Sciences And Cell Biology Conference 2010. 26-29 May 2010, Singapore.

CHAPTER 1

INTRODUCTION

1 Introduction

1.1 Introduction of neurulation

Neurulation is a complex morphogenetic process by which the rudiment of the adult central nervous system develops (Copp et al., 2003). It is composed of several co-dependent events overlapping temporally to some degree. In vertebrates, neurulation is divided into primary neurulation and secondary neurulation. Primary neurulation begins at the late stage of gastrulation, including initiation, elevation, apposition and fusion of the neuroepithelium and ends by the closure of the neural tube to form the precursor of the central nervous system, including the brain and most of the spinal cord. Subsequently, secondary neurulation forms the remaining sacral and all of the coccygeal regions of the spinal cord by different mechanisms (Catala, 2002; Kibar et al., 2007). Failure of closure of the neural tube during embryo development leads to neural tube defects (NTDs), the second congenital malformation in human (De et al., 2006; Wallingford, 2005).

Scientists have put a lot of efforts into investigation of neurulation in order to find solutions to NTDs. Currently, more than 200 genes are found related with neural tube closure (Copp and Greene, 2010b). Mutation of these genes cause NTDs in mice by interrupting functions of cell proliferation, cell differentiation, cell migration, cell adhesion and the integrity of cytoskeleton. Several signaling pathways have been identified involving in neural tube closure process, such as the planar cell polarity (PCP) pathway, the sonic hedgehog (*Shh*) signaling pathway, the retinoid acid (*RA*) signaling, and the bone morphogenetic protein (*BMP*) signaling. Although the exact molecular mechanism is still unclear, scientists tend to agree that neurulation is a highly synchronic process where highly-ordered regulation may exist.

Glycosaminoglycans (GAGs) are presented at cell surface or extracellular matrix, interacting with growth factors, morphogens, and adhesion molecules (Zhang, 2010a; Zhang, 2010b), and participating in many cellular functions such as cell proliferation, cell adhesion, and cell migration. They have also been found to regulate multiple signaling pathways such as *Wnt*, *hh*, etc. Different kinds of GAGs are found distributed at different axial levels of neurulation process. The roles of GAGs in neurulation activate the interests of biological scientists since early 19ths (Copp and Bernfield, 1988b). They are found distributed through multi-stages of mouse embryos, and accumulate specifically at the site of neural fold elevation, but not in the primitive streak where neurulation has not yet begun, and decreased progressively where neurulation was already complete (Copp and Bernfield, 1988b).

1.1.1 Primary neurulation

In vertebrates, primary neurulation begins when gastrulation ends, the notochord induces the ectoderm above it to become thick flat neuroectoderm-called the neural plate. The neural plate bends first in the midline to form the neural groove at early stage of neurulation, and the straight parts at both sides of the groove are called neural folds. Later at mid-stage of neurulation, bends take place at the lateral edges of the neural folds and the tips of the neural folds elevate and apposite each other in the upper midline to fuse into a closed neural tube (Copp et al., 2003; Greene and Copp, 2009). The neural tube later differentiates into the most important parts of the central nervous system, the brain and the spinal cord. Cells at the very lateral edges of the neural folds separate as the neural crest cells and migrate to become various different but important cells, such as pigment cells and the cells of the peripheral nervous system. The mesoderm

surrounding the neuroectoderm at the sides will develop into the somite which become future muscles, bones, etc.

To nominate the gestation time of embryo, in vertebrates, embryonic day 0.5 (E0.5) means if timed matings were made at night, noon on the day of discovering a copulation plug. The first somite presents at around E8.0 in the mouse embryo, and neural tube closure begins at the level of cervical/hindbrain boundary at around 4 to 5 somite stage (Sakai, 1989). Then closure extends cranially (towards the head) to form the anterior neuropore and caudally (towards the tail) to form the posterior neuropore. The posterior neuropore (PNP) refers to the region of open, elevating neural folds caudally adjacent to the just closed neural tube which represents the next axial region to experience neural tube closure. The anterior neuropore will be closed at E9.0 and the posterior neuropore will be closed at E10.0 to declare the end of primary neurulation.

Neurulation is a very short period in human. Gastrulation in human embryo begins at the 2^{nd} week and neurulation starts at the end of gastrulation and ends within the fourth week of pregnancy when the pregnant mother unaware of their pregnant. Genetic analysis of neural tube development has shown that different neurulation events have different molecular mechanisms. Failure of neural tube closure will lead to neural tube defects (NTDs), a common congenital disease most of which will be still birth (Botto et al., 1999). Most of the few survivors are due to failure of closure at spinal region which called spina bifida and they have to face many problems such as sensory missing and activity limiting.

1.1.1.1 Initiation of neurulation

Neural induction is the formation of the neural plate from the dorsal midline ectoderm into the neuroepithelium (De et al., 2006). Prior to neurulation, the notochord is formed from the mesoderm and secrets a variety of signals such as bone morphogenetic protein-4 (*BMP-4*). These signals induce the overlying ectodermal cells to differentiate into epidermis which will become skin. This action is blocked by neural inducers such as *chordin*, *noggin*, *follistatin*, *cerberus*, *Xnr3* (Xenopus nodal-related 3), and *TSG* (twisted gastrulation), which are secreted from the surrounding tissues such as the spemann's organizer, a tissue located in the dorsal side of the gastrula in Xenopus, (or hensen's node, a mouse homologous to the Xenopus organizer), and present in the ectoderm (Kuroda et al., 2004; Weinstein and Hemmati-Brivanlou, 1999). Ectodermal cells that do not receive *BMP-4* are allowed to become neural ectoderm which will become the future brain and spinal cord (De Robertis and Kuroda, 2004).

Wnt signaling interferes with *BMP4* function by blocking the activity of glycogen synthase kinase 3 (*Gsk3*) and activating the transcription function of *beta-catenin* (Baker et al., 1999). *Wnt* signaling was also found to specify posterior neural identity in combination with the *BMP* antagonists. A further study in Xenopus also showed that down regulation of Bmp signaling in dorsal ectoderm by *Wnt* signaling may be mediated by *Xiro1*, one of the Xiro homeodomain proteins of the Iroquois (*Iro*) family, which were shown to control the size of the neural plate in Xenopus embryo. A number of *Wnt* inhibitors, such as *Frzb-1*, *sFRP-2*, *Crescent*, *Dickkopf-1*, and *Cerberus*, secreted by organizer region, play important roles in neural induction by inhibition of *Wnt* signaling.

Growth factors are also found to contribute to neural induction (Weinstein and Hemmati-Brivanlou, 1999). Members of *FGF* signaling were reported to induce gastrula stage ectoderm

into posterior neural tissue in Xenopus and chick, and inhibition of *FGF* receptors blocks neural induction (Launay et al., 1996). Fibroblast growth factor (*FGF*) signaling, as secreted diffusible glycoproteins, can bind to extracellular receptors (*FGF* receptors, *FGFR*) and mediate their effects. They are required at neural induction stage to enable later neural differentiation (Streit et al., 2000; Wilson et al., 2000).

Insulin-like growth factors (*IGFs*) have also been identified as neural inducers acting as either potent *Wnt* inhibitors or through a common mechanism as *BMP* antagonists by low levels of Smad1 activity (Pera et al., 2001; Pera et al., 2003).

1.1.1.2 **Shaping of neuroepithelium**

Global deformations of the neural plate are driven by the changes of cell shape, number and position as the neural plate grows with neurulation. As cell number changes, cell position changes by intercalation. These changes result from the process of convergent extension (CE) which is found mainly regulated by the planar cell polarity (PCP) pathway.

CE was first studied in amphibian gastrulation, and then it has been studied in many other species. Cell tracing experiment demonstrated that wedged cells moving only short distances within tissues while the collective effect of this polarized cell motility caused a rapid change in tissue shape. Time-lapse recordings showed that a mediolateral intercalation in the future mesoderm and neural plate were formed by lamelliform protrusions which were directed to connect to adjacent cells. This intercalation results in medial-to-lateral narrowing (Convergence) in the middle and rostro-caudal lengthening (extension) along the body axis (Keller, 2002).

In neurulation, cells experiencing CE move medially with intercalation and result in a neural plate lengthening craniocaudally and narrowing transversely (Keller et al., 2008). These

cells were directed by polarized cellular protrusions to move and intercalate with adjacent cells. The process of CE results in an elongated neural plate with broad cranial region and narrow spinal region and is crucial for neural tube closure.

At the molecular level, CE is regulated by PCP pathway which is the so-called non-canonical *Wnt* signaling pathway because it shares components with the *Wnt* signaling pathway but does not function through the activation of β-catenin (Jones and Chen, 2007).

Planar cell polarity signaling (PCP), also known as tissue polarity for cells within the plane of an epithelium become polarized during the process and at least one of the core PCP genes were involved (Mlodzik, 2002; Zohn et al., 2003). Polarization of cells has been so far observed in many biological processes such as distal orientation of wing hairs in Drosophila, convergent extension, neural tube closure, hair bundle orientation in inner ear, hair follicle orientation in the skin and the more complex organization of the ommatidia (eye units) (Wallingford et al., 2002a; Wang et al., 2005; Wang et al., 2006a; Wang et al., 2006b; Wang et al., 2006c; Wang and Nathans, 2007). The PCP signaling seems conserved among these processes and species.

The *Wnt* ligand binds to transmembrane receptor *Frizzled* (*Fz*) to activate the *Dishevelled* (*Dsh* in Drosophila and *Dvl* in vertebrates). In vertebrates, this process is regulated by the proteins of *Vangl*, *Celsr*, *Prickle* (*Pk*), and *Diego* (Jenny and Mlodzik, 2006; Klein and Mlodzik, 2005; Schlessinger et al., 2009; Veeman et al., 2003; Wallingford et al., 2002b). Dishevelled then activates the downstream cascades of GTPases *Rho-Daam1-ROCK (Rho-associated kinase)*, resulting in cytoskeletal rearrangements (Habas et al., 2001). *Dsh* also activates *Rac* which then stimulates JNK signaling (Jun –terminal Kinase) with the functions of regulating cytoskeletal organization and transcription (Habas et al., 2003).

Disruption of the core-genes of PCP signaling lead to neural tube defects in vertebrates. These genes include Wnt ligands, such as Wnt5α (Qian et al., 2007), its receptors such as *frizzled-3* and *frizzled-6* (craniorachischisis in double knockout) (Wang et al., 2006d), the core transduction components such as *dishevelled* (*Dvl*) (Wallingford and Harland, 2001; Wallingford and Harland, 2002), *Vangl2* (the homolog of Drosophila *strabismus*/*Van gogh*, results in *Loop-tail mice*) (Kibar et al., 2001; Murdoch et al., 2001) , *Celsr1* (the homolog of Drosophila *flamingo*/*starry night*, results in the Crash mice) (Curtin et al., 2003), *Scrb1* (results in the Circletail mouse) (Murdoch et al., 2003), the tyrosine kinase *Ptk7* (Lu et al., 2004).

The common feature of these mutations is craniorachischisis, resulting from failure of convergent extension which abrogating the formation of MHP, leaving the neural folds too far from each other to close. These findings indicated the potential important link between convergent extension and neurulation and the importance of PCP pathway genes as candidates for NTDs.

1.1.1.3 Bending of the neuroepithelium-formation of MHP and DLHPs

Morphological studies during mouse spinal neurulation found a series of morphogenetic changes along the neuroaxis, and three modes were defined according to the morphology of the neural plate bending within the PNP region to represent the continuous process of spinal neurulation (Shum and Copp, 1996). In mode 1, at E8.5, bending occurs in the neuroectoderm overlying the notochord, creating a median hinge point (MHP). The non-bending portion of the neural folds remains straight, demonstrating a V-shaped image on transverse sections. Mode 1 exists mainly at upper spinal level of the neuroaxis. In mode 2, at E9.0, additional bending occurs at the lateral edges of the neural folds and the dorsolateral hinge points (DLHPs) forms in

addition to the MHP, but the other portions of the neuroepithelium do not bend. Neuroepithelium with the three bending sites form a rhombus-shaped image on the transverse sections. Mode 2 exists in neuroaxis of both the cranial and the posterior spinal region. In mode 3, at E9.5, the entire neuroepithelium exhibits bending, resulting in a circular-shaped image on the transverse sections. The MHP is not distinguished at the caudal spinal region of neuroaxis.

This bending and closing process is accompanied by cell shape changes (Colas and Schoenwolf, 2001). The neural plate cells first change shape from cubical to columnar as a region taller than the rest of the surface ectoderm. Then the cells become wedge-shaped at MHP and DLHP region including an apical narrowing and basal widening. Cells become high-columnar at the non-bending portions of neuroectoderm (NT), making the NT distinguished obviously from the surrounding mesoderm (MD) (Hildebrand and Soriano, 1999; Smith et al., 1994; Wallingford et al., 2002b).

Observation from these morphological studies hypothesize that neurulation of the neuroepithelium in early stage (mode 1) is driven basically by extrinsic forces generated in surrounding tissues such as the paraxial mesoderm and surface ectoderm, while neurulation in late stage (mode 3) is driven largely by intrinsic forces generated by the neuroepithelium itself. And mode 2 is a transition period in which both the intrinsic and extrinsic forces play roles (Shum and Copp, 1996).

Animal models demonstrated that both MHP and DLHPs play significant roles in the development of neural tube closure. In some mouse NTD models such as Circle tail (Ct), Loop-tail (Lp), and Crash mutants, they display nonappearance of MHP with an unusually wide floor plate, the neural fold tips were too far from each other so that the neural tube remains open (Curtin et al., 2003; Hildebrand and Soriano, 1999; Murdoch et al., 2001).

Current studies have demonstrated that DLHPs may play more important roles in neural tube closure in the spinal region than MHP does (Curtin et al., 2003; Hildebrand and Soriano, 1999; Murdoch et al., 2001; Ybot-Gonzalez et al., 2002). These scientists demonstrated that disruption of DLHP can definitely damage neural tube closure, while some mutants with MHP damage may not induce NTDs especially at lower spinal levels. They were also able to identify that this disruption may be due to mutation of certain genes, such as *Shh* (Curtin et al., 2003; Hildebrand and Soriano, 1999; Murdoch et al., 2001; Ybot-Gonzalez et al., 2002), *BMP* and its antagonists (Curtin et al., 2003; Hildebrand and Soriano, 1999; Murdoch et al., 2001; Stottmann et al., 2006; Ybot-Gonzalez et al., 2007), *Grhl* family genes (Gustavsson et al., 2008; Rifat et al., 2010) or *Zic* genes (Nyholm et al., 2009).

In vertebrates, *Shh* is secreted from notochord and floor plate cells and is not only essential for bending of the neuroepithelium at the midline but preventing dorsolateral bending at the upper spine level (Ybot-Gonzalez et al., 2002). At this time, another dorsolateral bending inhibitor, *BMP2*, is secreted from the dorsal-most surface ectoderm. At early neurulation stage mouse embryos, loss of function of *Shh* pathway inhibitory genes, such as *Ptc1* (Goodrich et al., 1997), *Gli2* (Ding et al., 1998), *Gli3* (Hui and Joyner, 1993), *Fkbp8* (Shirane et al., 2008), *Rab23* (Eggenschwiler et al., 2001; Shirane et al., 2008), *Tulp3* (Norman et al., 2009), and overexpression of *Shh* stimulating proteins such as *Smo* and *Shh* itself (Echelard et al., 1993; Shirane et al., 2008), can lead to NTDs in upper spinal level, possibly due to failure of formation of MHP. In contrast, loss of function of stimulating proteins such as *Smo* and *Shh* itself do not produce NTDs (Chiang et al., 1996; Shirane et al., 2008; Zhang et al., 2001). In contrast, in lower spinal level of mouse embryos at late neurulation stage, closure of the neural tube depends essentially on the DLHPs rather than the MHP. Embryos ablated of notochord were able to close

the neural tube by forming ectopic DLHPs along the entire neuraxis in the absence of MHP (Ybot-Gonzalez et al., 2002). This view was supported by a series of experiments using mouse with the targeted mutation of Shh pathway genes, such as *Shh*, *HNF3β* (*Foxa2*), *Gli2* or *Gli1/2* (Ang and Rossant, 1994; Chiang et al., 1996; Ding et al., 1998; Matise et al., 1998; Park et al., 2000; Weinstein et al., 1994), none of them display spinal NTDs but display a circular lumen of the neural tube along the neuraxis, implying a default-DLHP mechanism in the lower spinal region.

At the lower spinal region, production of *Shh* from the notochord is significantly reduced, whereas secretion of *Noggin*, a *BMP*-antagonist, from the tips of the neural folds, conquers the *BMP*-mediated inhibition and facilitates DLHPs formation (Ybot-Gonzalez et al., 2007). *Zic* family genes were found to be involved in bending of the neuroepithelium during neurulation. The expression pattern of *Zic* genes in *Wnt3a* mutant mice changed in the presence of notochord, its dorsal constriction is consistent with the *Shh* expression (Nagai et al., 1997). Mutation of *Zic2* in mouse embryo results in extensive spina bifida, with normal MHP but abrogation of DLHP formation (Nagai et al., 2000). A more recent experiment using Zebrafish demonstrated that both *Wnt* signaling and *Zic* genes were required for DLHP formation during cranial neurulation (Nyholm et al., 2009).

1.1.1.4 Closure of the neuroepithelium

Bending of the neuroepithelium enables the paired lateral neural folds to contact with their tips at the dorsal midline. Fusion of the neuroepithelium occurs at the contact region to close the neural tube. This closure is facilitated by the formation of cellular protrusions at the tips

of the neural folds and cell adhesion and forms the roof plate of the neural tube (Geelen and Langman, 1979).

The cellular and molecular mechanisms of fusion and closure of the neural tube are not clear. Several lines of evidence indicate the involvement of cell adhesion molecules such as Eph receptors, the neural cell adhesion molecules (*NCAMs*), as well as cadherins. Eph was the first identified member of the tyrosine protein kinase receptors family with a conserved cysteine-rich domain, two fibronectin repeats, and a tyrosine protein kinase domain. Eph receptors and their ephrin ligands are implicated in playing roles in neural tube formation. Mice that lack *Eph-A5*, a cell surface ephrin ligand, or *Eph-A7* receptor, a potential ephrin A5 ligand, exhibit cranial NTDs (Holmberg et al., 2000). Yet no further evidence is added to elucidate the potential mechanism.

The neural cell adhesion molecule (*NCAM*) is a GAG-binding protein, expressed in the developing neural tube. The expression pattern of *NCAM* during neural tube development in mouse embryo implicated a role in closure of neural tube (Bally-Cuif et al., 1993) null mutations in *NCAM* in mice do not result in neural tube defects, questioning their essential role in neural tube closure (Cremer et al., 1997; Radice et al., 1997a). However, a study of investigating the role of *NCAM1* in 132 spina bifida families established the expression pattern of *NCAM1* in the central nervous system of human embryos, shed light on a possible contribution of variations of *NCAM1* to NTDs risk (Deak et al., 2005).

Cadherins belong to cell adhesion molecule family. They have been found to be differentially expressed during neural plate formation. N-cadherin is expressed in the neural plate, while E-cadherin is expressed in the surrounding ectoderm (Rutishauser and Jessell, 1988). When both the neural tube and the surface ectoderm in Xenopus embryos express N-cadherin, they fail to separate the two tissues and result in NTDs (Detrick et al., 1990). However, Mouse

with null mutations in N-cadherin gene undergoes normal neural tube closure, implicating that these cadherin molecules may not play a major role in neural tube formation.

1.1.2 Secondary neurulation

Secondary neurulation starts at the end of primary neurulation. In human, this process develops from the caudal eminence, which is the counterpart of the tailbud in other mammals such as chick or mice, to the formation of the most distal segment of the spinal cord (Muller and O'Rahilly, 1987). The caudal eminence or the tail bud contains a group of stem cells which first proliferate and then differentiate to different kinds of tissues in the caudal region such as hindgut, somites, and notochord, etc (O'Rahilly and Muller, 1989). These stem cells then condense and cavitate to form a tube to connect with the central canal formed during primary neurulation. The newly formed neural tube shapes the remaining sacral and coccygeal part of the spinal cord.

Previous studies have thought that secondary neurulation is not just an extention of primary neurulation. The manner and timing is different as well as their roles in CNS development (Saitsu et al., 2004). But one study suggested that primary and secondary neurulation are parts of a continuous process with similar molecular and cellular mechanisms (Catala, 2002).

1.1.3 Neural tube defects (NTDs)

Neural tube defects (NTDs) are a group of congenital anomalies of the central nervous system (CNS) (Copp et al., 2003). It is among the most common birth defects only secondary to congenital cardiovascular defects. The prevalence of this congenital disease is reported at around 1 to 10 per 1000 births worldwide: 0.75 to 1.12/1000 in America (Mitchell, 2005), 2.74/1000 births in China (from Birth defects report in China,2000), and 0.58/1000 births in Singapore (Tan et al., 2007). The common types of NTDs due to failure of neural tube closure during neurulation

are anencephaly and spina bifida (Botto et al., 1999). They are “open” NTDs with tissues exposed to outside of the unclosed neural tube. In contrast, encephalocele is the kind of post-neurulation NTD due to failure of the secondary neurulation. It often occurs in the occipital region and is covered with skin. The mechanism of NTD developed from secondary neurulation is usually due to failure of separation of the neural tube from the attached tissues of the tail bud (Rossi et al., 2004). Most infants with anencephaly die, some survivors with spina bifida face the threat of death or severe physical and developmental disabilities.

Epidemiological studies found that recurrence risk is enhanced among siblings, frequency in twins is higher than in singletons and occurrence of disease is associated with particular genes (Padmanabhan, 2006). Spina bifida often takes place in autosomal trisomies. These findings point toward the existence of a strong genetic mechanism of NTDs. Clinical studies of periconceptional supplementation of folate (FA) reduce significantly not only the first occurrence but the recurrence of NTD in the offspring encouraged investigations on the genes involved in FA metabolism during neural tube development (Czeizel and Dudas, 1992). Experiments using animal embryos such as mouse, rat, chick, pig, rabbit, Xenopus, etc, provided insights into the mechanism of NTDs and suggested a gene-gene, and gene-environment mechanism in NTD, yet no clear evidence for causation genes of NTD have been declared.

There are more than 200 NTD genes so far, most of them are related with the unknown genetics of the common human NTDs, exencephaly (EX), spina bifida (SB), and craniorachischisis (CE) (Copp and Greene, 2010b). In mouse mutants, EX has a much higher number than SB, while in human, the case numbers of the two are almost the same, which indicates that candidate genes induce EX only in mouse but may induce SB in human. The mouse mutants examined during the time of normal neural tube closure displayed a dominant

failure of neural folds elevation compared with the small portion of inadequate adhesion and fusion (*Efna*) as well as reopening of a poorly closed tube (*Fkbp8, Prkaca*) (Harris and Juriloff, 2007). In both mouse and human NTDs, the common region of failure of neural folds elevation were the mid-brain and the posterior neuropore, the former causes EX in mouse and anencephaly in human, while the later results in SB in both. CE was seen mainly in mouse mutants, with a widened floorplate, and the neural folds are too far to contact.

Glycosaminoglycans (GAGs) are a group of heteropolysaccharides that have long been found related with neural tube closure （Copp and Bernfield, 1988b）. Newly synthesized GAGs accumulated especially in the active neurulation sites, while mutation of some GAG genes such as *Sdc4*, *Ndst1* can lead to neural tube defects in mouse embryos. These findings implicated an important role of GAG genes in neural tube closure and hold a promising for further investigation.

1.2 Microarray analysis

Scientists can only study a relatively small number of genes at a time by traditional methods. The development of microarray technology can generate gene expression profiling of a creature with thousands of genes in a single experiment. With microarray analysis, researchers can explore dynamic aspects of normal developmental process or genetic basis of various diseases.

1.2.1 Microarray and its classification

Microarray is a technology for analyzing a large number of genes in small supports. The supports could be glass microscope slides, silicon chips or nylon membranes, with gene

sequences known as probes attached onto it at fixed locations in an orderly arrangement. The gene sequences attached to the supports can be DNA, cDNA, or oligonucleotides. These immobilized target DNA hybridize with laboratory prepared fluorescent labeled cDNA or cRNA samples. The binding of the labeled molecules to the corresponding sites on the array reveals the genes expressed in each cell. Therefore, simultaneously monitoring the expression intensities of thousands of genes in one experiment can provide a global view of gene expression patterns in biological samples, promoting a better understanding of the underlying mechanisms of the biological events.

There are two basic microarray types: genomic or transcriptomic microarray. They are mainly different from each other in the kind of immobilized DNA, the type of control and sample DNA used in the hybridization solution, and the information that is generated from the chip. Genomic microarray, also called "spotted microarray", uses oligonucleotides, cDNA or PCR products as probes to be spotted on the array surface (Bertucci et al., 2001). It represents the nucleic acid profiles and is ready to hybridize with cDNA or cRNA samples. This kind of microarray can be manufactured using only a portion of the whole genome according to purpose of different experiments. It's relatively cheaper, but may be less sensitive owing to its small batch size and reduced efficiency.

Transcriptomic microarray are used to generate transcriptomic profilings to measure gene expression patterns or change in mRNA levels (Conway and Schoolnik, 2003; Dalma-Weiszhausz et al., 2006). The transcriptome is defined as the steady-state of all RNAs formed in a tissue at a defined time in development. The Affymetrix oligonucleotide microarrays use shorter sequence probes in high density directly onto the array surface with the purpose of matching specific parts of mRNA. By this method, most genes in one organism can be detected

on one Chip (Dalma-Weiszhausz et al., 2006). For example, the Affymetrix GeneChip Mouse genome 430 2.0 array allows wide-ranging analysis of over 39000 transcripts and variants, covering over 34000 well known mouse genes (Auer et al., 2009).

Microarrays can also be classified according to the methods of labeling probes. The two-color microarrays actually use two different fluorescent dyes, cy3 and cy5, to label cDNA of two different samples (Shalon et al., 1996), for example, diseased and control samples. The two labeled cDNA samples will be hybridized on the same microarray chip. The same gene will give two different colors for comparing their expression difference between the two samples. Although this method allows two samples in one chip to be processed under exactly the same experiment condition, the low quality of one sample can affect the gene expression of another. Another limitation is that it cannot be used to compare more than 2 samples from more than 2 groups.

Fortunately this problem can be addressed by the one-color microarray. Affymetrix microarrays is a one-color microarray, which means that all the cRNA probes in the sample were labeled with one dye and hybridized on one chip. Control probes are designed in the Chip to normalize the target probes. Different experiment samples are applied onto different chips separately. More chips are needed in one experiment. This makes it relatively costly. But the one-sample-on-one-chip method avoids inter-chip interference of raw data by other samples, especially when quality of one of the samples is low. Moreover, there is no limitation of sample numbers and easier comparison between data from different experiments.

Because of the complex features of biological science and numerous genes with various functions involved in the same biological process, traditional candidate gene approaches cannot meet the needs of understanding the genetic basis of certain biological process in a broad view.

Microarray technology provides a great tool to investigate the comprehensive biological systems with at least two advantages. One advantage is in its high-throughput to provide a global picture of all genes within the whole genome. Differentially expressed genes can be simply discerned by comparing the expression profiles. Another advantage of microarray analysis is to reveal a new or enhanced pathway of interested biological function. Novel genes with unknown functions can be discerned by the following verification experiments as well.

1.2.2 Application of microarray in biological science

The characteristics of microarray technology enable measurement of thousands of genes expressed simultaneously. It has been widely used for monitoring transcription patterns or gene expression changes during developmental processes, under certain disease or experimental conditions such as gene mutation, diagnostics, pharmacogenomics or drug treatment (Choudhuri, 2004; Conway and Schoolnik, 2003; Stoughton, 2005). Researchers have explored the gene expression changes of different stages of embryogenesis, at the very early oogenesis (Niemann et al., 2007), preimplantation (Hamatani et al., 2004), and gastrulation stages (Hue et al., 2007). The above studies have provided extensive knowledge representing early stages of mouse embryogenesis, the later studies could refer to the genes provided in these studies before they design new experiments. But no genome-wide expression profiling has been provided regarding neurulation, the most important developmental stage of nervous system development. Jiang, et al compared the expression difference of cranial neural tube closure between embryos of diabetic mice and normal embryos at the same stage (E11.5) (Jiang et al., 2008). They found 390 differentially expressed genes with more than two-fold changes, and identified several genes with certain functions which could disturb proliferation of neurogenesis in embryos of diabetic

mice and their survival. This work provided a framework for later studies of diabetic disease. Since the genes found were from embryos of diabetic mice, they may not reflect the normal status of embryogenesis. Moreover, differences may also exist between neural tube development of cranial and spinal region.

In summary, microarray experiment is expected to play significant roles in investigating the genetic mechanism of nervous system development. Yet no microarray experiment has been done to explore the difference between stages of neural tube formation in physiological states. The current research was designed to explore the transcriptomic profiling of critical time points of the closing neural tube in the spinal region of mouse embryos, with the hope of revealing important aspects of neurulation, such as finding novel genes and group genes into functional pathways in order to illustrate the genetic mechanism of neural tube defects (NTDs), a congenital disease caused by failure of neural tube closure.

1.2.3 Bioinformatics for microarray analysis

Microarray technology has been used widely in various biomedical areas, including research area and microarray-based clinical tests. Therefore, microarray data analysis is important for its potential impact on development of biomedical research fields. There are two steps to analyze the quality of a microarray experiment. In the first step, analysis is focused on experiment designing, set up quality control, and the process of performing. These analyses depend more on professional knowledge and expertise in use of microarrays, and can be done before and during the experiment process. The second step analysis refers to the final purpose such as establishing a relationship between disease and certain treatment, finding targeting genes, or setting up molecular pathways and networks, promoting understanding of biological implications from a huge amount of microarray data. The second step analysis will be performed

after the experiment and depend more on commercially available software in addition to professional knowledge (Mocellin and Rossi, 2007; Wang, 2008).

There are various commercially available software for analysis of microarray data. The techniques and algorithms are different, but the main principles and purpose are similar: to generate a differential gene expression profile, find the key variables affecting the difference, and find links between genes within the profile and crosstalk nets among profiles.

1.2.3.1 GeneChip Operating Software (GCOS)

Affymetrix offers a Microarray Analysis Suite (MAS) and its successor GeneChip Operating Software (GCOS) for organization and analysis of the Affymetrix microarray data (Dalma-Weiszhausz et al., 2006). It is an integrated software package for data storage, sample organization, image acquisition, cell intensity calculation and normalization, background noise controlling and gene expression comparison.

This software employs a detection algorithm to evaluate the Present (P), Absent (A), or Marginal (M) of the transcripts. Then the expression value of each transcript is calculated by Signal Algorithm. The intensity of the probe sets are normalized between experiment and baseline array. The changed transcripts have a robust increase or decrease when “Present”.

One of the advantages of GCOS is set a default average Signal intensity. This can quantitatively calculate signal intensity which helps users know more about the expression strength in addition to fold change to assess the gene function. Another advantage is capable of comparing files from the same experiment or different experiment simultaneously using the batch analysis tool.

1.2.3.2 DNA-Chip Analyzer (dChip)

DNA-Chip Analyzer (dChip) is an software package for analysis of probe-level Affymetrix gene expression microarray (Schadt et al., 2001). It meets the basic service for comparison of differentially expressed genes. In addition, it presents the hierarchical clustering analysis which can group genes according to their expression pattern in a clustering tree. Genes with the closest distance are merged together indicative of their high similarity in standardized expression values.

dChip can be used to compare data from different array types or species. It is a great advantage especially when samples are rare and experiment cannot be repeated or unknown genes are investigated. Hierarchical clustering is offered by dChip software and replicate samples or samples with similar variables are expected to be clustered together.

1.2.3.3 GeneSpring

GeneSpring^{TM} software (Silicon Genetics, Redwood City, CA, USA) includes a set of analytical tools such as Robust Multi-array Average (RMA), Guanine Cytocine Robust Multi-array Average (GCRMA), and Probe Logarithmic Intensity Error (PLIER) to analysis data from multiple array formats. The RMA algorithm is used to analyze the Affymetrix data begins by correcting the raw intensity values against their background, the background-corrected perfect-match intensities are $\log_2$-transformed followed by normalization using the quantile normalization method (Irizarry et al., 2003). The advantage of RMA is obtaining an expression measure by the justification of discrepancies arose during experimental procedures such as staining, as well as avoiding the affects from MM probes. The GCRMA platform is an enhanced form of RMA designed to account for background noise and non-specific binding, and calculate

PM and MM value based on sequence information as probe affinity, so it is possible to obtain more accurate gene expression values. PLIER is an improved method for calculating signal by accounting for handling error. It is designed based on the model-based expression analysis and robust multiple analysis and featured by avoiding bias.

In experiments that genes generated by one software are too many that they are beyond the ability for further analysis, combined use of different software are suggested to narrow down the new candidate gene lists. Millenaar FF et al (Millenaar et al., 2006) compared the reliability of 6 different calculating methods (MAS5, dChip PMMM, dChip PM, RMA, GC-RMA and PDNN) for the same Affymetrix microarray data and find that only 27% to 36% genes overlapped between the different methods. This study shows that combined use of different software can effectively narrow down the targeted genes if too many genes are found, though loss of some of the critical genes might occur. Proper literature research should be needed for more accurately picking up biologically meaningful targeted genes.

1.2.3.4 Gene ontology (GO) tool and the NetAffx™ Analysis Center

Gene Ontology (GO) (http://www.geneontology.org/) is one of a functional annotation tool from the database for annotation, visualization and integrated discovery (DAVID) website (Ashburner et al., 2000). It is a practical tool for understanding biological meaning behind large list of genes. It is a joint project from multiple organism databases: FlyBase, Mouse Genome Informatics (MGI) (http://www.informatics.jax.org/searches/GO_form.shtml), and the Saccharomyces Genome Database (SGD). Information for specific genes or proteins is also linked to multiple keyword databases in order to provide flexible biological knowledge. GO provides at least three categories to characterize a gene list: biological process, molecular function, and cellular

component. The biological process refers to what is the biological purpose of the gene product, molecular function refers to how the gene products carry out their purpose, and cellular component presents where the gene products take actions. Through GO ontology, a list of data sets can be turned into multiple sets of well-defined terms with well-defined functions.

The Affymetrix NetAffx^{TM} Analysis Center (www.affymetrix.com/analysis/) provides comprehensive functional annotations for creating of statistically and biologically significant gene lists by the Gene Ontology (GO) Mining Tool. It makes users life easier by offers gene function interpretations among several databases simultaneously based on their molecular functions.

1.3 Introduction to laser capture microdissection (LCM)

The development of microarray makes it possible to investigate genome, transcriptome, or proteome. Genome is the whole set of DNAs in cells of individual being. DNA can undergo transcription into RNA. The transcriptome includes the steady state levels of all the RNAs in individual cells and transcriptome profiling can reflect the whole or a selected part of the whole transcriptome of individual cells or tissues. RNAs can undergo translation into proteins and the steady state level of all the protein species is called proteome. Expression profiling at RNA levels represents the status of the epigenome more closely than expression profiling at protein levels as different cell state can have different signaling molecules.

The big challenge of getting reliable microarray results is the heterogeneity in tissue context as gene expression levels can be affected by cell types and status. For example, in the same lump of tissue samples, gene expression is different in cancer cells compared with normal cells. In a developing organ, genes expression levels can also be fundamentally different among

epithelium, mesenchyme or endoderm. Cell numbers of different cell types usually very different in one tissue or organ, so investigating the gene expression profiling of whole mount tissues may give confounding results for discussion. The invention of laser capture microdissection (LCM) offers a tool for isolating interested cells or tissue types from heteogeneous tissue contexts (Bonner et al., 1997; Emmert-Buck et al., 1996).

1.3.1 LCM systems and their working principles

LCM is a technique used for harvesting selected cells even single cells from tissue sections or cultured cells by laser cutting under the guidance of microscope (Bonner et al., 1997; Emmert-Buck et al., 1996). It was first devised by a group of collaborative researchers from the National Institutes of Health (NIH) and the first commercial instrument was manufactured by Arcturus Engineering (Mountain View, CA). The main principles of the laser microdissection are: visualization of interested cells via an inverted light microscopy; transfer of low power laser energy of near-infrared (IR) for melting the thermolabile polymer or UV for photo volatilization of cells surrounding a selected area; removal of the cut cells from the heterogeneous context.

There are three types of commercially available LCM systems with similar components but different modes of harvesting cells: (1) Thermoplastic polymer film attached to a MicroCap situated just up to targeted cells, the film melted by laser and bounded to underlying cells after selection and microdissection and lifted away from the tissue section. Pixcell is the original manual instrument conceived by NIH and manufactured by Arcturus Molecular Devices (Bonner et al., 1997; Emmert-Buck et al., 1996; Espina et al., 2006). (2) The polymer film attached to a slide for tissue sections, interested cells were selected and catapulted by a laser pressure into the cap of a special collection tube situated just top of the sections. The automated system from

Arcturus Molecular Devices belongs to this type. This technique was named laser microdissection and pressure catapulting (LMPC) from PALM instruments (Burgemeister, 2005; Niyaz et al., 2005). (3) The polymer film attached to slides also, but the interested cells were selected and dropped into a collection device. This type instrument was named Leica AS-LMD (Edwards, R.A. 2007). Each technique can harvest cell with several microns' precision, allowing procurement of single cell even portions of chromosomes. The harvested cells can be used for various downstream analyses such as isolating DNA, RNA, protein, and lipid samples for RT-PCR, microarray, Western blot, or 2D gel electrophoresis.

1.3.2 The application of LCM in developmental biology

LCM allows users to isolate interested cells or tissues from either frozen sections or formalin-fixed, paraffin-embedded tissue sections. Because of its capability of isolating interested cells from heterogeneity contexts, it has been widely applied on various disease conditions to compare the pathology of diseased tissue cells with normal cells, for example, it is especially well applied in comparing cancer cells with more malignant, less malignant, and normal cells. It also has been smattered in various stages of biological development process of many organs of all kinds of species, such as heart (Kuhn et al., 2007), lung, kidney (Stemmer et al., 2006; Woroniecki and Bottinger, 2009), pancreas (Marselli et al., 2009), brain, et ctr.

One of the key points for successful application of LCM is to pick up the interested cell populations accurately. Various staining methods used on tissue sections can help distinguish different cellular components under the light of microscope. The most often used dyes are hematoxylin, eosin, methylene blue, Wright-Giemsa and toluidine blue, thionin, according to different cell types and the users' preference. The dyes used may have an extra advantage of

molecular integrity by absorbing laser energy to prevent heat deposition. In some cases when interested cells are very meager, or it is more difficult to distinguish, immunohistochemical staining could be used for the selection of morphologically similar yet immunophenotypically different cells (Fend et al., 1999; Kuhn et al., 2007).

If downstream applications such as microarray analysis require RNA with high quality and quantity, certain strategies will be needed during processing of original tissue samples since the performance of LCM need more time which may practically affect the RNA quality. To protect RNA integrity, RNA-Later can be used on tissue samples before section. Some researchers tried to recover RNA from archived tissue samples and get ideal RNA results. The disadvantage of RNA-Later is that tissue immerged in RNAlater is soft and difficult to section, and tissue morphology can be damaged during section process. Other strategies used to protect RNA integrity include using snap-frozen tissues, preparing fresh and RNase free reagents and staining sections quickly (Stemmer et al., 2006).

Only limited quantities of LCM dissected samples can be acquired within certain period of time, the RNA isolated from it cannot meet the requirement of microarray analysis. To solve this problem, the RNA amplification method has been developed in addition to the in vitro transcription method (Ginsberg, 2005; Portillo et al., 2009). Researchers use RNA amplification method in combination with in vitro transcription for microarray process successfully getting RNA with good quality and high quantity. As such, the gene expression profiling from LCM samples are more specific compared with those using whole mount tissue samples.

1.4 RNA interference (RNAi) technology

1.4.1 What is RNAi?

RNA interference (RNAi) is a natural process existed in many organisms ranging from plants to mammals that introduction of RNA into cells interfere with the function of an endogenous gene in a sequence context (Jorgensen, 1990; Romano and Macino, 1992). Fire and his colleagues discovered the phenomenon of gene-silencing in 1998 by specifically targeting a functional gene (*unc22*) using an exogenous dsRNA to effectively produce a reduced gene activity of the silenced gene (Fire et al., 1998). Similar phenomena were found when other genes were targeted. The RNAi was first successfully demonstrated in several mammalian cells in 2001 and raised its potential application in biomedical research and therapy (Elbashir et al., 2001).

How RNAi works to regulate gene expression and function? The mechanisms of RNAi pathway were similar in Drosophila and mammals (Hamilton and Baulcombe, 1999; Hammond et al., 2000; Tuschl et al., 1999; Zamore et al., 2000). In this process, small double-stranded RNAs (dsRNAs) including small interfering RNA (siRNA) or short hairpin RNA (shRNA) are homologous in sequence to the silenced gene. They are either cleaved into small interfering RNA duplex by the RNaseIII-type enzyme called Dicer, or chemically or enzymatically synthesized, or synthesized by DNA-based systems. Consequently, siRNAs are incorporated into the RNA-induced silencing complex (RISC), which mediates the binding and cleavage of the target mRNA. This process is sequence-specific, homology-dependent, and triggering gene abolition through degradation or by inducing translational inhibition. Since its discovery in the late 1990s by Fire and Mello, RNAi has been progressed to become a powerful biological tool for its high specificity and selectivity and has been used for the investigation of gene function, as well as in target validation, translational repression, transcriptional inhibition, and DNA degradation.

1.4.2 Applications of RNAi

RNAi become a useful research tool for reverse genetic studies, which establish the gene function by targeted disruption. RNAi-mediated silencing is usually incomplete, a “knockdown” but not a “knockout”. To maximize silencing effects, several siRNA sequences (usually 3-6) are used for each targeted gene. Transfection of siRNAs into rapidly dividing cells has a maximal silencing effect 2-3 days after transfection, and the silencing effect could last for a week. However, in nondividing cells, such as macrophages or neurons, this siRNA-mediated silencing effect can last for several weeks. To prolong silencing effects, viral expression systems have been employed to express shRNAs, which is a siRNA precursor synthesized by DNA-based vector and processed intracellularly into siRNAs.

The sequencing of human genome has provided most of the genes expressed in humans as well as some other organisms. This provided a huge amount of information for RNAi to silence any gene in the genomes of human or any other organisms. In C elegans as well as in Drosophila, gene silencing can be induced by expressing long dsRNAs, and RNAi-mediated genome-wide screening have been used to characterize the biological function of predicted genes in a high-throughput manner. In mammalian genome, however, long dsRNAs can trigger an interferon response, so short designed dsRNAs have been used for genome-wide RNAi screens in mammalian cells. shRNAs can be used to generate transgenic animals with stably silenced gene expression. One of the advantages of these knockdown animals is less time involved (only a few months) because it only requires inserting a single transgene. Another advantage is that it can be used to animals or organisms that are not appropriate for gene knockout approaches.

1.5 Introduction of glycosaminoglycans (GAGs)

1.5.1 Glycosaminoglycans (GAGs) and Proteoglycans (PGs)

Glycans are complex carbohydrate conjugates that mediate various cell-cell and cell-matrix interactions. The most abundant linear unbranched glycans in the body are Glycosaminoglycans (GAGs). GAGs are long, negatively charged heteropolysaccharides that have molecular weight of roughly 10 to 100 kDa, containing a repeating disaccharide unit (Gandhi and Mancera, 2008; Jackson et al., 1991). They present on the cell surfaces or in the extracellular matrix (ECM) and can be classified as sulphated and non-sulphated. Sulphated GAGs include heparin, heparan sulphate (HS), chondroitin sulphate (CS), dermatan sulphate (DS), and keratin sulphate (KS), while hyaluronic acid (HA) is non-sulphated.

GAGs vary according to disaccharide unit contents, sulphation positions, as well as geometry of the glycosidic linkage. HS and CS are two main types of GAGs comprising repeating hexosamine-uronic acid disaccharides that are sulphated at various positions (Zhang, 2010a). Heparin and HS are called glucosaminoglycans for they contain glucosamine, and Heparin is most highly sulphated. CS and DS contain galactosamine and are called galactosaminoglycans. DS is one type of CS containing IdoA residues.

GAGs can be sulphated at different positions of the amino sugar or the sugar backbone to form hundreds of thousands of different molecules. The geometry of the glycosidic linkage also increases GAGs' variation and heterogeneity.

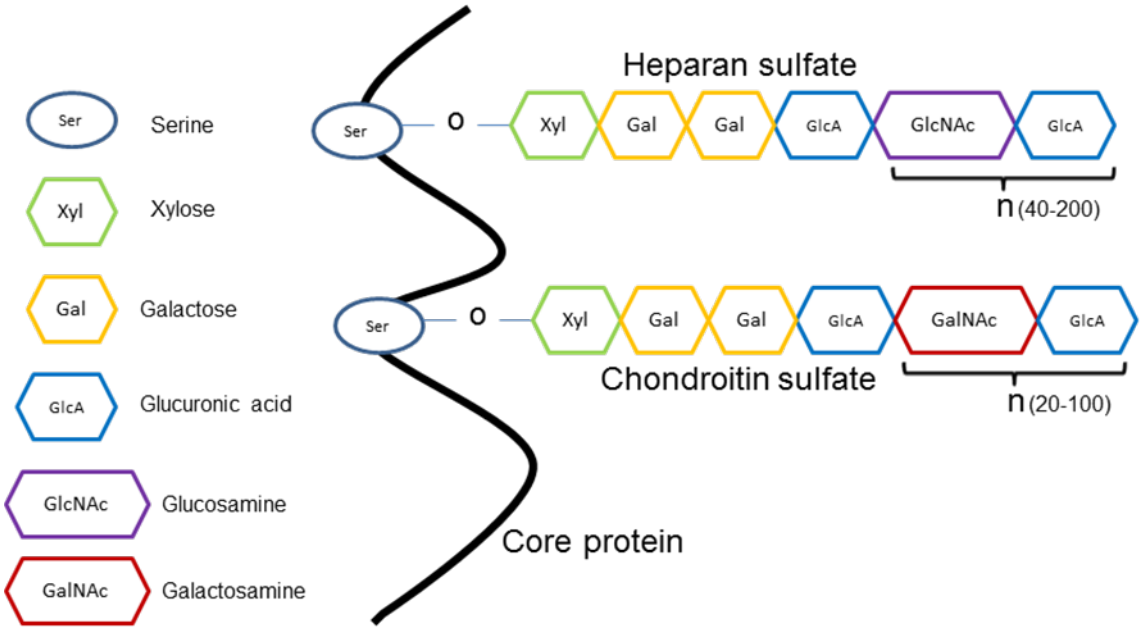

Fig. 1.1 Diagrammatic representation of GAGs linked to a proteoglycan core protein. Both heparan sulfate and chondroitin sulfate are linked to specific serine residues of proteoglycan by the linkage tetrasaccharide Xyl (green)-Gal (yellow)-Gal (yellow)-GlcA (blue). Alternating addition of GlcNAc and GlcA results in heparan sulfate, while alternating addition of GalNAc and GlcA leads to chondroitin sulfate.

GAGs can form proteoglycans (PGs) by linking to core proteins through a specific tetrasaccharide which are composed of one glucuronic acid (GlcA), two galactose residues (Gal), and a xylose residue (Xyl) (GAG-GlcA-Gal-Gal-Xyl-O-CH2-protein) (**Fig. 1.1**) (Zhang, 2010a). The tetrasaccharide linker is linked to a Serine residue (S) in the protein core through an O-glycosidic bond. Some forms of KS are attached to Asn in the protein core through an N-asparaginyl bond. The protein cores of proteoglycans have many S and Tryptophan (T) residues which allow various GAG attachments. Core proteins act as GAG carriers in PGs, besides, they usually determine the type (HSPGs or CSPGs), the number of GAG chains, and the ultimate destination (apical, luminal, intra- or extracellular) of the finished PGs (Zhang, 2010a). For example, glypicans as HSPGs carry more than 80% HS and much less CS, while the two CSPGs, biglycan and aggrecan, carry much more of CS and very low percentages of HS (Chen and

Lander, 2001). To explain these phenomena, a site-preference to multiple acidic residues, hydrophobic residues and Ser-Gly units for HS synthesis has been noticed.

PGs can be produced by almost all mammalian cells and exist in the extracellular matrix, plasma membrane, and some of them play functions in biological process (Zhang, 2010a). There are more than 23 types of PGs found in the nervous system (Hartmann and Maurer, 2001).

1.5.2 Biosynthesis of GAGs

GAGs are synthesized in the Golgi apparatus. The common so-called GAG-protein tetrasaccharide linker, GlcA β1,3-Gal β1,3-Gal β1,4-Xyl-β1-O-(Ser), is first synthesized by addition of a Xyl (xylose) to specific Ser residue on the proteoglycan core protein by two xylosyl-transferases, then two Gal (galactose) residues are added to the Xyl residue by galactosyltransferase I and II, followed by the addition of GlcA (glucuronic acid) by glucuronosyltransferase I (Zhang, 2010a).

After completion of the tetrasaccharide linkage region, GAGs synthesis on this linkage is triggered by the addition of the first HexNAc (N-acetyl-hexosamine, GalNAc or GlcNAc) residue. Addition of GalNAc to the nonreducing terminal GlcA by the key enzyme N-acetylgalactosaminyl transferase I commits the CS synthesis, followed by subsequent alternating addition of GlcA and GalNAc by chondroitin synthase (Silbert and Sugumaran, 2002). In contrast, HS synthesis occurs if GlcNAc is added to the linkage region by N-acetylglucosaminyltransferase followed by alternating addition of GlcA and GlcNAc residues by HS copolymerases (EXT-1 and EXT-2) from their corresponding UDP-sugars (Sugahara and Kitagawa, 2002). Chain modification of CS and HS are carried out by a series of enzymes which make the CS and HS the most abundant molecules in nature.

The enzymes for synthesizing the linkage region, GAGs (HS or CS) extension, as well as their modifications are very important for distribution and functions of GAGs. For example, GalT I, GalT II and GlcAT I (Almeida et al., 1999; Okajima et al., 1999) have been found largely expressed in human tissues, consistant with the omnipresent distribution of GAGs. Cells deficient in GalT-I, GlcAT-I, or GalT-II fail to synthesize the GAGs, while transfection of each enzyme cDNA into the corresponding mutant cells restores GAG synthesis (Bai et al., 2001; Okajima et al., 1999; Wei et al., 1999).

1.5.3 Biological roles of GAGs

The key properties of GAGs are high viscosity, low compressibility and rigidity (Gandhi and Mancera, 2008). They are found in mucous secretions as mucopolysaccharides for their viscous lubricating properties. These molecules provide structural integrity to cells and passageways between cells because of their rigidity.

GAGs can bind and regulate multiple protein partners, such as chemokines, cytokines, growth factors, morphogens, enzymes and adhesion molecule, and contribute to many biological processes, thus play multiple roles in development, health and disease through different molecular mechanisms (Casu and Lindahl, 2001; Jackson et al., 1991; Zhang, 2010b). More than 200 GAG-binding proteins have been described in literature (Zhang, 2010a). Heparin/HS are found to interact with more than 20% of the plasma proteins that are present on the cell surfaces and in the extracellular matrix (Saito and Munakata, 2007). CS acts as a biological activator independent of HS (Margolis and Margolis, 1997; Saito and Munakata, 2004). It is found to participate in modulation of axon growth, wound healing, *NFkB* transcriptional activation of endothelial cells. Moreover, GAGs can be involved to signaling pathways including, but not

limited to, Wnt signaling (Munoz et al., 2006), Sonic hedgehog (*Shh*) (Rubin et al., 2002), *BMP* signaling pathways (Ruppert et al., 1996), fibroblast growth factor (*FGF*)/*FGFR* (McDowell et al., 2006), platelet derived growth factor (*PDGF*/*PDGFR*) (Rolny et al., 2002), which are well known for embryonic development, in particular, neurulation process.

1.5.4 Galactosyltransferase (GalT, GalTase)

Glycosyltransferases (Glyco-T) are a super-family of enzymes residing in the Golgi apparatus of a cell, catalyzing the synthesis of carbohydrate moieties of cellular glycoconjugates (glycoproteins, glycolipids, and proteoglycans) by transferring a monosaccaride moiety from an activated glycosyl donor to an glycosyl acceptor molecule, forming a glycosidic bond, resulting in a carbohydrate, glycoside, oligosaccharide, or a polysaccharide (Paulson and Colley, 1989; Roseman, 2001).

Galactosyltransferase (GalT) is a type of Glyco-T that catalyzes the transferring of galactose from uridine-diphosphate-α-D-galactose (UDP-gal) to an acceptor sugar molecule. The galactosyltransferase subfamilies include β1, 4-(β4Gal-T), β1, 3-(β3Gal-T), β1, 6-(β6Gal-T), α1, 3-(α3Gal-T), and α1, 4-(α4Gal-T). All of these enzymes use UDP-α-D-Gal as the sugar donor but generate β-1,4-, β1,3-, β1,6-, α1,3-, and α1,4-linkages, respectively. Each of the above mentioned subfamily has additional members. For example, at least seven members have been found in the β4Gal-T subfamily, β4Gal-T1 to β4Gal-T7 (Amado et al., 1999). Although the β4Gal-Ts have 25% to 55% sequence homology and similar enzymatic functions, they are distinctive in structure, location, expression and tissue specific differences, and any alteration in the activity of subfamily members have been associated with various diseases. Among these GalTs, the β-1,4-galactosyltransferase (β4Gal-T) is the first mammalian Glyco-T that was cloned

in 1986, followed by the cloning and identifying of more Glyco-T and galactosyltransferase subfamily members and acceptor substrate specificities (Shaper et al., 1986). It is the initiation enzyme of biosynthesis of PGs and one of the biosynthesis enzyme of many kinds of GAGs. In addition, it also has functions in cell growth and cell adhesion, which are the most important functions for formation and closure of the neural tube. But the expression and function of B4galt1 in mouse embryo during neurulation has not been well studied.

1.5.5 Structure, expression and functions of B4galt1

β-1,4-galactosyltransferase1 (β4Gal-T1) is one of the first mammalian glycosyltransferases to be purified, cloned, sequenced, and its crystal structure has been established. β4Gal-T1 has 6 exons and encodes a type II integral membrane protein, synthesized mainly in the cytoplasm and localized in the Golgi apparatus as well as at the cell surface (Qasba et al., 2008). Like other β4Gal-Ts, it has an amino-terminal cytoplasmic tail, a transmembrane (TM) anchor domain, and an extended stem structure and large carboxyl-terminal catalytic domain (**Fig. 1.2.A**).

The β4Gal-T1 mRNA encodes for two isoforms differing at the cytoplasmic region (**Fig. 1.2.B and Fig. 1.2.C**). The longer form has 24 amino acids at the amino-termini, placing two Met residues in the cytoplasmic domain, while the short form has only 11 amino acids at the cytoplasmic region. Several studies supported that both long and short isoforms are found in the Golgi, but only a small percentage of long isoform is localized on the plasmic membrane and can function as a cell surface receptor (Hathaway et al., 2003; Lopez et al., 1991; Russo et al., 1990; Shaper et al., 1988). The transmembrane region is hydrophobic and plays an important role in the stability of the protein. The length of the TM region is consistent with the thickness of the lipid

layer and may play a role in their sorting and targeting mechanism (Masibay et al., 1993). The stem region has 45 to 145 residues in bovine β4Gal-T1. It can enhance the in vitro folding efficiency and flexible orientation of the catalytic domain in both bovine and human species (Boeggeman et al., 2003). The long catalytic domain of β4Gal-T1 facing the Golgi lumen has a GT-A fold, a globular protein with two dissimilar N- and C-terminal domains. The N-terminal domain identifies the nucleotide donor, while the C-terminal domain binds the acceptor substrate. The active sites reside between the two domains. A metal-binding site is also positioned in the cleft of the enzyme. β4Gal-T1 is a constituent of the trans-Golgi apparatus. It is one of the GAG synthesizing initiation enzymes that is responsible for adding the first Gal residue to Xyl residue in the tetrasaccaride linker. In addition, it catalyzes the transferring of galactose in a β-1,4-linkage from uridine diphosphate galactose (UDP-Gal) to N-acetylglucosamine (GlcNAc) residues on glycoprotein or glycolipid substrates.

A

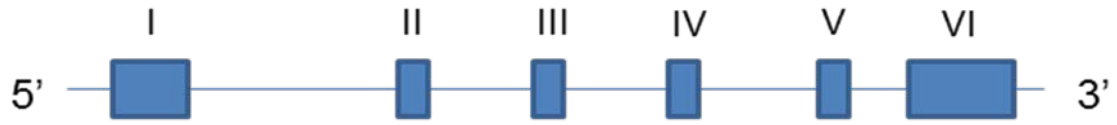

B Long form

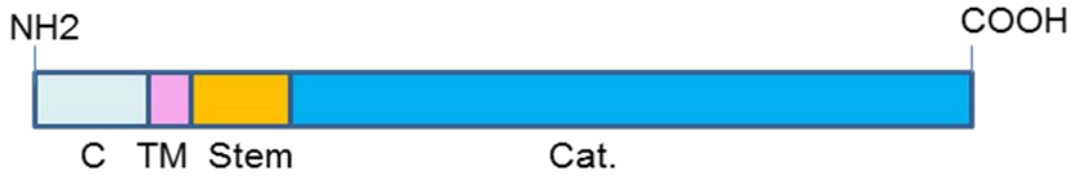

C Short form

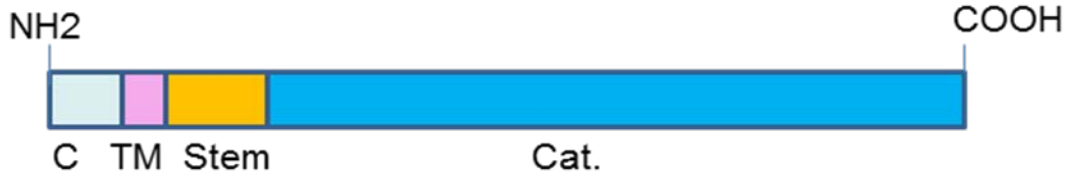

Fig. 1.2 Schematic representation of B4galt1 structure. (A) The genomic organization of mouse B4galt1 gene including six exons which encode two similar but not identical proteins. (B) and (C) show the two forms of proteins with a type II transmembrane topology. Both of them have identical transmembrane domain (TM, pink), short stem (yellow) and large carboxy-terminal catalytic domain (blue) but differ in the short amino-terminal cytoplasmic domain (C, light blue) with 13 amino acids difference. Figure was modified from *Rodeheffer C.R. and Shur B.D.(2002): Targeted mutations in β1,4-galactosyltransferase I reveal its multiple cellular functions. Biochimica et Biophysica Acta 1573:258-270.*

β4Gal-T1 is also detected on the plasma membrane of a wide variety of cell types, including early embryonic cells, spermatogenic cells, neuronal cells, epithelia, and mesenchymal cells, where it may function as cell surface receptors mediating multiple cell-cell and cell-matrix interactions (Roseman, 1970; Roth et al., 1971; Shur, 1993). Cell surface β4Gal-T1 mediates diverse biological functions by interacting with the multiple ligands, including:

(1) Laminin. GalT functions as the cell surface laminin receptor which recognizes specific oligosaccharide residues within laminin (Runyan et al., 1986).

(2) Focal adhesion kinase (FAK). Clustering of cell surface GalT in fibroblasts results in tyrosine phosphorylation of FAK and disorganization of actin stress fibers (Wassler and Shur, 2000).

(3) The presence of terminal GlcNAc glycosides on numerous glycoproteins in the extracellular environment and on cell surfaces(Rodeheffer and Shur, 2002).

(4) E-cadherin. On F9 embryonal cells, surface GalT I interacts with E-cadherin, a transmembrane receptor involved in cell-cell adhesion (Shur, 1983).

(5) EGF receptor. Surface GalT I has been shown to interact with the EGF receptor and affect its phosphorylation and activity, directly affect the cell proliferation rate (Hinton et al., 1995).

(6) Collagen IV. A study identifies GalTase as a calcium-dependent receptor for cell attachment to collagen type IV, a molecule commonly found associated with laminin within basement membranes. Enzyme perturbation or substrate pregalactosylation on cells possessing calcium-dependent mechanisms of adhesion can block the cell attachment to collagen IV (Eckstein and Shur, 1992).

1.5.6 B4galt1 in development

β4Gal-T1 localizes in the Golgi complex as galactose transferase and in a variety of body fluids as lactose synthetase. In addtition, it is also detected on the plasma membrane and cell surface function as receptors in cell-cell and cell-matrix interactions (Hathaway et al., 2003). Surface β4Gal-T1 can affect cell proliferation directly (Roth and White, 1972). Cell growth was inhibited by exogenous reagents to perturbe the GalTase function (Maillet and Shur, 1994), or by addition of UDP-galactose to transformed cells to increase surface galactosylation (Klohs et al.,

1982). Stably transfected cell lines with reduced surface GalTase grow faster than control cells, while those with overexpressed surface GalTase grow slower (Marchase et al., 1988). Moreover, the expression of GalTase was cell-cycle specific. GalT I-null animals exibit an increased rate of cell proliferation in some epithelial cell types (Asano et al., 1997).

The surface glycosyltransferase functions as an adhesion molecule by forming a stable adhesive bond with its glycoside substrate in the extracellular matrix or on an adjacent cell surface. In both Swiss 3T3 fibroblasts and F9 embryonal carcinoma cells, overexpression of the truncated long GalTase (TLGT) devoid of the catalytic domain affects the association of endogenous cell surface Gal Tase with the cytoskeleton, resulting in failure of intercellular adhesion (Evans et al., 1993). Further experiments identified binding sites on cytoskeleton for GalTase.

Both long form and short form of B4galt1 are found in Golgi, but only the long form can function as a surface receptor (Hathaway et al., 2003). As a type II transmembrane protein, the catalytic region of B4galt1 is exposed on the cell surface and can bind to terminal GlcNAc residues which are presented on various extracellular and cell surface glycoproteins and glycolipids. The cytoplasmic domain intracellularly would be predicted to interact with specific signaling networks if surface catalytic region acts as a signal-transducing receptor. On the other hand, sequences of the cytoplasmic domain of long form GalT I was expected to regulate the expression of long form at the cell surface.

Surface GalT I can be detected on various cell types, and if the cellular environment change, the expression levels and location change accordingly (Hathaway and Shur, 1992; Scully et al., 1987). GalT I might be able to interact with multiple extracellular ligands and have diverse biological functions. Its function is specific and regulated by the membrane microenvironment.

In addition to the terminal GlcNAc glycosides, GalT I can bind to laminin 1 in the extracellular matrix (ECM) to facilitate lamellipodia formation on migratory cells, or to facilitate the sperm-egg interaction by binding to the glycoprotein ZP3. GalT I can also function in cell-cell interaction by binding with other ligands such as E-cadherin, collagen IV, etc.

Though the relationship of GAGs and neurulation process is reported long ago, a few reports can be found for the direct relationship of B4galt1 with neurulation. The distribution of cell-surface glycosyltransferase activities implies the possibility that cell-surface glycosyltransferase are crucial to the embryonic morphogenesis. If so, perturbation of cell-surface glycosyltransferase activity may disturb the normal morphogenetic process. In an experiment using chick embryos, perturbation of cell-surface transferase activity during gastrulation stage would lead to morphogenetic defects such as NTD embryos manifested as abnormal embryos lacking of posterior components starting around the level of the hind limbs, or twist in the midtrunk level of the spinal column (Shur, 1977).

Cell surface B4galt1 (GalTase) seems to play a part in neural tube formation. An experiment using anti-GalTase Fab to specially recognize chick embryo GalTase and inhibite GalTase activity, induced neural tube defects in 61% of treated embryos, exibiting incomplete or improper neural tube closure with failure of neural fold elevation and lateral hinge formation (Hathaway and Shur, 1992). The possible mechanism for this might be that during the early neurulation time, there are a significant portion of the cell surface GalTase which mediate the contact of neural crest cells with the basal lamina that shapes the neural tube. Inhibiting of GalTase by anti-GalTase Fab perturbed the contaction by disturbing the binding of GalTase in the extracellular matrix or on adjacent cells. Since the critical significance of B4galt1 in

development, especially its association with neural tube closure, it is necessary to investigate the expression and function of B4galt1 in the neural tube formation.

1.6 Scope of Study

The genetic mechanism for the formation of neural tube along the neuroaxis is still not clear. Though more than 200 genes have been found related with closure of the neural tube, most of them were investigated by mutation of single or multiple genes, and the experiment conditions were varied. A comprehensive profile of the whole picture of the neurulation process was lacking. Microarray analyses have been used as a productive tool for capturing expression profilings of developmental process, such as preimplantation and gastrulation embryos, even on NTD embryos from treated diseased mice (Hamatani et al., 2004b; Hue et al., 2007; Jiang et al., 2008), and have made contributions to the knowledge of mouse embryo development, but no such work has been done on neurulation stage embryos.

The mechanism of neurulation is different at cranial and spinal region. Investigating gene expression profiling using roughly the whole embryo could not reflect the specific genetic mechanism of neurulation due to tissue heterogeneity. More accurate tissue acquirement method such as laser capture microdissection (LCM) is needed.

Currently, the role of glycosaminoglycan (GAG) genes in development has been recognized. A few studies also dipped into the expression and function of GAG genes in the nervous system development. But none of these studies have investigated the expression and role of GAG genes in the specific neurulation process.

The main objective of this study was to investigate the genetic mechanism of the spinal neurulation. The specific objectives of this study were to:

1) Generate specific transcriptomic profilings of neurulation in spinal region in mouse embryos by combined usage of Affymetrix GeneChips and LCM method, to set up a framework for future studies in this area.

2) Propose possible molecular interactions of different pathways and cascades involved in spinal neurulation according to the results of transcriptomic analysis.

3) Look into spatial and temporal expression of GAG genes in spinal region of mouse neurulation embryos. Investigate the knockdown effects of differentially expressed GAG genes on neuroepithelial cells by siRNA, and postulate the possible roles of GAG genes in the genetic mechanism of neurulation.

The results of the current study may have significance in providing the framework of gene expression on closing neural tube and the methodology of transcriptomic analysis in combination with LCM used firstly on neurulation studies. This framework can grant a comprehensive understanding of the mammalian spinal neurulation and aid in discovering the underlying genetic mechanism by functional studies of specific kinds of genes or cross-talks between different pathways. We can intensely explore the expression of GAG genes in the framework and study the roles of GAG genes in spinal neurulation.

It is understood that neurulation is a complex embryogenesis process. Morphological studies have found three modes marked transformation of neuroepithelium at three critical stages: E8.5, E9.0, and E9.5. MHP appears at E8.5, exists at E9.0, and disappears at E9.5, while DLHPs appear at E9.0 and exist through E9.5 till the end of the primary neurulation. Previous studies have found that disruption of MHP or DLHPs can lead to neural tube defects, and these defects may be due to alterations in biological functions such as proliferation, differentiation, adhesion, transcription, cell polarity etc by interrupting different molecule pathways. GAG genes have

been found involved in various cellular processes and interaction with multiple pathways during embryonic development. Expression of GAG genes along the neuraxis during spinal neurulation indicates a critical role in formation of the neural tube, but its potential role is not clear (Copp and Bernfield, 1988b; Yip et al., 2002). Any change in GAG associated genes may greatly influence the cellular functions and NT formation.

I selected two kinds of tissues at three critical timepoints according to morphological changes during neurulation and investigated. Although the transcriptomic profiling of one tissue at one timepoint can only reflect the spatial and temporal gene expression, the comparison analysis of gene expression between different timepoints may reflect the gene relationships during the whole process.

CHAPTER 2

MATERIALS AND METHODS

2 Materials and methods

2.1 Collection of mouse embryos and preparation of cryosections

Pregnant Swiss Albino mouse were euthanized by CO_2 asphyxiation at E8.5, E9.0, and E9.5. Timed matings were made at night, noon on the 8th day of finding a copulation plug is designated as embryonic day 8.5; morning on the 9th day is called E9.0; and noon on the 9th day is called E9.5. The uterus with mouse embryos inside were dissected out and put inside Petri dishes with DMEM containing 10% FBS. Mouse embryos were dissected out from the uterus. Their decidua, the amnion, as well as the Reichart's membrane were carefully dissected away. Intact embryos were staged based on the criteria of the Edinubrgh Mouse Atlas Project (http://www.emouseatlas.org/emap/home.html) and the work of Kaufman (1992), then were selected by global observation and the somite number was counted under the stereo dissection microscope. Preliminary experiment was done to decide on somite number of mouse embryos at different stages with the accordingly typical modes on sections according to Shum, A. S. et al (Shum and Copp, 1996). Embryos at stage of E8.5 with somite number of 9 to 12, E9.0 with somite number of 20 to 23, and E9.5 with somite number of 27 to 30 were choosen for embedding or fixed by 100% methanol and saved for further use (Copp et al., 1982).

To protect RNA quality and quantity, several methods were adopted: snap-frozen mouse embryos, RNA-later-ICE incubated cryosections, and optimized quick staining methods. Briefly, mouse embryos were embedded in cryomold with OCT™ (Tissue Tek™) and snap-frozen by liquid nitrogen immediately after microdissection and saved in -80°C till cryosection.

Cryosections were cut through posterior neuropore (PNP) region at 8-µm at container temperature (CT) -20°C, object temperature (OT) -15°C using a cryostat, attached to RNase free glass slides (treated by RNase Zap). Each section was immersed in prechilled RNA-later®-ICE

for 15 mins in a RNase-AWAY treated humid chamber (Sigma, Cat H6644) in -20°C before saved in -80°C for LCM microdissection.

Immediately before microdissection, the staining and dehydration solutions such as haematoxylin, ethanol and xylene were prepared freshly for use, and the slides were brought to equilibrium at room temperature (RT) for 5 mins after being taken out from -80 °C. It is necessary to fix the sections in 70% ethanol for 1 min before performing quick staining. Then wash out the OCT in distilled water, apply 100 µL of haematoxylin (Merck, Darmstadt, Germany) to cover all the sections on one slide for 10 secs, and wash away additional haematoxylin under running tap water for 10 secs. Transfer the slides to distilled water (II) for 10 secs, and then perform dehydration in serial ethanol of 75%, 95%, and 100% for 5 secs each. The sections were cleared by xylene twice, drying in the slide box for 5 mins and proceeded for LCM.

2.2 Laser capture microdissection

Before performing LCM on the dried sections, pipette 50 µL of RNA Extraction Buffer (XB) in 0.5 mL tube and prewarmed at 42°C before use for containing the LCM samples. The Arcturus microdissction program (version 2.0) was used for the Arcturus Pixcell™ laser capture microdissection system (Arcturus, Mountain View, CA). The microdissection parameters were set as laser power at 70 mW and duration at 2.0 ms. Neuroepithelium and the surrouding mesenchyme with similar size were dissected separately under direct visualization under the microscope (Arcturus Pixcell™). The microdissected tissues were attached to the CapSure™ Macro LCM Caps (Arcturus Engineering). The LCM samples were collected in Extraction Buffer (XB) by the aid of the CapSure Cap–microcentrifuge tube assembly. Then the LCM samples can be proceeded to extract RNA or saved at –80°C.

2.3 Isolation of RNA from Laser-Captured Tissue cells

Total RNA from microdissected cell populations was extracted using a PicoPure™ RNA Isolation Kit (Arcturus, KIT0204) according to the manufacturer's protocols. All the principal reagents were provided by the kit. DNase I (Qiagen, Cat 79254) treatment was applied to avoid genomic DNA contamination. Briefly, conditional buffer (CB) was added to wet the filter membrane of the purification column. 70% ethanol was mixed with the cell extract and added into the preconditioned purification column. The column was then centrifuged and the flow-through was throwed away. Wash buffer (W1) was added to wash the filter membrane, followed by DNase I incubation to remove the genomic DNA contamination. The purification column was then washed by W1 again and wash Buffer 2 (W2) twice, then centrifuged to remove any residual reagents. The cleaned purification column was transferred onto a microcentrifuge tube and RNA bound onto the membrane was washed down by elution buffer (EB). RNA was aliquoted and saved in -80°C for testing and future work.

2.4 RNA quality and quantity assessment

RNA quantity was assessed by NanoDrop spectrophotometer ND-1000 (NanoDrop technologies, Wilmington, DE, USA). RNA quality was tested by Agilent 2100 Bioanalyzer (Agilent Technologies, CA, USA) according to the manufacturer's instructions.

NanoDrop software provided analysis options for total RNA by measuring full-spectrum (220-750nm) UV-Vis absorbance. It was performed by just applying one micro liter of total RNA samples onto the testing table, selecting the option of RNA and clicking the testing button. The RNA quality was represented by ratio of 260/280 UV absorbance and quantity was presented as ng/µl.

To test RNA by Agilent 2100 Bioanalyser, the RNA 6000 Pico kit (Agilent Technologies, CA, USA) provided all the reagents needed and the 2100 expert software was used. All the procedures were performed according to the manufacturer's instructions.

Firstly, the Bioanalyser system was prepared by setting up the chip priming station, the Bioanalyser machine, and the vortex mixer. The electrodes were cleaned by the electrode cleaner before use. The second step was to prepare the gel. All reagents were equilibrated to room temperature for 30 mins before use. 550 µl of RNA 6000 Pico gel matrix (red labelled) was pipetted into the top container of a spin filter and the spin filter was spinned at 4000 rpm for 10 mins. The filtered gel was aliquoted into 65 µl per tube and store at 4°C before use. The next step was to prepare the gel-dye mix. RNA 6000 pico dye concentrate (blue cap) was vortexed for 10 secs and spined down. 1 µl of dye concentrate was added to a tube of 65 µl filtered gel and the gel and dye were mixed well by vortex thoroughly and centrifuge. The gel-dye mix should be protected from light and used within one day. The RNA samples were heat-denatured at 70 °C for 2 mins.

A new RNA pico chip was placed on the adjusted chip priming station, 9.0µl of the gel-dye mix was pipetted and dispensed into the bottom of the well marked "G" for 30 secs. Close the chip priming station when the plunger was positioned at 1 ml. The plunger of the syringe was pressed down to be held by the clip for 30 secs and was released when the plunger was moving back to the 0.3 ml mark, held for 5 secs, then was slowly pulled back to the 1ml position. 9.0 µl of the gel-dye mix, 9.0 µl of the RNA 6000 Pico conditioning solution (white cap), 5.0 µl of the RNA 6000 Pico marker (green cap), 1 µl of the diluted Pico ladder, and 1 µl of each sample were pipetted into specific wells according to the manuals. The prepared chip with samples was vortexd by the IKA vortex mixer at 2400 rpm for 60 secs.

Finally, the vortexed chip was inserted in the holder of the Bioanalyser. The "Eukaryotic Total RNA Pico Series II" was selected for the assay by the 2100 expert software. RNA Integrity Number (RIN) (Schroeder et al., 2006) was calculated by Agilent 2100 expert software. A RIN of 7-10 is indicative of high RNA quality and used for microarray work, whereas a RIN of 1 grade a completely degraded RNA sample (Fleige and Pfaffl, 2006).

2.5 Transcriptomic analysis using Affymetrix GeneChip™ Microarray

The 18 independent LCM RNA samples, triplicates for three stages (E8.5, E9.0, and E9.5) of two kinds of tissues (NT and MD), were prepared for hybridization on the microarray chips using the Two-Cycle target labelling and control reagents (Affymetrix, P/N 900494) in combination with the MEGAscript® high yield transcription kit (Ambion Inc, P/N 1334) for amplification and labelling. The labelled Bio-cRNA was fragmented and hybridized on the Affymetrix Mouse 430 2.0 Genechips. The Affymetrix GeneChip microarray system was used for probe array wash, stain, and scan. All procedures were performed according to the manufacturer's instructions (Affymetrix, Santa Clara, CA). The volumes were described for one reaction use, but all of the 18 samples were prepared at the same time to decrease discrepancy from different patches.

2.5.1 Preparation of T7-Oligo (dT) Primer/Poly-A RNA controls

The supplied Poly-A RNA controls act as positive controls to examine the whole target labelling process and the quality of the target RNA materials. Firstly, poly-A RNA serial dilutions for 15 ng of total RNA were prepared. 2 µl of the poly-A control stock and 38 µl of

poly-A control buffer were mixed for the first dilution. 2 µl of the first dilution and 98 µl of poly-A control dil buffer were mixed for the second dilution. 2 µl of the second dilution and 98 µl of poly-A control buffer were mixed for the third dilution. To prepare the fourth dilution, as 15 ng RNA is the intermediate starting amounts, calculating the ratio proportionally to the same final concentration of the spike-in controls in the sample was needed. For 15ng starting RNA, the ratio is 1:6.67, so 2 µl of the third dilution and 11.33 µl of poly-A control dil buffer were mixed for the fourth dilution. Finally, 2 µl of the fourth dilution of Poly-A RNA controls, 2 µl of 50 µM T7-Oligo (dT) Primer, and 16 µl RNase-free water were mixed together. This 20 T7-Oligo (dT) Primer/Poly-A RNA controls mix was used for one reaction for preparation of the First-Cycle, First-Strand cDNA.

2.5.2 Synthesis of the First-Cycle, First-Strand cDNA

15 ng total RNA, 2 µl of the T7-Oligo (dT) Primer/Poly-A RNA controls mix, RNase-free water were mixed to the volume of 5 µl and incubated at 70°C for 6 mins and cooled on ice. In a separate tube, for a single reaction, 2 µl of 5 x first strand reaction mix, 1µl of 0.1M DTT, 0.5 µl of RNase inhibitor, 0.5 µl of 10mM dNTP and 1 µl of SuperScript II were mixed for preparation of the First-Cycle, First-Strand Master mix.

The 5 µl of First-Cycle, First-Strand Master mix was combined with each total RNA sample/ T7-Oligo (dT) Primer/Poly-A RNA controls mix from the previous step to a final volume of 10 µl and incubated at 42°C for 1 hour. The sample was heated at 70°C for 10 mins to inactivate the RT enzyme.

2.5.3 Synthesis of the First-Cycle, Second-Strand cDNA

To prepare the first-cycle, second strand master mix, the following reagents were added for one reaction use: 4.8 µl of RNase-free water, 4.0 µl of freshly diluted 17.5 mM $MgCl_2$, 0.4 µl of 10mM dNTPs, 0.6µl of *E.coli* DNA polymerase I, 0.2 µl of RNase H to a final volume of 10 µl. 10 µl of the first-cycle, second strand master mix was pipetted to each sample of the First-Cycle, First-Strand cDNA Synthesis reaction to a total volume of 20 µl and incubated at 16°C for 2 hours and at 75°C for 10mins, then cool on ice.

2.5.4 IVT Amplification of cRNA after First-Cycle cDNA synthesis

30 µl of the first-cycle, IVT master mix were prepared for one reaction use by mixing of 5 µl of 10 x reaction buffer, 5 µl of ATP solution, 5 µl of CTP solution, 5 µl of UTP solution, 5 µl of GTP solution, 5 µl of enzyme. The above prepared 30 µl of the first-cycle, IVT master mix was added to each 20 µl of cDNA sample from the first round synthesis to a final volume of 50 µl and incubated at 37°C for 16 hours.

2.5.5 Cleanup of cRNA after First-Cycle Synthesis and IVT

The cRNA synthesized by the first cycle amplification and IVT was cleaned by vortexing in 50 µl of RNase-free water and then 350 µl of IVT cRNA binding buffer. The bound cRNA lysine was washed by 250 µl 100% ethanol, 500 µl of IVT cRNA wash buffer, and 500µl of 80% ethanol on the IVT cRNA cleanup spin column. The cleaned cRNA were diluted by 13 µl of RNase-free water. 1 µl of the cRNA was aliquot for assessing cRNA yield by Nanodrop. The remaining cRNA were used for the 2nd cycle amplification.

2.5.6 Synthesis of the Second-Cycle, First-Strand cDNA

Random primer was diluted in RNase-free water to a final concentration of 0.2 µg/µL. 2 µl of the diluted random primers was added to the purified cRNA from the last step, RNase-free water was added to a final volume of 11 µl and incubated at 70 °C for10 mins. The second-cycle, first-strand master mix was prepared by adding the following reagents for a single reaction: 4 µl of 5 x 1st strand reaction mix, 2 µl of 0.1 M DTT, 1 µl of RNase inhibitor, 1 µl of 10 mM dNTP and 1 µl of SuperSript II. The 9 µl of the second-cycle, first-strand master mix was ransferred to each cRNA/random primer sample to a final volumn of 20 µl and incubated at 42°C for 1 hour. 1 µl of RNase H was pipetted to each sample to a final volume of 21 µl and incubated at 37°C for 20 mins. The RNase H was deactivated by heating up the sample at 95°C for 5 mins.

2.5.7 Synthesis of the Second-Cycle, Second-Strand cDNA

4 µl of diluted T7-Oligo (dT) primer (5µM) was added to the sample from the second-cycle, first-strand cDNA synthesis step for a final volume of 25 µl and incubated at 70°C for 6 mins. The second-cycle, second-strand master mix was prepared by mixing the following reagents for one reaction use: 88 µl of RNase-free water, 30 µl of of 5 x 2nd strand reaction mix, 3 µl of 10mM dNTPs, 4 µl of *E.coli* DNA polymerase I to a final volume of 125 µl. The mixture was incubated at 16°C for 2 hours. 2 µl of T4 DNA polymerase was added into the incubated mixture and incubated for another 10 mins at 16°C.

2.5.8 Double-Stranded cDNA Cleanup

600 µl of cDNA binding buffer were added to the synthesized double-stranded cDNA by brief vortexing. The mixture was centrifuged in the cDNA cleanup spin column sitting in a 2 mL

collection tube. The binded cDNA was washed by 750µl of the cDNA wash buffer by centrifugation. The cleaned cDNA was diluted with 14 µl of cDNA elution buffer and around 12 µl would be eluted for the next step.

2.5.9 Biotin-Labeled cRNA synthesis

The IVT reaction mix was prepared by adding the following reaction components in a RNase-free microfuge tube: 8 µl of RNase-free water, 4 µl of 10 x IVT labelling buffer, 12 µl of IVT labelling NTP mix, 4 µl of IVT labelling enzyme mix to generate Biotin-labled cRNA. The mixture was transferred into the cDNA template and incubated at 37 °C for 16 hours.

2.5.10 Biotin-Labeled cRNA Cleanup and Quantification

The 40 µl of Biotin-labled cRNA was diluted by brief vortexing in 60 µl of RNase-free water. 350 µl of IVT cRNA binding buffer was added to the mixture and vortex for 3 secs. The cRNA was mixed with 250 µl of 100% ethanol and the total of 700 µl mixture was added to the IVT cRNA cleanup spin column sitting in a 2 mL collection tube for binding by centrifugation at 13000 rpm for 15 secs. The binded cRNA was washed by 500 µl of IVT cRNA wash buffer and 500 µl 80% ethanol and diluted into 21 µl of RNase-free water. Measure the cRNA quality and quantity by Nanodrop. The remaining cleaned Biotin-labled cRNA was ready for fragmentation.

2.5.11 Fragmentation of cRNA

The sample fragmentation reaction mix was prepared by adding 20 µg (1 to 21 µl) of cRNA, 8 µl of 5 x fragmentation buffer, and RNase-free water to a final volume of 40 µl and

incubated at 94℃ for 35 mins and cool on ice. 1 µl of the fragmented cRNA was aliquoted for analysis on the Bioanalyzer. The remaining fragmented cRNA was saved at -20℃ for hybridization.

2.6 Target Hybridization, washing, staining, and scanning of genechips

Related reagents were prepared for hybridization, washing, staining, and scanning use.

1. 12 x MES stock buffer 100 mL was prepared by adding the following into a bottle: 6.461 g of MES hydrate, 19.33 g of MES sodium salt, 800 mL of molecular biology grate water, mix and adjust volume to 100 mL by DEPC-water, the pH value was adjusted at between 6.5 and 6.7, then filter through a 0.2 µm filter. The buffer was stored at 2℃ to 8℃, and shield from light by aluminized paper.

2. 2 x hybridization buffer 50 mL was prepared by adding the following into a bottle: 8.3 mL of 12 x MES stock buffer, 17.7 mL of 5 M NaCl, 4.0 mL of 0.5 M EDTA, 0.1 mL of 10% Tween-20, and 19.9 mL water, store at 2℃ to 8℃, and shield from light by aluminized paper.

3. Non-stringent wash buffer A of 1000 mL was prepared by adding the following into a bottle: 300 mL of 20 x SSPE, 1.0 mL of 10% Tween-20, 699 mL water, filter through a 0.2 µm filter.

4. The stringent wash buffer B of 1000 mL was prepared by adding the following into a bottle: 83.3 mL of 12 x MES stock buffer, 5.2 mL of 5 M NaCl, 1.0 mL of 10% Tween-20, and 910.5 mL water, store at 2℃ to 8℃, and shield from light by aluminized paper.

5. 2 x stain buffer of 50 mL was prepared by adding the following into a bottle: 8.34 mL of 12 x MES stock buffer, 18.5 mL of 5M NaCl, 0.5 mL of 10% Tween-20, and 22.66 mL water, filter through a 0.2 µm filter, store at 2°C to 8°C, and shield from light by aluminized paper.

2.6.1 Target Hybridization

Firstly, probe array was equilibrated to room temperature for 30 mins before use. Hybridization cocktail was prepared by adding the following reagents as for one standard array use: 15 µg of fragmented cRNA, 5 µl of 3 nM control oligonucleotide B2, 15 µl of 20 x Eukaryotic hybridization controls (bioB, bioC, bioD, cre), 3 µl of 10 mg/mL herring sperm DNA, 3 µl of 50 mg/mL BSA, 150 µl of 2 x hybridization buffer, 30 µl of DMSO, and water to final volume of 300 µl. The hybridization cocktail was heated in a heat block at 99 °C for 5 mins, then to a 45 °C heat block for 5 mins. In the intervening time, the chips were wetted by putting two microtips in the septa at the back of the chip, one for allowing venting of air from the hybridization chamber, and another for wetting the array by filling in 80 µl 1 x hybridization buffer through the septa. The probe arrays filled with 1 x hybridization buffer were incubated at 45 °C for 10 mins with rotation at 60 rpm. The hybridization cocktail was centrifuged from step 3 at 13000 rpm for 5 mins to remove any insoluble material. The buffer solution was taken out from the probe array cartridge and 200 µl of the clarified hybridization cocktail was loaded into each array. The probe array was incubated with hybridization cocktail in the Hybridization oven 640 (Affymetrix, Santa Clara, CA, USA. P/N 800139) at 45 °C for 16 hours with rotate at 60 rpm.

2.6.2 Wash and Stain of Probe Array after Hybridization

At the latter part of the 16-hour hybridization, the fluidics station and reagents required for probe array wash and stain were prepared ready for use. In this experiment, fluidics station 450/250 and program of GeneChip® Operating Software (GCOS) were used for probe array wash, stain, and scan.

Briefly, the fluidics station was primed before washing. The SAPE solution mix was prepared by adding the following reagents in a tube: 600 µl of 2 x stain buffer, 48 µl of 50 mg/ml BSA, 12 µl of 1 mg/ml streptavidin phycoerythrin (SAPE), 540 µl of DI H_2O to a final volume of 1200 µl. Mix well and aliquote 600 µl to an extro microtube. The antibody solution mix was prepared by adding the following reagents in a tube: 300 µl of 2 x stain buffer, 24 µl of 50 mg/ml BSA, 6 µl of 10 mg/ml goat IgG stock, 3.6 µl of 0.5 mg/ml biotinylated antibody, 266.4 µl of DI H_2O to a final volume of 600µl. The correct experiment name and appropriate antibody amplification protocol was selected and run in the fluidics station dialog box. The probe array was inserted into the selected module of the fluidics station. The cartridge lever was set in the down position. The three experiment sample vials were placed into the sample holders 1, 2, 3 on the fluidics station in the order of vial 1-SAPE 1- sample holder 1, vial 2-antibody- sample holder 2, vial 3-SAPE 2- sample holder 3, the needle lever was pressed down to snap the needles into respective vials and to start the run. At the end of the run, the three experiment sample vials was removed and replaced with empty vials. The cartridge lever was pressed down to the eject position and remove the probe arrays from the fluidics station modules. The stained probe array was proceeded to scan on the GeneChip® Scanner 3000. The cartridge lever was pulled up to engage washblock and proceed to probe array scan.

2.6.3 Probe Array scan

The probe array was scanned using the Affymetrix GeneArray® scanner 3000 after the wash protocols were completed. The glass surface of the probe array was cleaned and both of the two septa on the back of the probe array cartridge were sealed with Tough-Spots prior to scanning to prevent leaking of fluids. The probe array cartridge was inserted into the scanner and the autofocus was tested to make sure that the Tough-Spots did not interfere with the focus. The experiment name of the probe array to be scanned was selected, the corresponding array was loaded into the scanner, and the scanning process was started by clicking the Start button. The images were quantified using Affymetrix GeneChip Operating Software (GCOS) and saved as an image file (.dat). The .cel image file was automatically generated from the .dat file, and a .chp file was created from a .cel image file. An expression analysis report file (.rpt) was generated for reviewing the quality control parameters.

2.7 Gene expression data analysis

2.7.1 Quality assessment of a .dat/.cel image data

Quality assessment of the image data was performed by the GCOS software. The average signal intensity of the array was set to a default target signal of 500. The expression signal of a probe set above 500 is designated as present and below 500 is designated as absent. The boundaries of the probe area were defined by hybridization of B2 oligo which serves as a positive hybridization control and was used by the software to place a grid over the image. The grid should align well before assessing the image. The pixel-to-pixel variation of probe cells on a GeneChip array was measured by the average background and Noise (Raw Q). Poly-A controls

of dap, lys, phe, and thr were present in all the samples with increasing values which indicate proper of the entire target labeling process. The hybridization controls of bioB, bioC, bioD, and cre were used to evaluate sample hybridization efficiency, assess RNA sample quality and adjust signal values among replicates. β-actin and GAPDH were used to assess RNA samples and assay quality. The ratio of 3'/5' probe set was assessed for amplification efficiency. The percent present of probe set of all samples and differences among triplicates were assessed.

2.7.2 Statistical algorithms for expression analysis of GeneChip probe arrays

The .cel file of each array was analyzed by GCOS. The detection algorithm in GCOS uses probe pair intensities to generate a Detection p-value. It measures the target-specific intensity difference of the probe pair (perfect intensity (PP)-mismatch intensity (MM)) compared to its overall hybridization intensity (PM +MM) and assign a Detection call of Present (P), Marginal (M) or Absent (A). The p-value is reversely related with the Present of a given transcript. The smaller the p-value and the more likely the given transcript is truly present in the sample. Signal for each probe set was calculated using the One-Step Tukey's Biweight Estimate to signify the relative level of transcript expression. The real signal was estimated by taking the log of Perfect Match intensity after subtracting the Mismatch intensity.

In a comparison analysis, a Change p-value and Signal log Ratio was generated using the Wilcoxon's Signal Rank test to quantify changes in gene expression. Change p-values close to 0.0, 1.0 or 0.5 indicate increase, decrease or no change in transcript expression in the experiment array compared to the baseline. The Signal Log Ratio helps to cancel out differences in individual probe intensities due to different probe binding coefficients. The log scale used is base 2, thus, a Signal Log Ratio of 1.0, -1.0, and 0 indicates an increase or decrease of the transcript

expression by 2 fold or no change. Selecting transcripts with a fold change of > 2 for increase or < -2 for decrease can help to get consistent verification biological results.

2.7.3 Comparison analysis by GeneChip Operating Software (GCOS)

Affymetrix provides software tools for data storage and analysis. GCOS was one of the integrated software packages for generating profiles of gene expression and comparison. Data were transferred into GCOS program and stored in local workstation. GCOS manager was used to create publish databases, in addition, to import and export data for analysis. Single array analysis was performed by analyzing the image data and generated the analysis results file (.chp) and the expression analysis report file (.rpt). The quality control parameters in the .chp files were reviewed for control gene presentations, percent present scaling, housekeeping control gene signal output and 3'/5' ratios, average background and noise (Raw Q).

Normalization was not necessary when performing signal array analysis but was required when comparison was performed between different arrays. Stage of E8.5 was set as baseline when compared with E9.0 or E9.5, and E9.0 was set as baseline when compared with E9.5. Data were compared with the statistical algorithm of change and change P-value. Probe sets of changed p-value of less than 0.05 and had 66% or more change on experiment versus baseline arrays were queried out and displayed as pivot table. The pivot table was used to display analysis output and descriptions for transcripts represented on the probe array. Data was sorted by Signal Log Ratio (fold change).

2.7.4 DNA-Chip Analyser (dChip)

dChip gene information file MOE 430 2.0, Gene Ontology file which include function, ontology and process.ontology, were downloaded from website (www.dchip.org). Affymetrix

array data files (in CEL or DAT format), and the CDF files were provided by GCOS. Affy CEl file converting tool which converted the version 4 CEL file to the text-format version 3 CEL file so that dChip can read.

Normalization was done to adjust the brightness of the arrays to comparable level by normalizing arrays at PM and MM probe level before computing model-based expression levels. Next, an array with median overall intensity was chosen by default as the baseline array, and other arrays were normalized at probe intensity against it. The model-based expression method was performed to have a globel view of mismatch probe (PM/MM difference) and confirm the expression changes reported by sample comparison or clustering. Model-based expression indexes (MBEI) indicated the signals that were not specific and may not biologically meaningful. The outlier detection method was used to identify single, array, and probe outliers. The base of log transformation was set to 2 for convenient interpretation. Filter genes criteria were set as: (1) the ratio of the standard deviation and the mean, also known as Coefficient of Variation (CV), was less than 10. (2) P call% in the array was more than 20%. (3) transcripts whose expression values were larger than a threshold presented in more than 50% samples. The filtered transcripts that met the above criteria were used for comparison analysis and hierarchical clustering.

When comparing samples, earlier stage samples were selected as baseline (B) and later stage samples were selected as experiment (E). For example, E8.5 was “B” and E9.0 was “E” when compare E8.5 with E9.0, while E9.0 was “B” and E9.5 was “E” when compare E9.0 with E9.5. The filtering criteria for comparing samples were: (1) fold change between E and B were more than 1 or less than 1 (E - B > 1 or E - B < 1). Confidence interval of fold change is within 95%. (2) threshold for absolute fold change difference (E/B or B/E) more than 1 or less than 1, and absolute mean difference (E - B or B - E) more than 1 or less than 1 (log fold change). (3)

The default p-value threshold was less than 0.05. (4) Percentage of genes called “Present” was more than 0 in B while more than “66%” in E, and vice versa. (5) p-value less than 0.05 for the paired t-test. (6) False discovery rate (FDR) was assessed for 100 times. Genes that passed these filter criteria were exported in an output compare result file for further analysis.

2.7.5 GeneSpring GX 9

Preliminary analysis of the scanned chips was performed using Affymetrix GeneChip® Operating Software as described above. The CEL. Files (raw Affymetrix data) to show normalized signal intensity values generated with the Affymetrix GCOS software were imported into GeneSpring GX 9 (Agilent Technologies Inc., Santa Clara, CA, USA) for further data analysis. Quality control on samples was performed by assessing internal hybridization control (BioB, BioC, BioD and Cre) plots, the 3’/5’ ratio of GAPDH, sample correlation matrix, and Principle Components Analysis (PCA). PCA is a valuable visualization tool to compare the expression profile of samples. Samples representing the same experimental condition should be more similar and group closer in a PCA plot. Additionally, the probe sets were processed with the robust multi-array average algorithm (RMA, GeneSpring) to adjust background, normalize genes to the median, and perform log-transformation for the perfect matched values. The normalized data were then subjected to identify differentially expressed genes by five algorithms: RMA, GC-RMA, GS-GCOS, GS-dChip, PLIER. Probe sets were filtered to remove the low-intensity unreliable expression measurements. Present (P) call was at least 50% present in all arrays of the selected group. Probe sets lists past the filter criteria were further analyzed by One-Way ANOVA. Only genes with fold change more than 2 between at least two groups and $P <$

0.05 were defined as significant differentially expressed genes. These genes were used for further analysis.

2.8 Acquirement of MHP- and DLHP- related genes by intersection

The probe set lists of differentially expressed genes compared between different biological stages with fold change more than 2 analyzed by the software GCOS, dChip, and GeneSpring (5 algorithms: RMA, GC-RMA, GS-GCOS, GS-dChip, PLIER) were exported in excel files: E85vsE90, E85vsE95, E90vsE95, E85+E90vsE95, and E85vsE90+E95. The principle of this comparison is to take the data of early-stage chips as Basement group (B), while the data on late-stage chips were taken as Experiment group (E). A gene with fold change (FC) higher than 2 means expression (Absolute intensity, AI) of this gene at the experiment group is 2-fold higher than its expression (AI) at the basement group. Overlapping genes generated with the 3 software in each group were combined by intersection of 7 data sets. This combination intended to reduce the number of targeted genes. Overlapping genes among the three gene groups of E85vsE95, E90vsE95, and E85+E90vsE95 were combined by intersection and taken as MHP- related genes. These genes were differentially expressed at E8.5 and E9.0 (when MHP presents) and genes at E9.5 (when MHP disappeared). A gene with FC more than 2 in the MHP-related gene lists means its expression (AI) at E9.5 is 2-fold higher than its expression (AI) at E8.5 and/or E9.0, and is defined as MHP-up-regulated genes. Similarly, a MHP-down-regulated gene is the expression (AI) of this gene at E9.5 is 2-fold lower than its expression (AI) at E8.5 and/or E9.0. Logically, overlapping genes among the three gene groups of E85vsE95, E85vsE90, and E85vsE90+E95 were combined by intersection as DLHP- related genes. These genes were differentially expressed at E8.5 (when DLHPs do not exist) and genes at E9.0 and E9.5 (when DLHPs develop and retain). A DLHP-up-regulated gene is defined as a gene with FC more than

2 in the DLHP-related gene lists, which means its expression (AI) at E9.5 is 2-fold higher than its expression (AI) at E8.5 and/or E9.0. In the same way, a DLHP-down-regulated gene is defined as a gene with FC less than 2 in the DLHP-related gene lists. The expression (AI) of this gene at E9.5 is 2-fold lower than its expression (AI) at E8.5 and/or E9.0.

2.9 Verification of microarray results by One-step Quantitative Real time polymerase chain reaction (qRT-PCR)

Differentially expressed genes analyzed by microarray analysis were randomly selected from the MHP- and DLHP- related gene lists. Expression pattern of these genes were verified by LightCycler® 2.0 System (Roche Applied Science, ID, USA) and compared with microarray to validate the microarray quality.

Primers for these chosen genes were designed by a free online primer design tool Primer 3.0 software (http://www.genome.wi.mit.edu) (Rozen and Skaletsky, 2000) according to primer design principles (Kampke et al., 2001) (**Table 2.1**). Then the designed primers were checked by the **B**asic **L**ocal **A**lignment **S**earch **T**ool (BLAST) (http://www.ncbi.nlm.nih.gov/blast) to make sure their specificity (Altschul et al., 1990). Then the primers were synthesized by First-base technologies and used for RT-PCR. The RT-PCR results were analyzed by recording the threshold cycle (Ct) of each reaction which was the cycle number at which the reporter fluorescence generated passed by a fixed base line. Ct value of 30 or less was selected as indicative of expression for a gene.

Table 2.1 Primers for genes selected for validation by real-time PCR

Gene	Forward	Reverse	Product size(bp)
Ckb	aagttctcggaggtgctcaa	agtttcactccgtccaccac	158
Col3a1	cacgcaaggcaatgagacta	tggggtttcagagagtttgg	125
Sall4	agtgatgtggcttgtgacca	aacccgcttctttccaaaat	186
Rhobtb3	tcagccaaaagcctgaattt	tatgcaaacgctcaggtcac	165
Lyrm4	gaaattcaagccctggtgaa	tgtcctgggcttctcttgat	123
Ammecr1	tccttggacacactttgtgg	tctctctctcgctcgctctc	143
Fgf9	gtgcgagtgcatgagtgagt	ttgaagtatggcagctgtgc	139
Socs2	gggactgcctttaccaacaa	cacatagctgcattcggaga	145
Cyp26a1	ttcgggttgctctgaagact	tcctccaaatggaatgaagc	191
Arg1	tcacctgagctttgatgtcg	cacctcctctgctgtcttcc	187
Fabp7	ccagctgggagaagagtttg	tttctttgccatcccacttc	113
Hoxd13	gaaaagggtgccttacacca	tgtccttcacccttcgattc	161
Oxct1	tcattttggaggaagccatc	ggtagttcctgcagctttgc	134
Sh3gl3	cacctgagaaagctggaagg	aatgccgcctctacaaacac	200
Prtg	ggaattccctcacccaaaat	tcgtcttccgggataatctg	116
Nr6a1	ctgtttccgtcccagatgat	tgttgcaaatgctcctcttg	132
Phlda2	tcagcgctctgagtctgaaa	cagcaagcacgggaatatct	188
Hoxc10	cgcctggagattagcaagac	gatccgattctctcggttca	105
Lpl	gggctctgcctgagttgtag	ccatcctcagtcccagaaaa	167
Trps1	aatgccaccagtgttccttc	gttggcctcctgtttgacat	104
Idh1	aggttctgtggtggagatgc	gacgcccacgttgtatttct	193
Pcolce	cgctctgaccctaagacagg	tgaccgcttgtactgctttg	159
Hoxa10	cgcctagagatcagccgtag	gattcggttttctcggttca	105
Ttr	ccttcgactcttcctcctttg	gacagcatccaggactttgac	112

The QuantiTect® SYBR® Green one-step RT-PCR kit (Qiagen, Cat 204243) was used and all the reagents were provided by the kit and the procedure was following the manufacturer's protocol. The SYBR Green RT-PCR master mix was prepared while keeping LightCycler® capillaries (20 µl) (Roche, Cat 11909339) cooled in LightCycler® centrifuge adapter (Roche, Cat 1909312). The following reagents were added in a tube, with the amount was for one reaction use: 10 µl of 2 x QuantiTect SYBR Green RT-PCR Master Mix, 0.5 µl of 10 µM left primer and right primer, 0.2 µl of QuantiTect RT Mix, and appropriate RNase-free water, mixed

thoroughly and dispensed into PCR capillaries. 10 ng of template RNA was added into each individual PCR capillary, and mixed thoroughly for 10 mins in the cooled centrifuge adapter. The PCR capillaries were put in the LightCycler and the program was started according to standard program as: 50°C 20 mins for reverse transcription, 95°C for 15 mins for initiation, followed by 40 cycles of amplification with the cycle parameters were: denaturation at 94°C for 15 secs, annealing at 60°C for 25 secs, and extension at 72°C for 20 secs.

2.10 Hierarchical clustering of the MHP- and DLHP- related genes by dChip

Hierarchical clustering was used to check the data quality of MHP- and DLHP- genes to see if replicate samples or samples at the same stage and of the same tissue are clustered together. The clustering algorithm of genes was used as follows: the distance between two genes is defined as 1 - r where r is the Pearson correlation coefficient between the standardized intensity values of the two genes across the samples used. Two genes with the closest distance are first merged into a super-gene and connected by branches with length representing their distance, and are then excluded for subsequent merging events. Then the next pair of genes with the smallest distance is chosen to merge and the process is repeated to merge all the genes.

2.11 To estimate the biological functions of the MHP- and DLHP- genes by Gene Ontology (GO) analysis and pathway studies

The MHP- and DLHP- genes were subjected to a functional annotation tool of Gene Ontology (GO) from the database for annotation, visualization and integrated discovery (DAVID) website. GO ontology terms were analyzed to identify enriched biological processes, molecular functions, and cellular components within each group. The probe sets found in each GO category with a significant enrichment (a P-value cutoff of 0.01 to be used as significant) to be

differentially expressed between different stages will be saved as a list under the name of the GO term.

2.12 Culture of the Neuroectodermal Cells

The Neuroectodermal (NE4C) cell line was obtained from American Tissue Culture Collection (ATCC, Manassas, VA, USA). It was derived from the cerebral vesicles of 9-day-old mouse embryos lacking the functional p53 genes (Schlett et al., 1997). The NE4C cell line is neural stem cells with doubling time of approximately 12 hours. The characteristics of NE4C cell line and culture condition are well established (Schlett and Madarasz, 1997). NE4C cells were cultured in complete growth medium: Eagle's Minimum essential medium (MEM) (Sigma, Cat. M5650) supplemented with 10% non-heat inactivated fetal bovine serum (FBS), and 2 mM L-glutamine. The culture flasks should be pre-coated with 15 µg/ml poly-L-lysine (Sigma, Cat. No. P-9155) at least 2 hours in advance.

2.12.1 Thawing of NE4C cells

The frozen NE4C cells was taken out from the liquid nitrogen storage tank, and thawed immediately in a 37°C water bath with gentle agitation. The cells were transferred to a centrifuge tube and mixed with 9.0 ml complete growth medium and spun at 125 g/min for 5 mins to remove the cytotoxic, cryoprotectant dimethyl sulphoxide (DMSO). The cell pellet was suspended with 10 ml of complete growth medium and transferred into a 75 cm^2 poly-L-lysine coated culture flask and incubated at 37°C humidified atmosphere supplied with 5% CO_2 incubator. The culture medium was changed 24 hours after thawing to remove dead cells and cell debris.

2.12.2 Subculture of NE4C cells

The monolayer of NE4C cells was subjected to subculture when 80% of cellular confluence was reached. The medium used for subculture was pre-warmed in 37°C water bath before use. The culture flask was shaken slightly and the culture medium was discarded. The cells were washed with 1x PBS to remove any remaining cell debris and culture medium which contains trypsin inhibitor. Then the cells were incubated with 2.5 ml of 1x Trypsin at 37°C for 5 mins to allow quick detachment of cells from the bottom of the flask which can be observed under an inverted microscope. The trypsin activity was inactivated by adding 10ml of MEM with 10% FBS and centrifuged at 125 g/min for 5 mins. The cell pellet was suspended with 10ml culture medium and divided into a 75 cm^2 poly-L-lysine pre-coated culture flask with estimated cell number of 4 x 10^4 viable cells/cm^2. The subcultured cells were placed at a 37°C incubator supplied with 5% CO_2.

2.12.3 Cryopreservation of NE4C cells

NE4C cells were cryopreserved for storage purpose. The culture medium was first removed and the cells were washed with 1x PBS, followed by trypsinisation as mentioned in the subculture step. MEM with 10% FBS was used to inactivate trypsin, and the cell pellet was suspended with the complete cell culture medium supplemented with 10% DMSO and transferred to cryovials. These cryovials with NE4C cells in cryopreservation reagents were placed in a freezing container, Mr. Frosty (Nalgene, Rocjester, NY) to achieve temperature of -80°C gradually before long-term storage in liquid nitrogen tank.

2.13 Quantitative real time PCR

Quantitative real time PCR was used to quantitatively assess the gene expression in NE4C cells. Because we can acquire enough RNA from the cultured NE4C cells by RNeasy mini kit, two-step RT-PCR method was used for it is more convenient and comparable.

2.13.1 Total RNA isolation for NE4C cells

Total RNA was extracted from NE4C cells grown in 6-well plates using the RNeasy mini kit (Qiagen, Hilden, Germany) according to the manufacturer's protocol. Cultured cells were washed with PBS and detached from the dish by typsinization. Trypsin activity was inactive by MEM with 10% FBS. Cell pellets were lysed by 350 µl of RLT buffer containing 1% of β-mercaptoethanol (β-ME) and were homogenized by a 21-gauge needle fitted to a syringe for 15 times. The cell lysate was mixed with 350 µl of 70% ethanol by pipetting and transferred to the RNeasy Mini column placed in a 2 ml collection tube and centrifuged at 13000 rpm for 30 secs. The flow through was discarded and the spin column was washed by 350 µl of Buffer RW1 twice, 500 µl of Buffer RPE, and dried by centrifugation for 1 min to ensure no leftover of reagents for the elution step. Finally the total RNA was eluted using 30 µl of RNase-free water in a 1.5 ml collection tube supplied by the RNeasy mini kit. The purity and concentration of total RNA was measured by NanoDrop ND-1000 spectrophotometer (Thermo Fisher Scientific, Wilmington, USA). NanoDrop was used to measure RNA quality by UV spectrophotometer to compare the absorbance ratio between the wavelength of 260 and 280 nm. It is reported that ratio of 260/280 between 1.8 and 2.1 indicative of RNA with good quality (Manchester, 1996).

2.13.2 First strand cDNA synthesis

First strand cDNA was synthesized by the SuperScript III first strand synthesis system (Invitrogen, Carlsbad, USA). In a nuclease-free microcentrifuge tube, 2 µg of total RNA, 50 ng of random primers, and 1 µl of 10 mM dNTP mix were mixed together, topped up to 13 µl with RNase-free water, and heated to 65 °C for 5 mins. The heated mixture was then incubated on ice and added to a mixture of 4 µl of 5 x First-Strand Buffer, 1µl of 0.1 M DTT, 1 µl of RNaseOUT™ Recombinant RNase Inhibitor (Cat.No. 10777-019, 40 Unit/µl), and 1µl of SuperScript™ III RT (200 Unit/µl). The mixture was then incubated at 25 °C for 5 mins, 50 °C for 60 mins, 70 °C for 15 mins, cool at 4 °C, used for PCR reaction or stored at -20 °C.

2.13.3 Quantitative real time polymerase chain reaction (qRT-PCR)

PCR reaction was done using the QuantiTect™ SYBR® Green PCR kit (Qiagen, Hilden, Germany) on the LightCycler system (Roche Applied Science, ID, USA) according to the manufacturer's protocol. Primers were designed using Primer 3 software and their specificities were confirmed by nucleotide BLAST from the NCBI website as described in 2.9. The primers were synthesized by 1st Base (1st Base, Singapore) and sequences were listed in **Table** 2.2.

Table 2.2 Primers for qRT-PCR.

Gene Symbol	Forward primer	Reverse primer	Product size
β-actin	gttaccaactgggacgacatg	tcgtagatgggcacagtatg	275bp
Gapdh	atcaccatcttccaggag	atggactgtggtcatgag	304bp
B4galt1	aatgatccggcattcaagag	cgatgtccactgtgatttgg	167bp

The SYBR Green master mix was prepared in a centrifuge tube with the amount for one reaction use of: 10 µl of 2 x QuantiTect SYBR Green PCR Master Mix, 0.5 µl of 10 µM left primer and right primer, 10 ng of the first strand cDNA as template, and topped up with appropriate RNase-free water. The master mix with the cDNA template was mixed thoroughly and appropriate volumes were dispensed into the LightCycler capillaries pre-cooled in lightCycler centrifuge adapter. The LightCycler was programmed as: 95°C 15 mins for initiation, followed by 40 cycles of amplification with the cycle parameters were: 94°C 15 secs for denaturation, 60°C 25 secs for annealing, and 72°C 20 secs for extension. The PCR capillaries were placed into the LightCycler and the cycling program was started with a melting curve analysis of PCR products performed.

2.14 siRNA transfection

For siRNA transfection, NE4C cells were cultured in the maintaining medium. The transfection was carried out using forward transfection method as recommended by DharmaFECT transfection reagents (DF1)-siRNA transfection protocol. Briefly, NE4C cells seeded in 6-well-plate were transfected with siRNA (Negative control, Positive control, and target genes) and DF1 complex 24 hours after seeding. Positive control was GAPDH siRNA. Optimization of transfection conditions was performed several times before formal experiments, including the transfection parameters of NE4C cell number, siRNA concentration, amount of DF1 transfection reagent and exposure time of NE4C cells to the transfection reagents. Triplicates were done for normal NE4C cells, negative siRNA, siGAPDH, and two sequences of the target gene. Two-step RT-PCR was done to analyze the transfection efficiency.

2.15 Proliferation assay

Proliferation assay was done by MTS method performed using the CellTiter96 Aqueous non-radioactive proliferation assay (MTS, Promega Corp., Madison, WI, USA). This is a colorimetric method for determining the number of viable cells in proliferation assays. The main components in the assay are the tetrazolium compound 3-(4,5-dimethylthiazol-2-yl)-5-(3-carboxymethoxyphenyl)-2-(4-sulphophenyl)-2H-tetrazolium (MTS) and phenazine ethosulphate (PES). MTS is chemically reduced by the mitochondrial dehydrogenase activity in the viable cells into a soluble purple-color formazan, the absorbance of which can be measured directly at 490nm. The quantity of the formazan formed (absorbance level) is directly proportional to the number of viable cells in the sample (Promega, 2007). The PES is an electron coupling reagent which enhances the chemical stability of MTS.

NE4C cells were seeded in 6-well-plate (8×10^4 cells/well) and transfected 24 hours after seeding using the optimized transfection condition: siRNA 5nM, DF1 5µl, exposure time of cells to transfection reagents was 24 hours. 48 hours post-transfection, 400 µl/well of MTS reagent was added into the transfected NE4C cells containing 2 ml of MEM without FBS. The cells were then incubated at 37°C for 4 hours. The absorbance of the formazan formed was measured hourly using the GENios Microplate Reader (Tecan, Mannedorf, Switzerland).

2.16 Adhesion assay

96-well plate was pre-coated with 20 µg/ml fibronectin (BD, Franklin lakes, NJ, USA) or 20 µg/ml Collagen I (Corning, Lowell, MA, USA) in 100µl of PBS at 4℃ overnight. Wells were then washed with PBS and blocked with 100 µl of 1% bovine serum albumin (BSA)

(Sigma-Aldrich, St.Louis, MO, USA) at 25°C for one hour. Wells were then washed twice with PBS and air-dried in the hood and stored at 4°C for later use.

48 hours post transfection NE4C cells were trypsinized and resuspended in MEM without FBS and reseeded in the pre-coated 96-well plate at a concentration of 1 x 10^4 cells/well in 100 µl for Collagen I and 3 x 10^4 cells/well in 100 µl for fibronectin. Within each treatment group, the wells were divided into the washed group and the unwashed group. For the washed group, wells were washed thrice with PBS after the cells were allowed to attach for 30 mins at 37°C in a humidified incubator containing 5% CO_2. Nothing was done for the unwashed group. MTS assay was performed to determine the number of adhered cells. 20 µl of MTS reagent diluted with 100 µl of MEM without FBS was added into each well of the washed group, while 20 µl of MTS reagent was directly added into each well of the unwashed group. Absorbance of formazan formed was taken at 490 nm one hour after MTS was added and was taken hourly for 4 hours. 8 replicates were done for the washed group and unwashed group within each treatment group. 3 blanks were done for control with 20 µl of MTS reagent diluted with 100 µl of MEM without FBS was added into each well.

CHAPTER 3

RESULTS

3 Results

3.1 Mouse embryos were dissected at different time points during neurulation

Mouse embryos were dissected at three stages of E8.5, E9.0, and E9.5 during neurulation which were critical for neural tube formation. Mouse embryo pictures were shown in **Fig. 3.1**. In **Fig. 3.1.A**, it shows one mouse embryo with 10 somites before turning at E8.5 in the posture of "U". The embryo is relatively transparent with cut edge amnion attached to the embryo body difficult to be torn away. Closed somites can be distinguished clearly at the mid-region along the neuroaxis. The two openings at the upper head fold and the bottom region are prominent. While in **Fig. 3.1.B,** the mouse embryo at the E9.0 stage with 20 somites was in the posture of "C" after turning. The rostral extremity of the neural tube is closed already, but the caudal region still remains open. A prominent ridge in the mid of the lateral body wall, at approximately the level of 11 to 12 somite region indicates the site of the forelimb bud. Cranially at the upper forelimb, the closed somites are difficult to count, but somites can be easily distinguished caudally from the forelimb bud region. Characteristics of embryos at this stage also include the indented otic and the optic pit at the ostral region, the transparent heart that was discernable. The amnion is easily torn away and the body of the embryo seems much smoother than at the E8.5 stage. At E9.5 as shown in **Fig. 3.1.C**, the mouse embryo grows much larger in size and not transparent any more. The outlines of the forebrain, midbrain and hindbrain become much clearer, and the forebrain vesicle subdivides into telencephalic and diencephalic vesicles. The posterior opening becomes a hole immediately adjacent to the closed neural tube which is the posterior neuropore (PNP) as designated by an arrow in **Fig. 3.1.C**. The forelimb bud becomes obvious at the 11 to 12 somites level, and a distinct condensation of the hind limb bud appears at just the upper level of the PNP region. The somites coalesce at upper of the forelimb bud and the somite number at

the forelimb bud region was designated as 11, and the somites were counted caudally till the one that is forming. The somite number at this stage is from 27 to 30, and the somite number of the mouse embryo in **Fig. 3.1.C** is 29. Practically, there are developmental differences among embryos between different litters or even from the same litter. Somite number was used as an indicator when selecting embryos for cryo-section. Mouse embryos with somite number of 9 to 12, 19 to 22, and 27 to 30 were selected and used as E8.5, E9.0 and E9.5 embryos (Copp et al., 1982; Shum and Copp, 1996a).

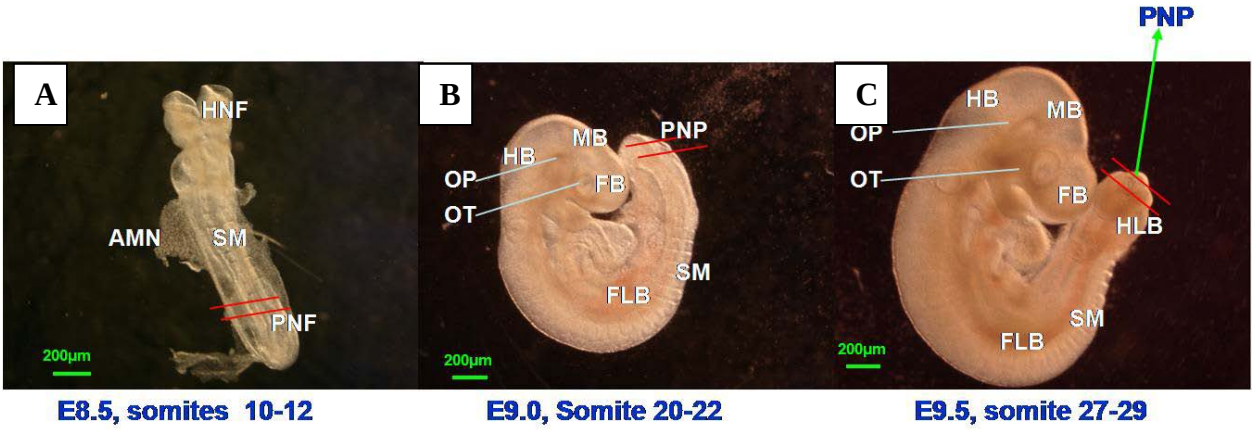

Fig. 3.1. Photographs A, B, and C represent embryos dissected at the three different timing of neurulation. (The three pictures were taken under the same magnification and scale bar equals 200µm.) AMN: amnion; SM: somite; HNF: head neural fold; PNF: posterior neural fold; FB: forebrain; MB: midbrain; HB: hindbrain; OP: optic pit; OT: otic pit; FLB: forelimb bud; HLB: hind limb bud; PNP: posterior neuropore. Red line indicates areas to be transversely cut.

3.2 Transverse sections through spinal region of mouse embryos

Transverse sections of 8um were sectioned by cryostat and quickly stained by haematoxylin. **Fig. 3.2.A** shows mode 1 of E8.5 embryos. Transverse sections of mouse embryo with 12 somites demonstrate mode 1 during neurulation process. The straight arrow in Figure 3.A indicates the median hinge point (MHP) at the upper middle of hind gut and notochord, the

neuroectoderm at both sides of the MHP remains straight and elevated, and the whole neuroectoderm demonstrated a V-shaped morphology.

Fig. 3.2.B shows mode 2 of E9.0 embryos with 20 somites. The two bilateral arrows in figure 3.B indicate the bending sites of dorsolateral hinge points (DLHPs) along the neuroectoderm, while the arrow in the middle point to MHP. The morphology of neuroectoderm in mode 2 is like a diamond, the length of the DLHP bending sites to the MHP varies according to somite number or stage of embryos. The bending NT becomes more prominent compared with the NT in mode1. The size of paraxial mesoderm in mode 2 and mode 3 is reduced compared with the mesoderm surrounding the NT at mode 1, implicating less influence of paraxial mesoderm on neurulation at later stage.

The morphology of mode 3 at E9.5 mouse embryo is demonstrated in **Fig. 3.2.C**. The MHP is not distinguished, the whole neuroepithelium bends and the DLHPs become more powerful with the tips of the neural folds become sharpen and stretch to connect towards each other, implicating that NT may play more important roles at the end of neural tube closure.

It is estimated that the posterior neuropore is about 40 to 60 um in length along the neuroaxis (van Straaten et al., 1992). 5 sections of 8 μm across the closure sites were selected for microdissection by LCM, and a total of 15 sections from 3 embryos were microdissected and pooled for extracting RNA for one sample. Such selection is made because if selecting less sections, the RNA extracted from the LCM samples is not enough for microarray, and more embryos will be needed; while if selecting more sections from the same embryo, the sections from the sites may be closed too long or be too far from the closing site and may not be proper to represent the closing status. The RNA from LCM samples will be amplified and used for microarray analysis and RT-PCR.

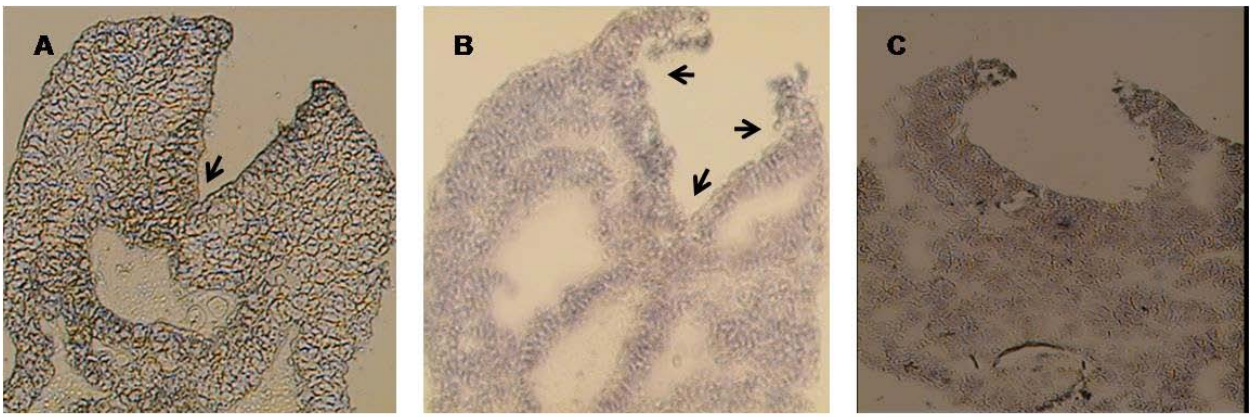

Fig. 3.2 Transverse sections through the posterior neuropore of mouse embryos at E8.5, E9.0, and E9.5 demonstrate three modes of spinal neurulation. Sections were quickly stained by Haematoxylin and pictures were taken under microscope attached to the LCM system under the same magnificent of x40. Arrow in A points to the MHP, the upper two arrows in B point to DLHPs, and the lower one point to MHP.

3.3 Procurement of selected tissues by LCM

Targeted NT and MD tissues were selected and microdissected separately by the Arcturus LCM system. The sections were observed under microscope and only those sections with the typical features for each mode were used for microdissection. **Fig. 3.3** shows the microdissction process of the mode 2 section. **Fig. 3.3.A** shows the picture of the section with a diamond-shaped NT viewed under microscope, and a CapSure Macro LCM cap was situated on it, after a selection, the NT was microdissection by laser and attached to the film under the cap as shown in **Fig. 3.3.B**. The cap with the NT was lifted up but the unwanted tissues were still left on the section as shown in **Fig. 3.3.C**. **Fig. 3.3.D** shows the NT microdissected just now. NT from sections of about 5 embryos were dissected on one MicroCap and the cap with microdissected tissues was transferred to be incubated in extraction buffer under the help of the CapSure Insertion Tool for RNA extraction. Then another round microdissection of the paraxial MD

tissue was carried out on the same section using a clean MicroCap. The paraxial MD was selected immediately adjacent to the selected NT with a comparable size as shown in **Fig. 3.3.E**. **Fig. 3.3.F** shows the remaining tissues left on the slides after the second microdissection and the microdissected MD tissue is shown in **Fig. 3.3.G**. Background colors on different pictures were slightly different because of the different distance from the objective light. The tissue cells seem to be a little bit unclear and this may be due to three reasons: first reason may be due to the Microcap situated onto the sections, the light must traverse the translucent film when taking pictures; another reason is due to no cover slip on the tissue as usual; last but not least is may be due to the quickly stain method which is just for determining targeted tissues so the staining is not quite prominent.

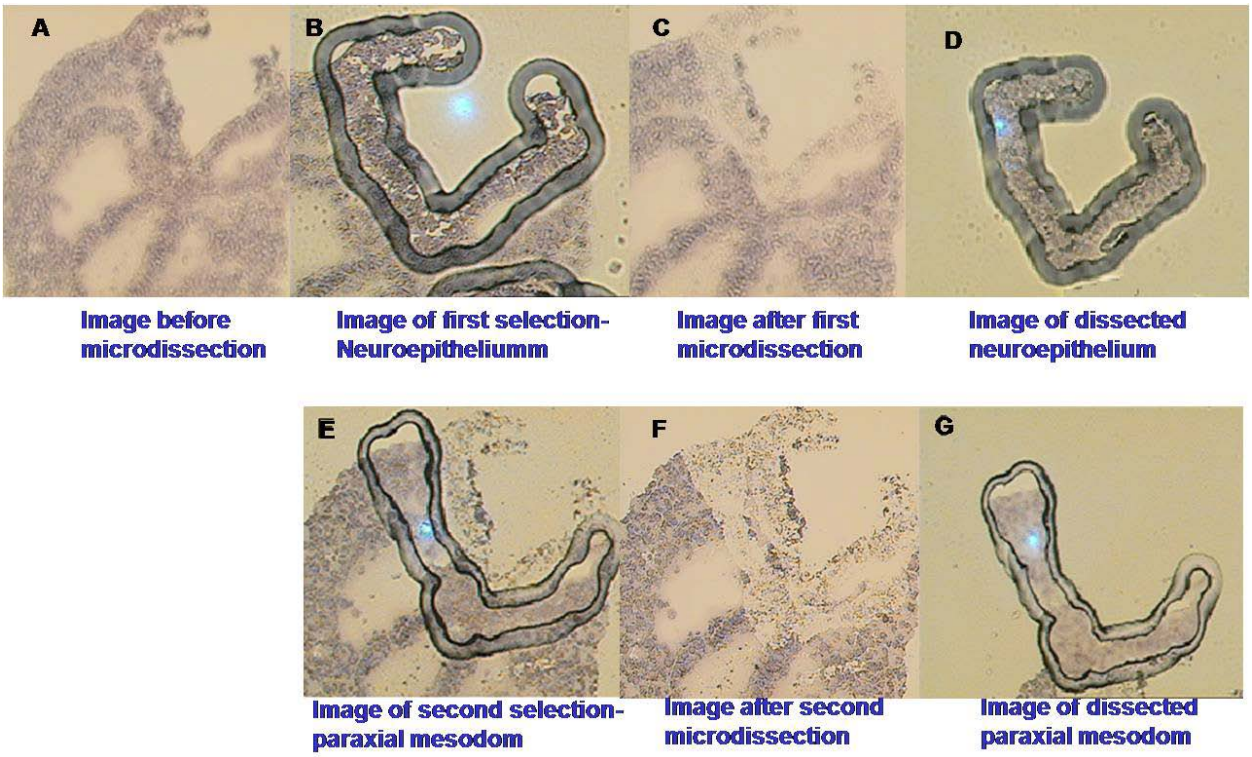

Fig. 3.3 A representative example demonstrating precise procurement of selective populations of cells by laser capture microdissection (Haematoxylin staining; Magnification of pictures of the three modes taken by LCM machine is 40 times.) (A-G, mode 2, E9.0). Quickly stain and isolation of neuroepithelium and mesenchymal cells from E9.0 mouse embryo transverse sections though posterior neuropore region. (A), Sections were quickly-stained by Haematoxylin. Neuroepithelium in E9.0 was in Diamond shape. (B) and (E), Selected populations of cells were targeted with laser and attached to membrane on the Microcap used for their isolation. (C) and (F), After lifting off the membrane, selected cell populations were removed from the tissue section. (D) and (G), Isolated cell populations stuck to the membrane, (D) was neuroepithelium and (G) was surrounding mesenchymal cells.

3.4 Assessment of Quality and quantity of total RNA extracted from laser capture microdissected NT and MD samples

The quality of starting total RNA is important for the success of microarray analysis (Jones et al., 2006; Tomita et al., 2004). I assessed the quality and quantity of total RNA carefully using a combined method of Nanodrop and Agilent 2100 bioanalyzer. The very low sample consumption of 1-2 µl is one advantage of Nanodrop and it was used to measure RNA quantity for LCM samples.

The Agilent 2100 Bioanalyzer is an advanced innovative lab-on-chip technology to assess RNA quality and quantity widely used in the gene expression profiling platforms (Bustin, 2002; Mueller et al., 2000). It detects RNA samples applied on a micro-fabricated chip via laser induced fluorescence. Total RNA samples as small as 50 pg can be used for assessment. RNA ladder was used to estimate the RNA band sizes. RNA Integrity Number (RIN) (Schroeder et al., 2006) was calculated according to the shape of the curve in the electropharogram by Agilent 2100 expert software. A RIN of 7-10 is indicative of High RNA quality and used for microarray work, whereas a RIN of 1 indicates a completely degraded RNA sample (Fleige and Pfaffl, 2006; Jones et al., 2006).

All of the 18 RNA samples had good quality with RIN number of more than 7.5, and the quantity were more than enough for minimum requirement of starting RNA for amplification (**Table 3.1**). The two peaks at positions of 18s and 28s of all 18 samples displayed by the electropharogram were high with all RIN numbers above 7.5, and the gel pictures of all 18 samples displayed by Bioanalyzer were with two clear bands at the positions of 18s and 28s (**Fig. 3.4**).

Table 3.1 Total RNA quality and quantity of pooled microdissected samples assessed by Nanodrop and Agilent 2100 Bioanalyzer.

Sample group	Sample type	Mode	RNA concentration (ng/µl) (mean±SD)(n=3)	RIN (mean±SD)(n=3)
1	E8.5-NT	1	10.8±2.86	8.93±0.49
2	E9.0-NT	2	12.73±4.47	8.13±0.55
3	E9.5-NT	3	17.7±8.85	8.26±0.64
4	E8.5-MD	1	15.8±4.01	8.5±0.87
5	E9.0-MD	2	14.47±5.4	8.4±0.26
6	E9.5-MD	3	13.5±8.05	7.9±0.32

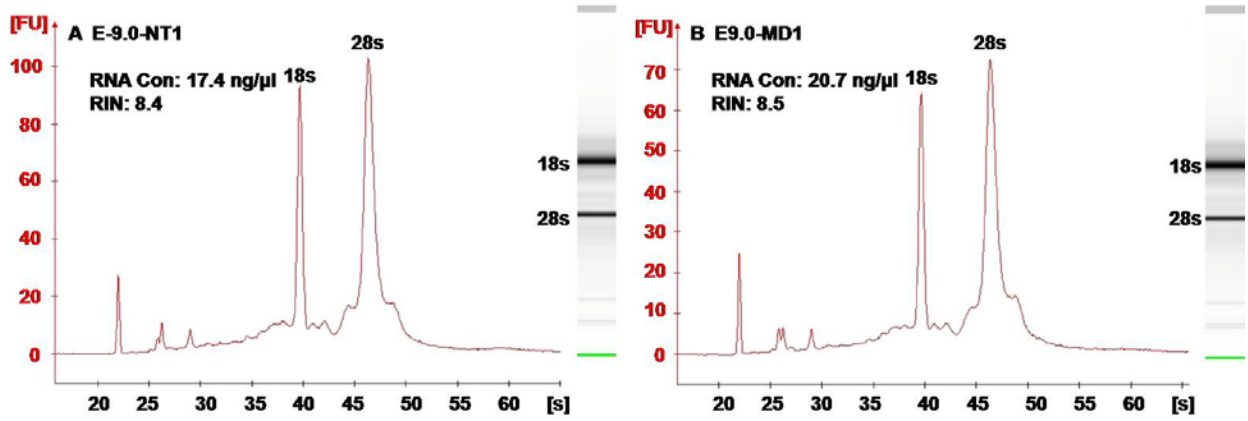

Fig. 3.4 Assessment of total RNA of laser capture microdissected NT and MD samples by Agilent 2100 Bioanalyzer. Representative examples of total RNA after microdissection, before amplification, tested by Bioanalyser (A, E9.0-NT1; B, E9.0-MD1). The two peaks at the position of 18s and 28s were high displayed by the electrophoretogram, and the two bands indicative of the two peaks were clearly visible in the left gel picture. The RNA quality and quantity were similar for NT and MD tissues.

3.5 Assessment of quality and quantity of total cRNA and fragmented cRNA for microarray analysis

For nanogram level amounts (in the range of 10ng to 100 ng) of starting total RNA from LCM samples, a two-cycle cDNA synthesis and IVT amplification is necessary to get sufficient amounts of labeled cRNA for microarray analysis. 15 ng of total RNA for each sample was used as starting material. After two cycle cDNA synthesis with IVT amplification, Biotin labeled cRNA were acquired. The quality and quantity of the labeled Bio-cRNA was measured by Nanodrop. The ratio of 260/280 was between 1.8 and 2.1 for all the 18 samples, indicating RNA was amplified and purified with good quality, and the quantity is above 27 μg for each sample, which is sufficient for hybridization on GeneChips (**Table 3.2**). The total amount of Bio-cRNA did not have obvious relation with the starting 18S/28S ratios of the starting total RNA just as reported by Dumur *et al* (Dumur et al., 2004b). Starting total RNA with RIN more than 7 used in this experiment can provide sufficient amount of Bio-cRNA, indicating their good quality.

The number of genes presented among each group was similar with the starting RIN number more than 7 as indicated in the hybridization results in **Table 3.3**. This is consistent with the previous study that a RIN of 7-10 is indicative of high RNA quality and good enough for microarray work (Fleige and Pfaffl, 2006; Jones et al., 2006). After 2 rounds of amplification and purification process, all of the final cRNA hybridized on the genechips were of good quality as indicated by the RNA260/280 ratio (**Table 3.3**). Then 20 μg of labeled Bio-cRNA were cleaned up and fragmented. The fragmented Bio-cRNA was measured by Agilent 2100 Bioanalyzer. **Fig. 3.5** shows the Bioanalyzer electrophoretogram of the fragmented Bio-cRNA with the size between 25 and 200 bp which indicates a proper feature for microarray hybridization.

Table 3.2 Bio-cRNA results amplified by two cycle cDNA synthesis and IVT amplification.

Sample group	Sample type	Mode	RNA260/280 (mean±SD)(n=3)	cRNA yield(μg) (mean±SD)(n=3)
1	E8.5-NT	1	1.89±0.10	123.35±58.26
2	E9.0-NT	2	1.96±0.06	92.36±56.07
3	E9.5-NT	3	2.01±0.03	79.98±20.39
4	E8.5-MD	1	1.92±0.09	97.08±46.21
5	E9.0-MD	2	1.99±0.01	93.94±38.25
6	E9.5-MD	3	2.03±0.01	54.67±42.35

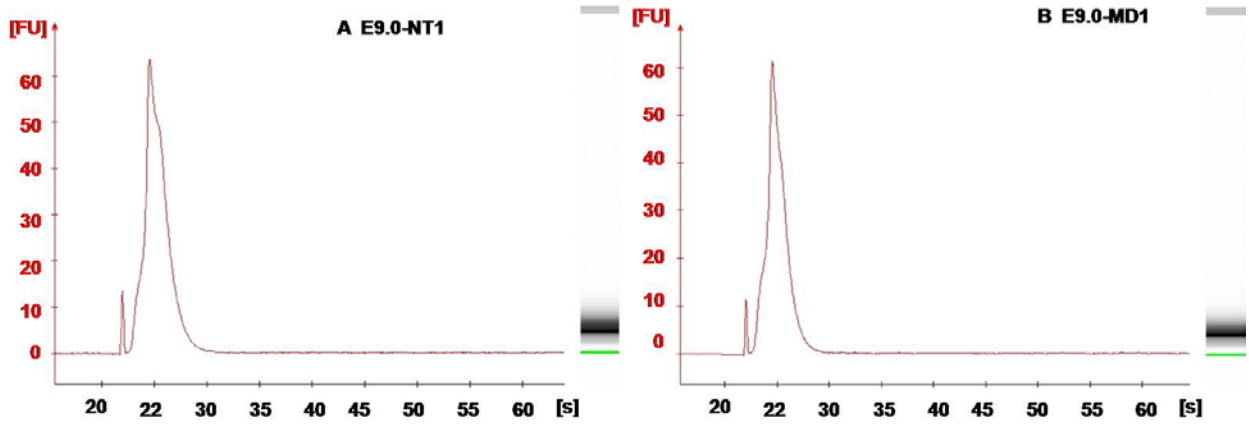

Fig. 3.5 Assessment of fragmented Bio-cRNA using Agilent 2100 Bioanalyzer.
Representative examples of fragmented Bio-cRNA after 2 rounds amplification, before hybridization, tested by Bioanalyser (A, E9.0-NT1; B, E9.0-MD1). The peak of fragmented Bio-cRNA was at the size of 25bp displayed by the electrophoretogram, indicated by a clear band on the gel picture at the left side.

3.6 Analysis of microarray data

Microarrays were used to provide quantitative and comprehensive profiling of gene expression levels for different neurulation stages. Each stage was examined in triplicate using independent biological samples for each Affymetrix gene array. 10 µg of the fragmented biotin-labeled cRNA samples was hybridized to Affymetrix Mouse 430.2.0 Genechips according to the manufacturer's instructions. After probe array wash and stain steps, the probe arrays were scanned with an Affymetrix GeneChip Scanner and the images quantified using Affymetrix GeneChip Operating Software (GCOS) and saved as an image file. The resulting gene expression profiling from 18 microarrays were analyzed with three software: dChip, GCOS, and GeneSpring, providing a global view of almost all genes during different neurulation stages.

3.6.1 Quality assessment of a .dat/.cel image data

The average signal intensity of the array was set to a target signal of 500 by default. The expression signal of a probe set above 500 is designated as present and below 500 is designated as absent. Affymetrix suggested that average background values for arrays scanned with the GeneChip Scanner 3000 range from 20 to 100. The detected noise values (background) of all the samples were between 30 to 50 and comparable among triplicates in this experiments which indicates a less pixel-to-pixel variation on the GeneChip arrays. Poly-A controls of dap, lys, phe, and thr were present in all the samples with increasing values which indicate proper of the entire target labeling process. All of the hybridization controls of bioB, bioC, bioD, and cre were present with increasing values which indicate higher hybridization efficiency on gene arrays and a good RNA sample quality.

The housekeeping genes of GAPDH were used as internal control genes to assess RNA samples and assay quality. Measurement of hybridization signal ratios from the 3' and 5' ends is used as a quality control for robust, full-length target synthesis. The 3'/5' ratios range is generally no more than 3 for the 1-cycle assay and could be higher for the 2-cycle assay due to additional cycle of amplification. It is reported that the ratio of hybridization signals at the 3' and 5' end of GAPDH transcript could be at least ten-fold for the 2-cycle assay (Luzzi et al., 2003). In the current microarray analysis, the 3'/5' ratio of GAPDH of all samples was measured (**Table 3.3**). Affymetrix GeneChips used multiple probes to measure expression for each transcript, and preferentially selected probes from the 3' end of each transcript as well in order to minimize the influence that both RNA degradation and probe position can have on the final estimation of gene expression. The probe position effects are less likely influence measurement of whole expression data as long as the relative overall expression levels are considered (Cope et al., 2006).

Two other parameters that reflect signal intensity were recommended to be used as measurement of sample quality for 2 round amplification microarrays, scale factor (SF) and percentage of presented genes (%P) (Luzzi et al., 2003). Scale factor is the relative amount of a defined target intensity value compared to the average signal intensity of all probe pairs on the microarray. The higher the scale factor, the lower the overall signal intensity. The scale factors in the current microarray analysis results were below 10 and no obvious difference among groups (**Table 3.3**), indicating comparable microarray results. The percent present of probe set of all samples were above 43%, and differences among triplicates were below 5% (**Table 3.3**). These results also indicate a good sample quality and the results were proper for comparison among replicates.

Table 3.3 Comparison of scale factor and percentage of number of genes presented on Genechips .

	Sample group	Background	GAPDH 3'/5' ratio	Scale Factor (SF)	Present(%) genes (%P)
1	E8.5-NT	37.33±0.01	15.80±3.09	8.47±0.005	46.73±0.009
2	E9.0-NT	38.85±0.01	12.07±2.21	7.63±0.011	46.00±0.02
3	E9.5-NT	42.52±0.02	3.91±0.08	4.28±0.017	52.87±0.014
4	E8.5-MD	41.92±0.01	12.52±3.56	7.32±0.007	46.73±0.076
5	E9.0-MD	34.94±0.03	10.18±0.69	6.37±0.029	49.20±0.003
6	E9.5-MD	37.42±0.01	3.10±0.23	5.70±0.008	53.73±0.007

All data are presented as mean±SD, n=3. Scale factor (SF): utilized to generate an average signal intensity of 150 using GCOS software; Present(%) genes (%P): percentage of genes scored detected ("P") by GCOS.

3.6.2 Comparison of the differentially expressed genes by microarray analysis

All raw data of the 18 samples were analyzed by three common used software, GCOS, dChip, and GeneSpring, with the same filtering conditions of AI > 500 and FC > 2 **(Fig. 3.6)**. Five probe set lists for neuroepithelium (NT) and surrounding mesoderm (MD) were generated by each of the algorithms of the software.

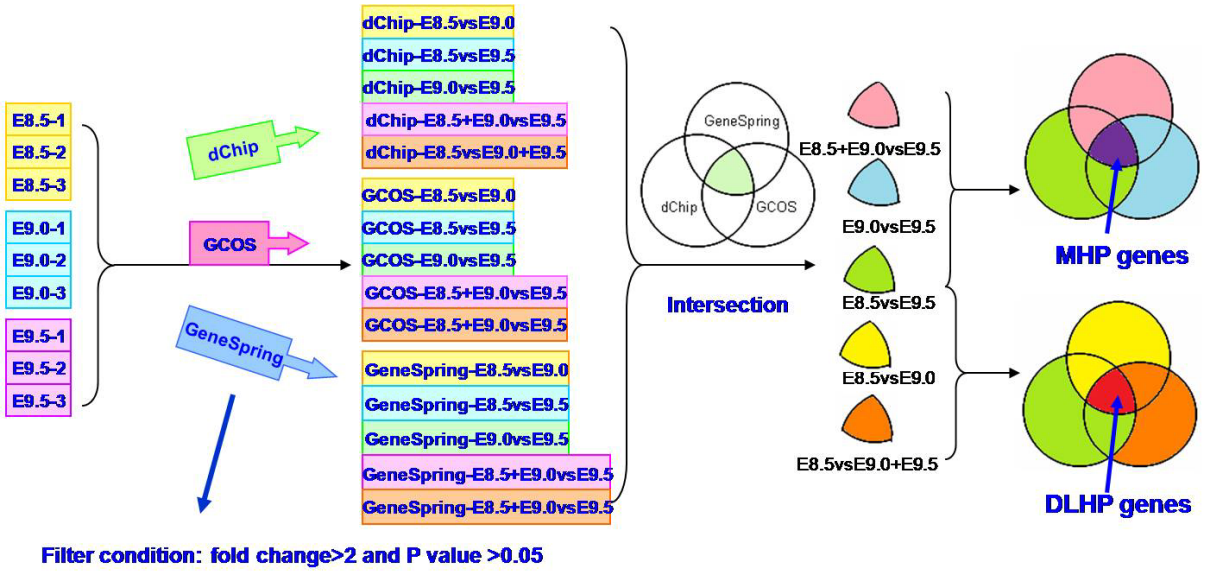

Fig. 3.6 Experiment design and comparison of the overlapped probesets among 3 analysis software. See materials and method for detailed analysis process.

In GCOS software generated probe set lists which are summarized in **Table 3.4**, the total numbers of differentially expressed transcripts by at least 2 fold change in NT groups of E8.5 compare with E9.0, E8.5 compared with E9.5, and E9.0 compared with E9.5 were 572, 1882 and 1148, respectively; While the total numbers of transcripts differentially expressed in MD groups of E8.5 compared with E9.0, E8.5 compared with E9.5, and E9.0 compared with E9.5 were 642, 1870 and 1194, respectively. It seems that the number of differentially expressed transcripts were direct proportional to the length of time in development. 2199 transcripts were differentially expressed when the MHP disappeared at E9.5 compared with when MHP presented at E8.5 and E9.0. Among these transcripts, 1102 were from the NT, and 1097 were from MD. Besides, a total of 1206 transcripts were differentially expressed when the dorsolateral hinge points (DLHPs) presented at E9.0 and E9.5 compared with the profile just before the formation of the DLHPs at E8.5. Among these transcripts, 533 were from NT and 673 were from MD**.**

The same raw data were analyzed by software dChip and 5 different algorithms of GeneSpring (**Table 3.4**). The number of differentially expressed genes of dChip and 3 algorithms of GeneSpring (RMA, GC-RMA, and GS-GCOS) gave the most similar results as GCOS**.** GS-dChip gave the most nonstringent calculation with the number of differentially changed transcripts being the highest among all groups, while PLIER gave the most stringent calculation with the number of differentially changed transcripts being the lowest, especially in all of the NT groups**.** These similarities and differences indicate that every algorithm has its own advantages and disadvantages, and combined calculation using more software may increase the accuracy by presenting the overlapping genes from all software (Millenaar et al., 2006). This

combined application of several software is suggested when a lot of genes changed (more than thousands or hundreds) using only one software**.**

A combined probe set list for each comparison was obtained by intersection of the 7 probe set lists generated by the above software. A total of 442, 1318, and 892 transcripts showed differential expression for comparison between E8.5 and E9.0, E8.5 and E9.5, and E9.0 and E9.5 and the numbers of these genes were listed as the intersection of 7 data sets lists (**Table 3.5**). The overlapped genes presented a decrease in numbers compared with numbers filtered by only one software, the GCOS**.** The combined usage of 3 software presented less genes but still contained more than hundreds of transcripts for future analysis. This indicates the effectiveness of combined use of different algorithms in narrowing down the scope of studies**.** The gap between the number of differentially expressed transcripts of E8.5vsE9.5 and the number of E8.5vsE9.0 together with E9.0vsE9.5 add up to 16 while the gaps calculated by each one of the software were more than 100**.** This may indicate an improvement in the accuracy of filtered genes**.**

A total of 847 differentially expressed transcripts were presented in all of the 7 probesets lists in E8.5+E9.0vsE9.5 group list, with 411 transcripts for NT and 436 for MD (**Table 3.5**). These genes may be involved in the formation and existence of the MHP**.** Besides, a total of 365 differentially expressed probe sets were presented in all of the 7 datasets in E8.5vsE9.0+E9.5 group list, with 215 transcripts for NT and 150 for MD (**Table 3.5**)**.** These genes may contribute to the formation and existence of the DLHPs**.**

To know the distribution of these transcripts more clearly, the transcripts from E8.5vs9.5, E9.0vsE9.5 and E8.5+E9.0vsE9.5 gene lists as well as the transcripts from E8.5vsE9.0, E8.5vsE9.5, and E8.5vsE9.0+9.5 were calculated by intersection to generate the MHP- and

DLHP- related transcript lists. After removal of duplicates of probesets and probesets with uncharacterized expressed sequences, a total of 433 transcripts were generated for MHP-related genes with 214 for NT and 219 for MD, and a total of 151 transcripts were found for DLHP-related genes with 95 for NT and 56 for MD (**Table 3.6).** These differentially expressed transcripts were functionally clustered by GO file from DAVID database, and partially listed in tables (data not shown here). Further analysis of these genes will increase the possibility of finding MHP- and DLHP- related key genes. These findings may be further explored to unveil the neurulation mechanism.

Table 3.4 Number of differentially expressed probe sets at different stages analyzed by different software.

	dChip	**GCOS**	**GeneSpring**				
			RMA	**GC-RMA**	**GS-dChip**	**GS-GCOS**	**PLIER**
NT-E8.5vsE9.0	559	572	467	729	1279	703	383
NT-E8.5vsE9.5	1698	1882	1504	2322	3241	2453	1227
NT-E9.0vsE9.5	1328	1148	1157	1778	2718	1916	928
NT-E8.5+E9.0vsE9.5	1237	1102	1066	1753	2658	1803	855
NT-E8.5vsE9.0+E9.5	666	533	492	788	1533	777	414
MD-E8.5vsE9.0	798	642	602	936	2250	870	721
MD-E8.5vsE9.5	2148	1870	2037	2703	4576	2560	2235
MD-E9.0vsE9.5	1287	1194	1065	1523	2679	1634	864
MD-E8.5+E9.0vsE9.5	1406	1097	1165	1660	3137	1603	1054
MD-E8.5vsE9.0+E9.5	1016	673	797	1183	3002	1059	941

Table 3.5 Intersection of 7 datasets by Microsoft access to narrow down the scope of the differentially expressed transcripts.

	NT	MD	Total
E8.5vsE9.0	209	233	442
E8.5vsE9.5	615	703	1318
E9.0vsE9.5	453	439	892
E8.5+E9.0vsE9.5	411	436	847
E8.5vsE9.0+E9.5	215	150	365

Table 3.6 Calculation of MHP- and DLHP- related transcripts by Microsoft Access.

		up	down	total
MHP-NT	NT-E8.5vsE9.5	138	76	214
	NT-E9.0vsE9.5			
	NT-E8.5+E9.0vsE9.5			
MHP-MD	MD-E8.5vsE9.5	176	43	219
	MD-E9.0vsE9.5			
	MD-E8.5+E9.0vsE9.5			
DLHP-NT	NT-E8.5vsE9.0	57	38	95
	NT-E8.5vsE9.5			
	NT-E8.5vsE9.0+E9.5			
DLHP-MD	MD-E8.5vsE9.0	35	21	56
	MD-E8.5vsE9.5			
	MD-E8.5vsE9.0+E9.5			

As adjacent tissues, the NT and MD share some genes in common that may function sequentially or together. The MHP-NT and MHP-MD transcripts as well as the DLHP-NT and DLHP-MD transcripts were intersected by Microsoft Access specifically to compare their distribution among NT and MD tissues. The comparison results were present as Venn diagrams in **Fig. 3.7.A** for MHP and **Fig. 3.7.B** for DLHPs. In **Fig. 3.7.A**, there are 69 transcripts present in common among both MHP-NT and MHP-MD related genes, with 55 up-regulated and 14 down-regulated. In **Fig. 3.7.B**, there are 24 transcripts that in common among both DLHP-NT and DLHP-MD transcript datasets, with 17 up-regulated and 7 down-regulated.

There were 136 transcripts in MHP-NT list only with 75 up-regulated and 61 down-regulated, and 141 transcripts in MHP-MD list only with 116 up-regulated and 25 down-regulated in **Fig. 3.7.A**. Similar as in **Fig. 3.7.B**, there are 64 transcripts in DLHP-NT list only with 36 up-regulated and 28 down-regulated, while there are 29 differentially changed transcripts in DLHP-MD list only with 17 up-regulated and 12 down-regulated. With the Venn diagram, we can easily note the distribution of transcripts in a spatial and temporal manner.

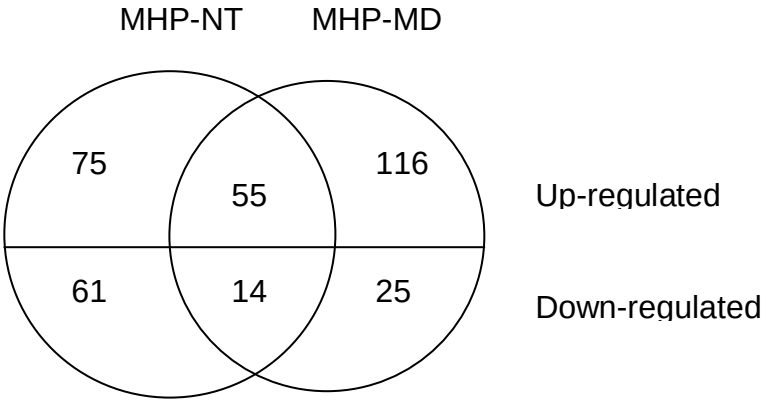

A. Venn diagram for MHP-NT and MHP-MD genes.

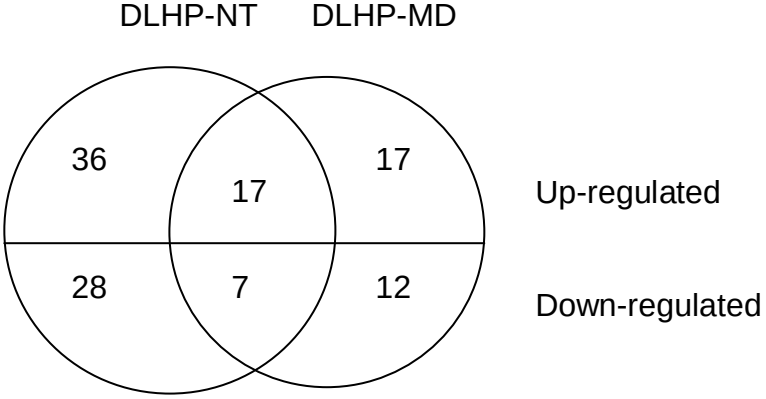

B. Venn diagram for DLHP-NT and DLHP-MD genes.

Fig. 3.7 Venn diagram of temporally expressed transcripts distributed spatially in NT and MD. Transcripts from NT and MD were intersected by Microsoft access, and the distribution of expressed genes was shown in separate groups. The numbers of separated transcripts was counted and Venn diagrams were drawn to show the distribution of transcripts in NT and MD. Fig. 3.7.A shows the results for MHP-related genes and Fig. 3.7.B for DLHP-related genes.

3.6.3 Verification of differentially expressed genes from microarray data by RT-PCR

To confirm that the microarray platform was acceptably measuring differential expression between different stages of the LCM samples, 42 differentially expressed genes from the MHP- and DLHP- related gene lists were selected for RT-PCR analysis. The excess RNA produced by the microarray target preparation was used as template for the RT-PCR work (Day et al., 2008). Expression pattern of all genes were consistent in RT-PCR compared with microarray data (**Table 3.7**). The expression ratios produced by RT-PCR is similar as microarray. There is no obvious trend that the expression ratio of RT-PCR is higher than microarray as reported (Kultima et al., 2004). These results are highly supportive of the microarray data.

Table 3.7 Verification of differential gene expression by quantitative RT-PCR compared with microarray.

Group	gene	qRT-PCR	microarray(dChip)
MHP-NT	Fabp7	↑	↑
	Pcolce	↑	↑
	Sall4	↓	↓
	Rhobtb3	↓	↓
	Ammer1	↓	↓
	Ttr	↓	↓
	Col3a1	↑	↑
	Ckb	↑	↑
	Hoxd13	↑	↑
	Lyrm4	↓	↓
MHP-MD	Pcolce	↑	↑
	Oxct1	↑	↑
	Col3a1	↑	↑
	Fabp7	↑	↑
	Ckb	↑	↑
	Fgf9	↓	↓
	Phlda2	↓	↓
	Ammercr	↓	↓
	Lyrm	↓	↓
	Ttr	↓	↓
DLHP-NT	Idh1	↑	↑
	Trps1	↑	↑
	Fabp7	↑	↑
	Sh3gl3	↑	↑
	LPL	↑	↑
	Phlda2	↓	↓
	Prtg	↓	↓
	Arg1	↓	↓
	Nr6a1	↓	↓
	Ttr	↓	↓
	Hoxc10	↑	↑
	Hoxd13	↑	↑
DLHP-MD	Fabp7	↑	↑
	LPL	↑	↑
	Trps1	↑	↑
	Cyp26a1	↑	↑
	Nr6a1	↓	↓
	Prtg	↓	↓
	Phlda2	↓	↓
	Socs2	↑	↑
	Arg1	↓	↓
	Ttr	↓	↓

3.6.4 Hierarchical clustering of differentially expressed transcripts in 3 different stages of mouse spinal NT and MD

A high level analysis of Hierarchical clustering was performed using dChip V5.0 to further visualize the expression pattern. A total of 584 differentially expressed probe sets from the comparison of MHP- and DLHP- related genes were sent into the software for hierarchical clustering.

Changes in gene expression profiles of the total 18 samples, including 3 replicates for 2 different tissues (the NT and MD) at 3 critical stages (E8.5, E9.0 and E9.5) of neurulation were displayed as a clustering figure as in **Fig. 3.8**. In the clustering figure, each row represents a gene and each column represents a sample with the sample name displayed on top of each column.

On the left is the gene cluster tree which is called dendrogram and genes close to each other indicate that they have high similarities in their standardized expression values across the 18 samples. Each gene in each sample was represented by a colored box and colored according to its expression level. On the bottom of the clustering figure is the color scale: the red color signifies expression level above mean expression of a probe set across all samples, the white color represents mean expression and the blue color represents expression level lower than the mean.

Situated on the top is the sample clustering tree. The replicate samples collected for the same tissue at the same stage are clustered together, and samples from the same stage are clustered together, which indicate that samples used in this experiment have good quality, replicate samples have high similarity, and the data generated by microarray are reliable.

The clustering figure was roughly divided into 4 parts from top to bottom according to the expression levels among the 18 samples displayed by different colors. They are numbered as

1, 2, 3, and 4 for each cluster. Genes in cluster 1 exhibited a down-regulation at E8.5 and E9.0 of both NT and MD samples, but were up-regulated at E9.5 of NT and MD. This expression pattern indicates that they were MHP-up regulated genes. Genes in cluster 2 with an expression pattern of down-regulation at E8.5, but up-regulation at E9.0 and E9.5, these genes represent DLHP-up regulated genes. Genes in cluster 3 showed an up-regulation at E8.5 and down-regulation at E9.0 and E9.5 which indicate them as DLHP-down regulated genes. Finally, genes in cluster 4 demonstrated an up-regulation at E8.5 and E9.0, but a down-regulation at E9.5 signified the MHP-down regulated genes.

In the left panel on the screen also shows functional clusters, a local cluster enriched by genes with a particular function, by which a gene can be classified according to molecular function, biological process and cellular component using GO terms. 9 functionally significant gene clusters were displayed in the left panel with a default p-value < 0.005. They can be highlighted in blue as shown for the cell proliferation cluster in the clustering figure. The functional clusters were displayed as: a, development and enzyme linked receptor protein signaling pathway; b, cell proliferation; c, signal transduction activity; d, cell communication; e, cell motility; f, cell migration; g, nervous system development and morphogenesis. The genes in the same cluster can be represented by different functional clusters if they are enriched by several different functional terms as in cluster a and cluster g. Most of these functions were consistent with those from GO analysis and can assist in further investigation.

From the hierarchical cluster tree, we can tell that all the MHP- and DLHP- related genes by the microarray analysis have involved in nervous system development and morphogenesis. More than half of the genes have the function of cell migration. These genes expressed lower at both NT and MD at stage E8.5, the expression signaling increase gradually at E9.0 and reach the

highest at E9.5 at both NT and MD gene lists. A few genes among these function at the top of the map with an increased expression only in MD but decreased in NT at E9.5. Within the scope of cell motility the function, a few genes that involved in the enzyme linked receptor protein signaling pathway have a differential expression pattern with a relatively higher expression in NT at E8.5 and the most lower expression at E9.0 NT, while other group of genes with cell proliferation roles were demonstrated as have relatively higher expression levels in MD than in NT at all stages. At the lower 1/3 part of the map were a group of genes with signal transducer activity, the expression pattern of which were relatively different from the cell migration genes. They expressed high at E8.5 and decreased at E9.5. It seems that most of the signal transducer genes were from the MHP- and DLHP- down-regulated gene lists, while the genes involved in cell migration, cell proliferation, cell communication, and the enzyme linked receptor protein signaling pathway were distributed in the MHP- and DLHP- up-regulated gene lists.

This hierarchical cluster figure displays visually and directly of the expression pattern for all the samples, in addition, it can help the researchers to understand the distributed pattern of genes with different functions. More information can also be acquired by further analysis such as displaying profile plot for interested genes by linking to online resources.

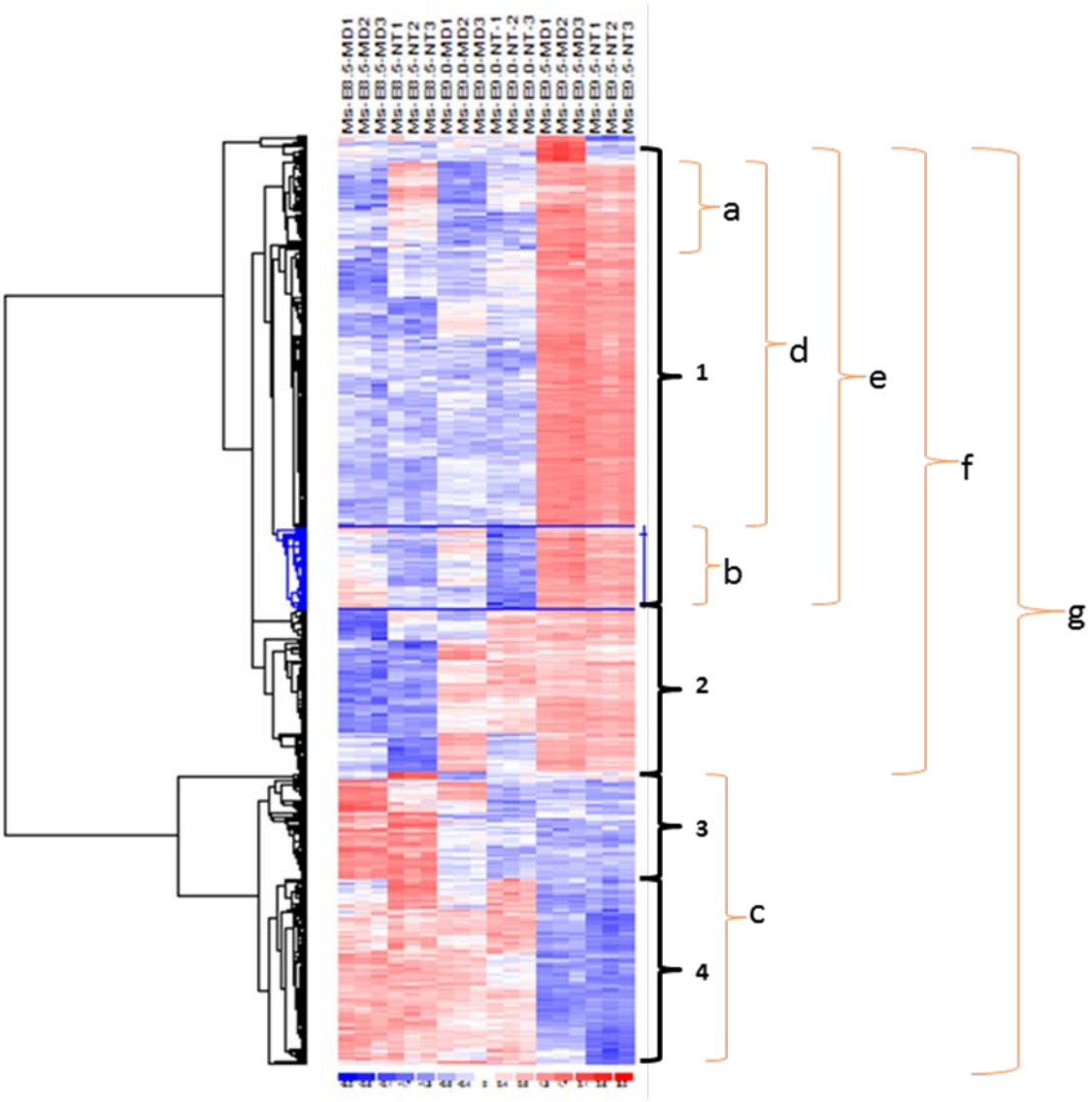

Fig. 3.8 Hierarchical cluster map of MHP- and DLHP-related genes. The trend analysis of gene expression patterns for the MHP- and DLHP- related genes were conducted by hierarchical clustering by dChip. Upper side indicated the 18 independent samples, including three triplicates of 3 stages (E8.5, E9.0 and E9.5) and 2 kinds of tissues (NT and MD). Each row represents one gene and each column represents one sample. Left side was the clustering tree which showed the genes with close relationship were clustered closer (high similarity in expression value and possible gene functions). Right side showed different clusters for different gene groups and functional clusters enriched by GO ontology terms for biological processes. Detailed interpretation can be seen in the main text. The bottom of the map showed the color scale. Red: up-regulated genes. Blue: down-regulated genes. White: no changed genes. Cluster 1: MHP-up-regulated genes; Cluster 2: DLHP-up-regulated genes; Cluster 3: MHP-down-regulated genes; Cluster 4: DLHP-down-regulated genes; Cluster a: Development; Enzyme linked receptor protein signaling pathway; Cluster b: Cell proliferation; Cluster c: signal transduction activity; Cluster d: Cell communication; Cluster e: Cell motility; Cluster f: Cell migration; Cluster g: Nervous system development; Morphogenesis.

3.6.5 Gene Ontology enrichment of differentially expressed genes related to MHP and DLHP formation

In order to assess the association of gene expression with cellular events during biological process, the differentially expressed genes from the 8 MHP- and DLHP- related groups were analyzed by gene ontology (GO) of DAVID: The online **D**atabase for **A**nnotation, **V**isualization and **I**ntegrated **D**iscovery (**DAVID**). 10 main functional gene clusters related with embryonic development were defined based on the functional classification terms used in GO (**Table 3.8**). Each of these clusters indicate functional-related gene groups that having similar biological meaning and sharing similar genes. Shared genes were counted only once to be included in the number (No.) of genes in each cluster. Analysis of GO enrichment revealed multiple developmental functions and pathways dominated by the genes associated with: growth-related (GR), cell structure and communication (CSC), morphogenesis, cell motility and migration (CMM), signal transduction (ST), transcription (TX), nucleic acid metabolism and chromosome dynamics (NMCD), carbohydrate, lipid, and amino acid metabolism (CLAM), intra/inner cellular molecular transport (ICMT), and pathways such as TGF-β signaling pathway, FGFR signaling pathway, and Wnt receptor signaling pathway. This table could help us interpret the biological events during critical stages of neurulation in a group level.

A detailed analysis of the distribution of functional clusters implicated a dynamic distribution of biological events during neurulation in temporal as MHP-related genes compared with DLHP-related genes, and in spatial as MHP-NT genes compared with MHP-MD genes, and DLHP-NT compared with DLHP-MD genes. Cell growth, communication, signal transduction, transcription, as well as molecular metabolism seems more active in earlier stages of neurulation than in late stages since more related genes expressed in MHP-related gene lists than in DLHP-

related gene lists (**Table 3.8**). However, cell motility and morphogenetic ability seems similar in late stages as compared with earlier stages. Moreover, functions in development, cell maturation, transcription, molecular metabolism, as well as intra/inner cellular molecular transport were also active in late stages with many genes expressed in both DLHP-NT and DLHP-MD lists. This dynamic distribution of functional clusters may reveal the biological events during the process of neural tube closure: cells grow and differentiate fast in earlier stages while become mature in late stages, while requirement of morphogenesis of cells as well as neural tube are all through the neurulation process.

As for the similarity or difference between the two adjacent tissues, it seems that there is not much difference in activity of development, cell maturation, cell structure and communication, morphogenesis and cell motility, signal transduction, transcription, as well as metabolism between NT and MD in earlier stages revealed by MHP-NT and MHP-MD related genes (**Table 3.8**). Almost all cellular events except molecule transport were more active in DLHP-NT than in DLHP-MD. This may be due to at the late stages of neurulation, the forces of NT closure comes from interior NT more than in the surrounding MD, the paraxial mesoderm in mode 3 is reduced and cells here more simplex (**Fig.3.2**). Gene expression indicates that in earlier stages, genes highly expressed in both NT and MD, while in later stages, genes expressed mainly in NT rather than MD. This result is consistent with the hypothesis that forces for neural tube closure were from surrounding tissues in earlier stages while mainly depend on interior forces in later stages (Shum and Copp, 1996).

Table 3.8 GO analysis of MHP- and DLHP-related genes.

Functional clusters	MHP-NT (No. of genes)	MHP-MD (No. of genes)	DLHP-NT (No. of genes)	DLHP-MD (No. of genes)
Growth- related (GR)	70	67	37	10
Cell proliferation-related	11	6	11	2
Cell differentiation-related	18	20	5	3
Others (development and maturation)	41	41	21	7
Cell structure and communication (CSC)	17	22	7	4
Cell adhesion and recognition-related	10	10	7	1
Cytoskeleton-related	7	12	1	4
Morphogenesis	18	18	19	6
CMM	10	10	10	4
ST	6	9	4	2
TX	17	26	13	8
NMCD	18	22	12	8
CLAM	20	30	15	7
ICMT	4	1	4	3
Pathway genes	10	6	4	2

CMM: Cell motility/cell migration; ST: Signaling transduction; TX: Transcription; NMCD: Nucleic acid metabolism and chromosome dynamics; CLAM: Carbohydrate, lipid, and amino acid metabolism; ICMT: Intra/inner cellular molecular transport.

3.6.6 Transcriptomic analysis of gene expression during critical stages of neurulation reveals associations to diverse biological processes and multiple pathways

Since each gene has multiple functions during different biological events, in order to know the most possible role that it does during the neurulation process, the functions of the genes enriched by GO analysis were compared with their functions recorded in NetAffex gene information cards and in the Pub med gene cards. Additionally, all genes in the MHP- and DLHP-related lists were checked in investigations of PubMed by literature research. More functions have been found for these genes, e.g., cell cycle, apoptosis, migration, RTK, GPCR, as well as intracellular signaling cascades, proteolysis, pigmentation, phosphorylation, etc. One common function for each gene, especially those involved in development, nervous system development, or neural tube closure has the privilege to be selected as possible functions during

neurulation process and listed in the tables below (from **table 3.9** to **table 3.16**). These tables provided preliminary data and setup a framework for potential candidate genes for further investigation. Since all microarray analysis software gave similar fold change for each gene, results presented here based on the results generated by GCOS.

The first three columns of each table presented the Affymetrix probe set ID, full name, and gene symbol for each gene. Fold changes between different stages for each gene were listed which revealed its differential expression during neurulation. Up-regulated genes in Table 3.9 and 3.11 refer to the genes presented in NT (**Table 3.9**) and surrounding MD (**Table 3.11**) that expressed lower at E8.5 and E9.0 when MHP presents but their expression increased more than 2 fold at E9.5 when MHP disappears. They may play a role in inhibiting MHP. At the same time, down-regulated genes in table 3.10 and 3.12 denote genes with higher expression in NT (**Table 3.10**) and MD (**Table 3.12**) at E8.5 and E9.0 when MHP presents, but their expression decreased more than 2 fold at E9.5 when MHP disappears. These genes may play a part in sustaining the MHP. Genes listed in other four tables were related with the formation of DLHPs. Up-regulated genes in Table 3.13 and 3.15 refer to the genes presented in NT (**Table 3.13**) and surrounding MD (**Table 3.15**) that expressed lower at E8.5 in absent of DLHPs but their expression increased more than 2 fold at E9.0 and E9.5 when DLHPs take shape and sustain. They may motivate and accelerate the formation of DLHPs. At the same time, down-regulated genes in table 3.14 and 3.16 represent genes with higher expression in NT (**Table 3.14**) and MD (**Table 3.16**) at E8.5 before DLHPs present, but their expression decreased more than 2 fold at E9.0 and E9.5 when DLHPs appear. These genes may function in inhibiting DLHP formation, and inhibition of them can contribute to the formation of DLHPs.

The genes of multiple functions display a dynamic temporal and spatial difference among all stages. We describe most of the listed genes here and discuss their potential functions of the critical genes in neurulation later.

3.6.6.1 Expression of genes related with cell growth

We identified more than 60 cell growth-related genes including many that were not previously associated with neurulation. These genes were related with proliferation, differentiation, cell cycle regulation, apoptosis, cell maturation and/or embryonic development. Some genes have more than one function revealed by GO, but only one of the function were listed in the tables as mentioned above.

Genes related with cell growth were expressed in all of the 8 MHP- and DLHP- related gene groups, but they were highly represented in up-regulated gene groups of MHP-NT (19 in **Table 3.9**), MHP-MD (10 in **Table 3.11**), DLHP-NT (9 in **Table 3.13**) and DLHP-MD (3 in **Table 3.15**), while less genes with the same function presented in down-regulated gene groups of MHP-NT (8 in **Table 3.10**), MHP-MD (4 in **Table 3.12**), DLHP-NT (3 in **Table 3.14**) and DLHP-MD (2 in **Table 3.16**). There were more than a dozen genes with regulation function of cell proliferation in the MHP-NT related gene groups revealed by GO, 5 of which have negative regulation function of cell proliferation. The 5 genes were: *Pthr, Serpinf1, and Tgfb2* in **Table 3.9**, *Gtpbp4*, and *Spry2* in **Table 3.10.** And the remaining genes were: *Foxp2, Hoxd13, Igf1, kdr, Pdgfc, Fabp7*, and *Cdk4* in **Table 3.9,** and *Vzg1* **in Table 3.10**. There were 12 genes related with regulation of proliferation function in the DLHP-NT groups revealed by GO, and 5 of them were having negative regulation function. The 5 genes were: *Igfbp3, Serpinf1*, and *Wnt5a* in **Table 3.13**, *Cer1*, and *Rbp4* in **Table 3.14**. The other 6 genes were: *CD40, Sox2, Fgf17, Fabp7,*

Hoxd13 in **Table 3.13**, and *Ccnd2, Tcfl5* in **Table 3.14**. There were 7 genes with function of proliferation revealed by GO in the MHP-MD related gene lists, *Foxp2, Ccnd2, Fabp7,* and *Tgfbi* in **Table 3.11**, and *Fgf9, Spry2, Ppp1r14b* in **Table 3.12**. In DLHP-MD related genes, 3 genes related with cell proliferation were listed, *Fgf17,* and *Fabp7* in **Table 3.15**, and *Rbp4* in **Table 3.16**. Theoretically, when the genes of *Gtpbp4* and *Spry2* with negative regulation of cell proliferation function expressed in MHP-down-related gene groups, growth of certain cell populations will be inhibited during MHP formation, but the formation of MHP has positive correlation with these genes. In the MHP-up-regulated gene groups, expression of genes with negative regulation of cell proliferation function, such as *Pthr, Serpinf1,* and *Tgfbi* may have negative correlation with the formation of MHP. The Absolute Intensity of these 3 genes at E8.5 and E9.0 were low when the MHP existed, but the expression became high at E9.5 when the MHP was inhibited. The expression of genes with cell proliferation function in the MHP-up-regulated groups were negatively related with the formation of MHP, for their expression were low at E8.5 and E9.0 when MHP existed, but the expression became high at E9.5 when the MHP was inhibited. Similarly, expression of genes with negative regulation of cell proliferation function such as *Cer1* and *Rbp4* in DLHP-down-regulated groups were negatively correlated with the formation of DLHP. Because the expression of these genes were high at E8.5 when there was no DLHP, while their expression became low at E9.0 and E9.5 when the DLHPs forms and existed. Besides, the other 3 genes with negative regulation of cell proliferation function in the DLHP-up-regulated groups, *Igfbp3, Serpinf1*, and *Wnt5a* may have positive correlation with the formation of DLHP, because they were lowly expressed at E8.5 when there was no DLHP, but highly expressed at E9.0 and E9.5 when the DLHP were formed and existed. It is postulated that these two groups of genes may act on the same populations of genes with reverse actions.

Likewise, genes with regulation function of cell proliferation function in DLHP-up-regulated groups, such as *CD40, Sox2, Fgf17,* may have positive correlation with formation of DLHPs, while genes with regulation of cell proliferation function in the DLHP-down-regulated groups, such as *Ccnd2* and *Tcfl5,* may have negative correlation with formation of DLHPs.

Genes regulating cell cycle were highly down-regulated in MHP-NT group (5 genes of *Gtpbp4, Seh1l, Aspm, Ppp1cb, Rbbp4* in **Table 3.10**), and DLHP-NT group (*Ccnd2* in **Table 3.12**), but few of the cell cycle genes were up-regulated in MHP-NT group (*Cdk4* in **Table 3.9**). Genes with apoptosis function were mainly expressed in the up-regulated groups: MHP-NT-up (3 genes of *Psme3, Eya1,* and *Rnf216* in **Table 3.9**), MHP-MD-up (3 genes of *Actc1, Tia1,* and *Psme3* in **Table 3.10**), DLHP-NT-up (*Dhcr24* in **Table 3.13**), DLHP-MD-up (*Actc1* and *Alx3* in **Table 3.15**), and only one expressed in the MHP-MD-down-regulated group (*Rffl* in **Table 3.12**). The expression patterns of cell cycle and apoptosis genes shows that growth is regulated during the presence or absence of MHP and DLHPs in addition to the universal growth feature in neurulation stage embryos.

Cell differentiation at the end of neurulation became active, which were reflected by the expression pattern of genes with function of cell differentiation revealed by GO. Most of the cell differentiation genes were up-regulated in the MHP- and DLHP- related groups, including Epha7, *Top2b, Tubb3, Isl1, Mtap2, Rncr2, Nefl2, Onecut2* in MHP-NT-up-regulated group (**Table 3.9**), *Irx5, Cutl1, Dclk1, Kif5c, Mtap1b,* and *Stmn3* in MHP-MD-up-regulated group (**Table 3.11**), which may be positively correlated with the differentiation of cells at the MHP; and *Socs2, Foxd1, Hoxc10,* and *Lpl* in DLHP-NT-up-regulated group (**Table 3.13**), and *Socs2* in DLHP-MD-up-regulated group (**Table 3.15**), which may be positively correlated with the differentiation of cells at the DLHPs. A few genes with function of cell differentiation were presented in the

down-regulated gene groups, including *Cxcr4, Aspm, Ttc3* in MHP-NT-down-regulated group (**Table 3.10**), *Ubc* in MHP-MD-down-regulated group (**Table 3.12**). These genes may be negatively related with cell differentiation at MHP. *Nrcam, Alcam, Ptprz1*, and *Ret* in DLHP-NT-down-regulated group (**Table 3.14**), *Ptprz1* were presented in DLHP-MD-down-regulated group (**Table 3.16**), which may be negatively correlated with cell differentiation at DLHPs. The formation of MHP and DLHPs by bending and folding of the neural folds during neurulation were accompanied with cell morphogenesis (Colas and Schoenwolf, 2001). It was revealed by GO that some of the cell differentiation genes have function involved in morphogenesis which were important for neurulation. These genes include: *Nefl, Nefm, Ttc3, Epha7, Isl1*, and *Top2b* in MHP-NT-up-regulated group (**Table 3.9**), *Cxcr4* in MHP-NT-down-regulated group (**Table 3.10**), *Dclk1* and *Kif5c* in MHP-MD-up-regulated group (**Table 3.11**), *Alcam* and *Foxd1* in DLHP-NT-up-regulated group (**Table 3.13**), *Nrcam* and *Ptprz1* in DLHP-NT-down-regulated group (**Table 3.14**).

3.6.6.2 Cell structure and adhesion related genes:

Cell structure and adhesion related genes provide mechanical support and transport for the process of neural tube closure. The extracellular matrix interacting with cell surface receptors via cytoskeleton-mediated events are important for cell shape and polarization. Cytoskeleton has a potential role for formation and movement of the neural folds, while the initiation of fusion at the tips of the closing neural folds could be facilitated by cell adhesion molecules. In the current microarray results, the cell structure and adhesion related genes were dominantly expressed in the up-regulated groups: 15 in **Table 3.9**, 13 in **Table 3.11**, 5 in **Table 3.13**, and 3 in **Table 3.15**,

while less genes were down-regulated: 5 in **Table 3.10**, 4 in **Table 3.14**, 1 in **Table 3.12** and **3.16**.

Cytoskeleton proteins have been shown playing an essential role in neural tube defects, especially for cranial closure (Copp and Greene, 2010b). Actin neurofilaments are localized at the apical side of cells in the neural folds (Sadler et al., 1982; Zolessi and Arruti, 2001). The neuroepithelial cells wedged within the hinge points involves apical narrowing with the presence of circumferential microfilaments (Lee and Nagele, 1985), and basal expansion which may be due to the position of nuclei of newly formed daughter cells migrating from the apex toward the base of neuroepithelial cells mediated by microtubules (Smith and Schoenwolf, 1988). Microfilaments may play a role in stabilizing the shape of the neural folds or newly formed neural tube (Schoenwolf and Smith, 1990).

Cell structure related genes such as *Nefl, Nefm, Mtap2, Tubb3, Epb4.1l3,* and *Synpo* were up-regulated in the MHP-NT related group (**Table 9**), and Seh1l was down-regulated in the MHP-NT group (**Table 10**). In the MHP-MD related groups, *Kif21a, Kif5c, Mtap1b, Mtap2, Stmn3, Tmsb10, Mid1, Actc1,* and *Mgl2* were up-regulated (**Table 11**), while *Seh1l* was down-regulated (**Table 12**). These are newly found genes that are not reported related with neurulation. Adhesion molecules were also found mostly up-regulated with a few down-regulated in the microarray results. Those presented in MHP-NT group include: *Cdh11, Cldn5, Col3a1, Col9a1, Megf10, Thbs1, Edil3, Itga9 Epha7* and *Nid1*in **Table 9,** and Epha5 in **Table 10**. In MHP-MD group presented: *Celsr2, Gpr98, Cad11, Cd2a1, Lgals,* and *Tgfbi* (**Table 11**). Expression of these genes were high at E9.5 when MHP disappeared compared with at E8.5 and E9.0 when MHP existed, this may imply that adhesion may not be important for MHP formation.

In DLHP-NT related groups, *CD44*, *Fat4*, *Antxr*, and *Postn* were up-regulated (**Table 13**), while *Alcam*, *Nrcam*, and *Ret* were down-regulated (**Table 14**). This expression pattern indicates that cell adhesion was actively regulated during the formation of DLHP and imply an essential role of adhesion function in initiation of neural tube closure.

It is noticed that 2 of the 4 adhesion molecules in DLHP-NT-down-regulation group, *CD44*, and *Sdc4*, were found related with neural tube defects. Both *CD44* and *Sdc4* belong to GAG genes, the former was involved in tube morphogenesis and the later played a role in cell proliferation. *Celsr2*, *Epha5*, and *Epha7*, which were found in MHP-related gene groups were also found related to neural tube defects, though their roles were not confirmed.

3.6.6.3 Transcription factors and NMCD molecules:

The activity of transcription factors were found active through stages of neurulation in both NT and MD. Many genes with function of differentiation and proliferation are transcriptional factors in molecule level, some of them also play roles in morphogenesis, which was a critical process for neurulation. Many NMCD genes were transcription factor, too. They were important in regulation of gene expression, mutation of which lead to all kinds of diseases. The transcription factors, *Zic3* and *Twist 1* in **Table 3.9**, *Jmjd3*, *Zic2* and *Sall4* in **Table 3.10**, *Celsr2* in **Table 3.11**, *Wnt5a* in **Table 3.13**, were well known critical genes to neural tube closure, mutation of which lead to NTDs, especially spida bifida.

3.6.6.4 Genes linked to multiple pathways

There were 4 main pathways revealed by GO biological process: Transmembrane receptor protein tyrosine kinase signaling pathway (TRPTK), enzyme linked receptor protein signaling pathway (ERP), Wnt receptor signaling pathway (Wnt), and regulation of transforming growth factor beta receptor signaling pathway (TGFbR). The TRPTK pathway has high similarity with ERP pathway since they have 11 common genes: *Epha7, Ddr2, Fgf17, Fgf9, Igf1, Kdr, Pdgfc, Ror1, Ret, Mrf1l,* and *Tgfb2*. In addition, TRPTKS pathway has another 3 genes found in the neurulation process: *Epha5, Rgs2*, and *Arid5b*, while ERP pathway has one more: *Rgmb*. 6 Wnt pathway genes were found: *Wnt5a*, *Wif1*, *Frd3*, *Frd5*, *Celsr2*, and *Sostdc1*. In addition, *Fgf9* was a known Wnt pathway related gene. TGFbR pathway genes include: *Onecut2, Thbs1, Prdm16*, Gdf10 (Bmp3b), and *Cer1*. Furthermore, gene analysis by NetAffyx center and literature research also revealed 5 more pathways: GPCR, Notch (*Dtx4*), Fgf (*Fgf9, Fgf17*, and *Igf1*), Smoothened (*Tgfbr2* and *Fgf9*), and PDGF (*Arid5b*). Among these, GPCR pathway has more genes: *Gper, Edg3, Edg2, Cxcr4, Vzg1, Gng4, Rgs2* (also known as TRPTK pathway gene), and *Celsr2* (also known as Wnt pathway gene). These pathway genes were differentially expressed among stages of neurulation in NT and/or MD. Further investigation of their function and regulation are sure to promote our knowledge about the neurulation process.

Table 3.9 MHP-NT related up-regulated genes

			Fold change			
Probe set	**Gene name**	**Gene Symbol**	**85vs95**	**90vs95**	**85+90vs95**	**gene function**
1452163_at	E26 avian leukemia oncogene 1, 5' domain	Ets1	6.38	6.91	6.63	differentiation
1441956_s_at	cut-like homeobox 1	Cutl1	2.52	3.07	2.78	differentiation
1449077_at	erythroid associated factor	Eraf	3.39	2.47	2.86	differentiation
1418698_a_at	ferrochelatase	Fech	2.25	2.06	2.15	differentiation
1415978_at	tubulin, beta 3; tubulin, beta 3, pseudogene 1	Tubb3	10.24	2.43	3.93	differentiation
1455325_at	myocardial infarction associated transcript (non-protein coding)	Rncr2	2.98	2.82	2.89	differentiation
1460044_at	one cut domain, family member 2	Onecut2	5.59	3.07	4	differentiation
1456688_at	topoisomerase (DNA) II beta	Top2b	4.06	2.59	3.16	differentiation
1434194_at	microtubule-associated protein 2	Mtap2	7.21	3.06	4.29	differentiation
1454672_at	neurofilament, light polypeptide	Nefl	3.16	4.27	3.63	differentiation
1451991_at	Eph receptor A7	Epha7	6.9	6.51	6.7	differentiation
1450723_at	ISL1 transcription factor, LIM/homeodomain	Isl1	3.41	4.08	3.71	differentiation
1438658_a_at	sphingosine-1-phosphate receptor 3	Edg3	2.4	2.49	2.44	differentiation
1426801_at	septin 8	Sept--8	2.34	1.93	2.11	proliferation
1437401_at	insulin-like growth factor 1	Igf1	4.35	5.66	4.92	proliferation
1419123_a_at	platelet-derived growth factor, C polypeptide	Pdgfc	2.7	1.97	2.28	proliferation
1426397_at	transforming growth factor, beta receptor II	Tgfbr2	3.22	2.96	3.09	proliferation
1454867_at	meningioma 1	Mn1	3.99	3.92	3.95	proliferation
1417092_at	parathyroid hormone receptor 1	Pthr	2.35	4.75	3.14	proliferation
1416168_at	serine (or cysteine) peptidase inhibitor, clade F, member 1	Serpinf1	6.69	2.26	3.38	proliferation
1440626_at	homeo box D13	Hoxd13	29.86	7.57	15.03	proliferation
1449379_at	kinase insert domain protein receptor	Kdr	2.15	2.23	2.19	proliferation
1438231_at	forkhead box P2	Foxp2	2.85	2.27	2.53	proliferation
1450779_at	fatty acid binding protein 7, brain	Fabp7	26.49	7.8	12.05	proliferation
1422440_at	similar to Cell division protein kinase 4 (Cyclin-dependent kinase 4) (PSK-J3) (CRK3); cyclin-dependent kinase 4	Cdk4	2.18	1.98	2.08	cell cycle
1418078_at	proteaseome (prosome, macropain) 28 subunit, 3	Psme3	2.64	2.84	2.74	apoptosis
1457424_at	eyes absent 1 homolog (Drosophila)	Eya1	2.35	5.63	3.31	apoptosis
1437532_at	ring finger protein 216	Rnf216	2.57	2.12	2.32	apoptosis
1450757_at	cadherin 11	Cdh11	5.27	2.45	3.35	adhesion
1417839_at	claudin 5	Cldn5	3	2.75	2.87	adhesion
1427883_a_at	collagen, type III, alpha 1	Col3a1	14.84	4.92	7.39	adhesion
1428571_at	collagen, type IX, alpha 1	Col9a1	3.16	4.01	3.54	adhesion
1429841_at	multiple EGF-like-domains 10	Megf10	4.94	3.42	4.05	adhesion
1416808_at	similar to Nidogen precursor (Entactin); nidogen 1; similar to Nid1 protein	Nid1	4.13	4.65	4.37	adhesion
1421811_at	thrombospondin 1; similar to thrombospondin 1	Thbs1	3.23	3.1	2.4	adhesion
1460285_at	integrin alpha 9	Itga9	1.84	2.53	2.13	adhesion
1433474_at	EGF-like repeats and discoidin I-like domains 3	Edil3	2.75	2.6	2.67	adhesion
1436568_at	junction adhesion molecule 2	Jam2	5.78	3.52	4.38	adhesion
1440595_at	erythrocyte protein band 4.1-like 3	Epb4.1l3	2.41	2.5	2.46	cytoskeleton organization
1422520_at	neurofilament, medium polypeptide	Nefm	10.77	19	13.75	cytoskeleton organization
1434089_at	synaptopodin	Synpo	3.17	3.53	3.34	cytoskeleton organization

1438239_at	similar to midline 1; midline 1	Mid1	4.84	4.32	4.56	cytoskeleton organization
1416159_at	similar to COUP-TFI; nuclear receptor subfamily 2, group F, member 2	Nr2f2	3.08	5.34	3.91	migration
1429372_at	SRY-box containing gene 11	Sox11	2.1	1.87	1.98	transcription
1454758_a_at	TSC22 domain family, member 1	Tsc22d1	1.93	1.86	1.89	transcription
1444615_x_at	runt-related transcription factor 1; translocated to, 1 (cyclin D-related)	Runx1t1	5.02	5.41	5.21	transcription
1435670_at	transcription factor AP-2 beta	Tcfap2b	9.04	8.3	8.65	transcription
1437556_at	zinc finger homeodomain 4	Zfhx4	6.26	8.32	7.15	transcription
1438737_at	zinc finger protein of the cerebellum 3	Zic3	4.09	6.05	4.88	transcription
1418733_at	twist homolog 1 (Drosophila)	Twist1	2.85	7.47	4.13	transcription
1440870_at	PR domain containing 16	Prdm16	4.22	5.2	4.66	NMCD
1439123_at	PHD finger protein 21A	Phf21a	2.74	2.14	2.4	NMCD
1441333_at	trichorhinophalangeal syndrome I (human); similar to Trps1 protein	Trps1	3.63	2.62	3.05	NMCD
1421923_at	SH3-domain binding protein 5 (BTK-associated)	Sh3bp5	3.56	2.17	2.69	intracellula signaling cascades
1433919_at	ankyrin repeat and SOCS box-containing 4	Asb4	2.71	2.44	2.57	intracellula signaling cascades
1418364_a_at	ferritin light chain 1	Ftl1	3.26	1.88	2.39	transport
1437165_a_at	procollagen C-endopeptidase enhancer protein	Pcolce	6.57	3.37	4.45	proteolysis
1424886_at	protein tyrosine phosphatase, receptor type, D	Ptprd	4.61	2.7	3.4	dephosphorylation
1417750_a_at	solute carrier family 25, member 37	Slc25a37	2.11	2.22	2.16	transport
1425315_at	dedicator of cytokinesis 7	Dock7	3.2	1.9	2.38	pigmentation
1448346_at	cofilin 1, non-muscle	Cfl1	2.22	1.76	1.96	
1460436_at	N-deacetylase/N-sulfotransferase (heparan glucosaminyl) 1	Ndst1	2.43	1.97	2.17	GAG synthesis
1423091_a_at	glycoprotein m6b	Gpm6b	14.4	11.81	12.98	Glycoprotein
1455604_at	frizzled homolog 5 (Drosophila)	Fzd5	2.92	3.07	2.99	Wnt signaling

Table 3.10 MHP-NT related down-regulated genes

Probe set	Gene name	Gene Symbol	Fold Change			gene function 1
			85vs95	90vs95	85+90vs95	
1421144_at	retinitis pigmentosa GTPase regulator interacting protein 1	Rpgrip1	-8.06	-3.99	-6.03	differentiation
1416484_at	tetratricopeptide repeat domain 3	Ttc3	-2.33	-2.38	-2.36	differentiation
1458560_at	asp (abnormal spindle)-like, microcephaly associated (Drosophila)	Aspm	-3.69	-3.1	-3.39	differentiation
1448710_at	chemokine (C-X-C motif) receptor 4	Cxcr4	-2.59	-2.59	-2.59	differentiation
1448606_at	lysophosphatidic acid receptor 1	Vzg1	-3.45	-3.12	-3.32	proliferation
1423143_at	GTP binding protein 4	Gtpbp4	-3	-4	-3.5	proliferation
1436584_at	sprouty homolog 2 (Drosophila)	Spry2	-3.67	-3.77	-3.72	proliferation
1431328_at	protein phosphatase 1, catalytic subunit, beta isoform	Ppp1cb	-3.22	-3.58	-3.4	cell cycle
1456260_at	retinoblastoma binding protein 4	Rbbp4	-2.47	-2.53	-2.5	cell cycle
1419967_at	SEH1-like (S. cerevisiae)	Seh1l	-3.16	-3.08	-3.12	cell cycle
1437920_at	Eph receptor A5	Epha5	-3.71	-3.25	-3.48	adhesion
1426865_a_at	neural cell adhesion molecule 1	Ncam1	-3.77	-3.89	-3.83	adhesion
1449799_s_at	plakophilin 2	Pkp2	-4.92	-3.52	-4.22	adhesion

1438556_a_at	tropomodulin 3	Tmod3	-2.77	-3.16	-2.97	cytoskeleton organization
1422719_s_at	nucleoporin 50	Nup50	-2.9	-2.52	-2.71	morphogenesis
1440346_at	Jumonji domain containing 3	Jmjd3	-3.14	-2.78	-2.96	transcription
1418024_at	NMDA receptor-regulated gene 1	Narg1	-3.22	-3.14	-3.18	transcription
1421933_at	chromobox homolog 5 (Drosophila HP1a)	Cbx5	-3.43	-4.16	-3.79	transcription
1424153_s_at	sal-like 4 (Drosophila)	Sall4	-4.66	-9.97	-7.31	transcription
1449578_at	suppressor of Ty 16 homolog (S. cerevisiae)	Supt16h	-2.8	-2.27	-2.54	transcription
1434644_at	transducin (beta)-like 1 X-linked	Tbl1x	-2.51	-2.84	-2.67	transcription
1421301_at	zinc finger protein of the cerebellum 2	Zic2	-2.86	-2.67	-2.76	transcription
1450035_a_at	PRP40 pre-mRNA processing factor 40 homolog A (yeast)	Prpf40a	-2.53	-2.79	-2.66	NMCD
1452540_a_at	similar to Hist1h2bj protein; histone cluster 1, H2bl; predicted gene	Hist1h2bm	-2.23	-2.5	-2.37	NMCD
1418227_at	origin recognition complex, subunit 2-like (S. cerevisiae)	Orc2l	-2.69	-3.83	-3.26	NMCD
1427262_at	inactive X specific transcripts	Xist	-3.53	-3.14	-3.34	NMCD
1447869_x_at	Rho-related BTB domain containing 3	Rhobtb3	-6.77	-3.55	-5.16	transport
1452454_at	SDA1 domain containing 1; similar to SDA1 domain containing 1	Sdad1	-2.55	-3.38	-2.97	transport
1426269_at	predicted gene 14338; vesicle-associated membrane protein 7	Vamp7	-2.36	-2.73	-2.55	transport
1416062_at	TBC1 domain family, member 15	Tbc1d15	-4.58	-3.44	-4.01	regulation of Rab, GTPase, Ras activity
1417695_a_at	sterol O-acyltransferase 1	Soat1	-4.46	-3.94	-4.2	CLAM
1458347_s_at	transmembrane protease, serine 2	Tmprss2	-3.81	-2.82	-3.32	proteolysis
1450954_at	YME1-like 1 (S. cerevisiae)	Yme1l1	-2.79	-3.75	-3.27	proteolysis
1418014_a_at	betaGlcNAc beta 1,4- galactosyltransferase, polypeptide 1	B4galt1	-2.5	-1.65	-2.68	GAG synthesis
1423674_at	ubiquitin specific peptidase 1; predicted gene 5841	Usp1	-2.71	-3.25	-2.98	regulation of cellular response to stress

Table 3.11 MHP-MD related up-regulated genes

			Fold change			
Probe set	**Gene name**	**Gene Symbol**	**85vs95**	**90vs95**	**85+90vs95**	**gene function**
1421072_at	Iroquois related homeobox 5 (Drosophila)	Irx5	4.37	5.65	4.93	differentiation
1441956_s_at	cut-like homeobox 1	Cutl1	4.27	2.78	3.37	differentiation
1436659_at	doublecortin-like kinase 1	Dclk1	3.39	2.73	3.02	differentiation
1452163_at	E26 avian leukemia oncogene 1, 5' domain	Ets1	2.15	2.04	2.09	differentiation
1451991_at	Eph receptor A7	Epha7	16.12	5.92	2.5	differentiation
1418467_at	SWI/SNF related, matrix associated, actin dependent regulator of chromatin, subfamily d, member 3	Smarcd3	2.49	2.32	2.4	differentiation
1450397_at	microtubule-associated protein 1B	Mtap1b	4.64	4.73	4.68	differentiation
1434194_at	microtubule-associated protein 2	Mtap2	10.93	4.93	6.79	differentiation
1422945_a_at	kinesin family member 5C	Kif5c	5.09	2.59	3.44	differentiation
1435113_x_at	stathmin-like 3	Stmn3	3.58	4.47	2.29	differentiation
1419247_at	regulator of G-protein signaling 2	Rgs2	3.36	3.15	3.25	differentiation
1438232_at	forkhead box P2	Foxp2	3.62	2.86	3.2	proliferation
1448123_s_at	transforming growth factor, beta induced	Tgfbi	6.73	2.93	4.09	proliferation
1450779_at	fatty acid binding protein 7, brain	Fabp7	45.52	3.94	7.26	proliferation
1430127_a_at	cyclin D2	Ccnd2	2.26	2.24	2.25	cell cycle

1431708_a_at	cytotoxic granule-associated RNA binding protein 1	Tia1	2	1.93	13.1	apoptosis
1418078_at	proteaseome (prosome, macropain) 28 subunit, 3	Psme3	2.91	2.63	1.96	apoptosis
1415927_at	actin, alpha, cardiac muscle 1; similar to alpha-actin (AA 27-375)	Actc1	25.11	8.85	8.66	apoptosis
1435336_at	cadherin, EGF LAG seven-pass G-type receptor 2 (flamingo homolog, Drosophila)	Celsr2	2.21	2.41	2.31	adhesion
1450567_a_at	collagen, type II, alpha 1	Col2a1	3.64	3.09	3.35	adhesion
1455439_a_at	lectin, galactose binding, soluble 1	Lgals1	2.02	2.07	2.04	adhesion
1445740_at	G protein-coupled receptor 98	Gpr98	6.77	4.92	5.7	adhesion
1446245_at	Cadherin 11	Cad11	2.78	2.47	2.62	adhesion
1448394_at	myosin, light polypeptide 2, regulatory, cardiac, slow	Myl2	10.11	11.82	10.9	cytoskeleton organization
1415927_at	actin, alpha, cardiac muscle 1; similar to alpha-actin (AA 27-375)	Actc1	25.11	8.85	8.66	cytoskeleton organization
1455029_at	kinesin family member 21A	Kif21a	3.24	2.93	3.08	microtubule-based process
1417219_s_at	predicted gene 3787; predicted gene 9844; predicted gene 8034; similar to thymosin, beta 10; thymosin, beta 10	Tmsb10	3.35	2.85	3.08	cytoskeleton organization,
1418370_at	troponin C, cardiac/slow skeletal	Tnnc1	5.69	8.6	6.85	cytoskeleton organization
1450641_at	vimentin	Vim	3.96	2.2	2.83	cytoskeleton organization
1427883_a_at	collagen, type III, alpha 1	Col3a1	6.89	4.48	5.43	extracellular matrix organization
1456062_at	natriuretic peptide precursor type A	Nppa	8.89	8.86	8.87	regulation of tube size
1441107_at	doublesex and mab-3 related transcription factor like family A2	Dmrta2	2.64	4.95	3.44	transcription
1436931_at	regulatory factor X, 4 (influences HLA class II expression)	Rfx4	6.16	10.03	7.63	transcription
1444615_x_at	runt-related transcription factor 1; translocated to, 1 (cyclin D-related)	Runx1t1	4.96	4.95	4.95	transcription
1418157_at	similar to COUP-TFI; nuclear receptor subfamily 2, group F, member 2	Nr2f1	9.17	60.82	15.9	transcription
1437556_at	zinc finger homeodomain 4	Zfhx4	2.94	3.77	3.3	transcription
1423895_a_at	CUG triplet repeat, RNA binding protein 2	Cugbp2	2.55	3.72	3.02	NMCD
1417440_at	similar to AT rich interactive domain 1A isoform a; AT rich interactive domain 1A (SWI-like)	Arid1a	5.24	2.95	3.77	NMCD
1421923_at	SH3-domain binding protein 5 (BTK-associated)	Sh3bp5	2.24	2.33	2.77	intracellula signaling cascades
1434369_a_at	crystallin, alpha B	Cryab	3.18	2.19	2.59	response to abiotic stimulus,
1425315_at	dedicator of cytokinesis 7	Dock7	3.81	2.11	2.72	pigmentation
1436545_at	deltex 4 homolog (Drosophila)	Dtx4	2.42	1.88	2.12	signal transduction
1449010_at	heat shock protein 4 like	Hspa4l	4.27	3.29	3.71	response to protein stimulus,
1449059_a_at	3-oxoacid CoA transferase 1	Oxct1	5.23	3.25	2.87	CLAM
1440286_at	F-box and leucine-rich repeat protein 16	Fbxl16	3.07	3.07	3.07	CLAM
1448987_at	acyl-Coenzyme A dehydrogenase, long-chain	Acadl	2.9	2.16	2.47	CLAM
1448553_at	myosin, heavy polypeptide 7, cardiac muscle, beta	Myh7	20.09	32.15	24.7	CLAM
1425506_at	myosin, light polypeptide kinase	Mylk	2.25	1.92	2.07	phosphorylation
1435486_at	p21 protein (Cdc42/Rac)-activated kinase 3	Pak3	7.75	6.04	6.79	phosphorylation,
1424886_at	protein tyrosine phosphatase, receptor type, D	Ptprd	4.98	3.09	3.81	dephosphorylation
1437165_a_at	procollagen C-endopeptidase enhancer protein	Pcolce	5.26	2.77	3.63	proteolysis
1431057_a_at	protease, serine, 23	Prss23	5.45	5.1	5.27	proteolysis,

1439500_at	secernin 1	Scrn1	4.56	4.98	4.76	transport
1455106_a_at	similar to creatine kinase, brain; predicted gene 12892; creatine kinase, brain	Ckb	10.66	5.82	7.52	cellular homeostasis
1438239_at	similar to midline 1; midline 1	Mid1	2.32	2.81	2.54	proteolysis
1434249_s_at	tripartite motif-containing 9	Trim9	3.76	4.74	4.19	cell-cell signaling,
1454867_at	meningioma 1	Mn1	3.03	4.7	3.69	ossification
1433551_at	vesicle amine transport protein 1 homolog-like (T. californica)	AI427515	2.79	3.17	2.97	oxidation reduction
1449340_at	sclerostin domain containing 1	Sostdc1	2.43	2.95	2.67	Wnt signaling
1438101_at	Frizzled homolog 3 (Drosophila)	Fzd3	3.71	3.93	2.34	Wnt signaling

Table 3.12 MHP-MD related down-regulated genes

			Fold Change			
Probe set	**Gene name**	**Gene Symbol**	**85vs95**	**90vs95**	**85+90vs95**	**gene function**
1454373_x_at	ubiquitin B; similar to Ubc protein;	Ubc	-8.07	-4.84	-6.45	differentiation
1438718_at	fibroblast growth factor 9	Fgf9	-3.17	-2.74	-2.96	proliferation
1436584_at	sprouty homolog 2 (Drosophila)	Spry2	-3.59	-3.64	-3.61	proliferation
1436716_at	Protein phosphatase 1, regulatory (inhibitor) subunit 14B	Ppp1r14b	-2.95	2.9	-2.93	proliferation
1434432_at	ring finger and FYVE like domain containing protein	Rffl	-3.72	-2.93	-3.33	apoptosis
1419967_at	SEH1-like (S. cerevisiae	Seh1l	-2.62	-3.36	-2.99	cytoskeleton organization
1452085_at	GATA zinc finger domain containing 1	Gatad1	-2.88	-2.58	-2.73	transcription
1440346_at	Jumonji domain containing 3	Jmjd3	-3.44	-2.43	-2.93	transcription
1457473_at	chromodomain helicase DNA binding protein 1	Chd1	-2.84	-2.73	-2.78	NMCD
1427263_at	inactive X specific transcripts	Xist	-5.57	-3.39	-2.48	NMCD
1456565_s_at	mitogen-activated protein kinase kinase kinase 12	Map3k12	-4.28	-3.79	-4.03	NMCD
1448606_at	endothelial differentiation, lysophosphatidic acid G-protein-coupled receptor, 2	Edg2	-3.25	-3.88	-3.56	intracellula signaling cascades
1417695_a_at	sterol O-acyltransferase 1	Soat1	-5.02	3.51	-4.27	CLAM
1458347_s_at	transmembrane protease, serine 2	Tmprss2	-5.69	-4.3	-4.99	proteolysis
1421556_at	serine (or cysteine) peptidase inhibitor, clade A, member 3A	Serpina3a	-7.41	-10.63	-5.89	proteolysis
1451440_at	chondrolectin	Chodl	-4.56	-2.83	-3.69	GAG binding
1418014_a_at	betaGlcNAc beta 1,4- galactosyltransferase, polypeptide 1	B4galt1	-2.21	-2.77	-2.51	GAG synthesis
1437729_at	Predicted gene, EG665189	EG665189	-10.45	-6.03	-8.24	_?

Table 3.13 DLHP-NT related up-regulated genes

Probe set	Gene name	Gene Symbol	Fold Change			gene function
			85vs90	85vs95	85vs90+95	
1454086_a_at	LIM domain only 2	Lmo2	2.35	4	3.18	differentiation
1419430_at	cytochrome P450, family 26, subfamily a, polypeptide 1	Cyp26a1	3.25	2.59	2.92	differentiation
1418876_at	forkhead box D1	Foxd1	5	3.14	4.07	differentiation
1439798_at	homeo box C10	Hoxc10	14.02	18.44	16.2	differentiation
1416168_at	serine (or cysteine) peptidase inhibitor, clade F, member 1	Serpinf1	2.96	6.69	4.83	differentiation
1415904_at	lipoprotein lipase; similar to Lipoprotein lipase precursor (LPL)	Lpl	6.25	3.63	4.94	differentiation
1449109_at	suppressor of cytokine signaling 2; predicted gene 8000	Socs2	3.43	3.55	3.49	differentiation
1449473_s_at	CD40 antigen	CD40	3.71	2.54	3.12	proliferation
1456781_at	SRY-box containing gene 2	Sox2	-6.7	-4.92	-5.78	proliferation
1440626_at	homeo box D13	Hoxd13	3.42	20.1	11.8	proliferation
1423062_at	insulin-like growth factor binding protein 3	Igfbp3	3.64	3.52	3.58	proliferation
1456239_at	fibroblast growth factor 17	Fgf17	3.56	4.23	3.89	proliferation
1437673_at	wingless-related MMTV integration site 5A	Wnt5a	3	4.58	3.79	proliferation
1450779_at	fatty acid binding protein 7, brain	Fabp7	3.4	26.49	14.9	proliferation
1418129_at	24-dehydrocholesterol reductase	Dhcr24	3.03	5.28	4.15	apoptosis
1459749_s_at	FAT tumor suppressor homolog 4 (Drosophila)	Fat4	5.25	4.98	5.12	adhesion
1451446_at	anthrax toxin receptor 1	Antxr1	3.12	5.34	4.23	adhesion
1423606_at	periostin, osteoblast specific factor	Postn	3.88	2.86	3.37	adhesion
1456292_a_at	vimentin	Vim	3.25	4.16	3.71	Cytoskeleton organization
1416361_a_at	dynein cytoplasmic 1 intermediate chain 1	Dync1i1	4.18	2.94	3.56	intracellular transport,
1459790_x_at	aristaless-like homeobox 3	Alx3	4.05	4.02	4.04	transcription
1436050_x_at	hairy and enhancer of split 6 (Drosophila)	Hes6	2.39	2.07	2.23	transcription
1446408_at	homeo box A10	Hoxa10	16.06	12.8	14.4	transcription
1434286_at	trichorhinophalangeal syndrome I (human); similar to Trps1 protein	Trps1	3.59	2.92	3.26	transcription
1433638_s_at	homeo box D8	Hoxd8	3.07	2.55	2.81	transcription
1417392_a_at	solute carrier family 7 (cationic amino acid transporter, y+ system), member 7	Slc7a7	4.11	5.44	4.78	transmembrane transport
1416561_at	glutamic acid decarboxylase 1	Gad1	2.49	3.93	3.21	cell-cell signaling
1434642_at	hydroxysteroid (17-beta) dehydrogenase 11	Hsd17b11	3.77	2.47	3.12	CLAM
1419821_s_at	isocitrate dehydrogenase 1 (NADP+), soluble	Idh1	3.06	2.58	2.82	CLAM
1423078_a_at	sterol-C4-methyl oxidase-like	Sc4mol	4.04	3.08	3.56	CLAM
1432103_a_at	SH3-domain GRB2-like 3	Sh3gl3	2.36	2.71	2.53	membrane invagination

Table 3.14 DLHP-NT related down-regulated genes

Probe set	Gene name	Gene Symbol	Fold Change 85vs90	85vs95	85vs90+95	gene function
1452284_at, 1427019_at	protein tyrosine phosphatase, receptor type Z, polypeptide 1	Ptprz1	-5.33	-4.29	-4.75	differentiation
1424007_at	growth differentiation factor 10	Gdf10	-3.96	-2.77	-3.26	differentiation
1426225_at	retinol binding protein 4, plasma	Rbp4	-2.68	-3.1	-2.87	proliferation
1450256_at	cerberus 1 homolog (Xenopus laevis)	Cer1	-3.97	-3.3	-3.6	proliferation
1456515_s_at	transcription factor-like 5 (basic helix-loop-helix)	Tcfl5	-3.7	-6.22	-4.64	proliferation
1448229_s_at	cyclin D2	Ccnd2	-2.37	-2.27	-2.32	cell cycle
1423760_at	CD44 antigen	Cd44	-2.35	-3.29	-2.74	adhesion
1426301_at	activated leukocyte cell adhesion molecule	Alcam	-2.26	-2.41	-2.33	adhesion
1434709_at	neuron-glia-CAM-related cell adhesion molecule	Nrcam	-3.19	-2.66	-2.9	adhesion
1417654_at	syndecan 4	Sdc4	-4.41	-7.62	-5.47	adhesion
1434283_at	similar to modulator recognition factor 2; AT rich interactive domain 5B (MRF1-like)	Arid5b	-5.37	-2.68	-3.58	migration
1436359_at	ret proto-oncogene	Ret	-6.84	-8.59	-7.61	morphogenesis
1447360_at	TSC22 domain family, member 1	Tsc22d1	-3.16	-2.22	-2.61	transcription
1428825_at, 1428826_at	nuclear receptor subfamily 6, group A, member 1	Nr6a1	-7.45	-9.7	-8.43	transcription
1455345_at	PHD finger protein 15	Phf15	-2.06	-2.91	-2.41	NMCD
1419549_at	arginase, liver	Arg1	-5.84	-5.77	-5.81	CLAM
1455593_at	protein tyrosine phosphatase, receptor type Z, polypeptide 1	Apob	-8.75	-19.58	-12.1	CLAM
1443824_s_at	carbonic anhydrase 7	Car7	-4.24	-4.85	-4.53	CLAM
1441927_at	synaptotagmin VII	Syt7	-2.45	-3.18	-2.77	plasma membrane organization
1416855_at	growth arrest specific 1	Gas1	-2.11	-2.18	-2.15	Shh signaling
1447669_s_at	guanine nucleotide binding protein (G protein), gamma 4	Gng4	-5.8	-4.59	-5.12	GPCR

Table 3.15 DLHP-MD related up-regulated genes

Probe set	Gene name	Gene Symbol	Fold Change 85vs90	85vs95	85vs90+95	gene function
1449109_at	suppressor of cytokine signaling 2; predicted gene 8000	Socs2	3.19	4.28	3.73	differentiation
1456239_at	fibroblast growth factor 17	Fgf17	7.53	8.77	8.15	proliferation
1450779_at	fatty acid binding protein 7, brain	Fabp7	11.55	45.52	28.6	proliferation
1415927_at	actin, alpha, cardiac muscle 1; similar to alpha-actin (AA 27-375)	Actc1	2.84	25.11	14	apoptosis
1459790_x_at	aristaless-like homeobox 3	Alx3	3.41	5.49	4.45	apoptosis
1450757_at	cadherin 11	Cdh11	2.42	4.02	3.22	adhesion
1418599_at	collagen, type XI, alpha 1	Col11a1	2.36	4.58	3.47	adhesion
1429438_at	BCL6 interacting corepressor	Bcor	2.24	2.5	2.37	transcription
1436050_x_at	hairy and enhancer of split 6 (Drosophila)	Hes6	2.63	2.95	2.79	transcription
1449530_at	trichorhinophalangeal syndrome I (human); similar	Trps1	2.46	2.98	2.72	transcription

	to Trps1 protein					
1417392_a_at	solute carrier family 7 (cationic amino acid transporter, y+ system), member 7	Slc7a7	2.39	3.72	3.05	transmembrane transport
1423078_a_at	sterol-C4-methyl oxidase-like	Sc4mol	4.13	5.3	4.71	CLAM
1419430_at	cytochrome P450, family 26, subfamily a, polypeptide 1	Cyp26a1	3.55	4.49	4.02	CLAM
1415904_at	lipoprotein lipase; similar to Lipoprotein lipase precursor (LPL)	Lpl	4.95	4.04	4.5	CLAM

Table 3.16 DLHP-MD related down-regulated genes

			Fold Change			
Probe set	**Gene name**	**Gene Symbol**	**85vs90**	**85vs95**	**85vs90+95**	**gene function**
1452284_at	protein tyrosine phosphatase, receptor type Z, polypeptide 1	Ptprz1	-2.32	-3.44	-2.77	differentiation
1426225_at	retinol binding protein 4, plasma	Rbp4	-2.75	-3.89	-3.22	proliferation
1449582_at	caudal type homeo box 1	Cdx1	-3.26	-9.84	-4.9	transcription
1428826_at	nuclear receptor subfamily 6, group A, member 1	Nr6a1	-4	-5.35	-4.58	transcription
1435386_at	Von Willebrand factor homolog	Vwf	-2.24	-3.26	-2.66	adhesion
1447583_x_at	G protein-coupled estrogen receptor 1	Gper	-3.93	-6.24	-4.83	GPCR
1451461_a_at	aldolase C, fructose-bisphosphate	Aldoc	-3.61	-7.5	-4.87	CLAM
1419549_at	arginase, liver	Arg1	-8.92	-16.35	-11.6	CLAM
1452270_s_at	cubilin (intrinsic factor-cobalamin receptor)	Cubn	-4.76	-5.82	-5.24	vesicle-mediated transport
1425425_a_at	Wnt inhibitory factor 1	Wif1	-3.35	-5.62	-4.2	Wnt signaling
1437339_s_at	proprotein convertase subtilisin/kexin type 5	Pcsk5	-2.69	-4.37	-3.33	proteolysis

NMCD: Nucleic acid metabolism and chromosome dynamics; CLAM: Carbohydrate, lipid, and amino acid metabolism (CLAM).

3.6.6.5 **Expression profiling of GAG genes during neurulation:**

GAG associated genes have been found abundantly expressed during neurulation, including core proteins, synthesis enzymes, and binding proteins. Core protein *Sdc4* were found differentially expressed in the DLHP-NT-down regulated gene list (**Table 3.14**). Differentially expressed GAG synthesize enzymes including the initiation enzyme *B4galt1* (**Table 3.10**) and chain modification enzyme *Ndst1* (**Table 3.9**). In addition, many GAG binding proteins have been found by data analysis, such as *Igf1* (Table 3.9), *Thbs1* (Table 3.9), *Ncam1* (Table 3.10), *Postn* (Table 3.13), *Aplp1*, *Lpl* (Table 3.13, 3.15), *CD44* (Table 3.14), *Has2* (Table 3.15), *Fgf9*

(Table 3.12), *Chall*, *Col11a1* (Table 3.15), *Lyve1*, and *Vwf* (Table 3.16). Some of the above mentioned genes have been reported to have association with neurulation such as *Ndst1* and *Sdc4*, but most of them were first reported in this research area. The abundant expression of GAG associated genes implicate that GAGs play critical roles in neurulation.

3.6.6.6 Expression of NTD genes during the neural tube closing process of mouse embryo

Around 50 genes related with NTD have been shown presented in the microarray data, 13 of which were presented in the MHP- or DLHP-related gene lists, while the rest of them have been found differentially expressed by at least one software. Among them, some are key members of certain pathways, some are transcription factors, cell cycle regulators or cell adhesion components that have been found highly involved in neurulation, such as *Zic2* and *Zic3* (*Shh* signaling), *Prakaca* (negative regulator of *Shh* signaling), *Bmp2* (*Bmp* signaling), *Lrp6* (*Wnt* signaling), *Cyp26a1* and *Aldh1a1* (RA signaling), *Celsr2* and *Cer1* (cell adhesion molecules), *Ccnd2*, *Cdk4* (cell cycle regulator), *Jmjd3*, *Sall4*, *Twist1*, *T* (*brachyury*) (Transcription factors), as well as some GAG genes such as *Ndst1*, *Postn*, *CD44*. The presence of these genes in the microarray results may be indicator for finding new critical genes, and the potential role of them for bending of MHP and DLHPs will be discussed and investigated further.

3.7 Studies on phenotypic alterations in NE4C cells after silencing B4galt1 gene

In the current microarray results, dozens of GAG associated genes have been found differentially expressed. The GAG synthesizing enzyme, B4galt1, was down-regulated in both MHP-NT and MHP-MD groups, implying that it may play a role in formation of MHP and its sustaining.

GAGs have been implicated in the process of neural tube closure, but their function in neurulation in spinal region has not been studied in detail (Copp and Bernfield, 1988b). Though they participate in many biological processes such as cell signaling and development, their functions depend on the biosynthesis enzymes and chain modifications. Galactosyltransferase are responsible for initiating the synthesizing of tetra-link between the GAGs and their core proteins which is most important for functions of GAGs in biological processes. It is also responsible for specifically transferring Gal from UDP-gal to the acceptor substrate, which is a very important step for synthesizing many glycoconjugates. B4galt1 is one of the Galactosyntransferases whose structure and dynamics of the catalytic function has been known clearly, but as for its biological functions in mammalian cells, it is seldom investigated. In order to know the possible function played by B4galt1 in neurulation, we knockdown its mRNA in NE4C cells by siRNA and check its effects on cell behaviors.

3.7.1 Optimization of the transfection parameters for knocking down of B4galt1 mRNA expression by siRNA

To silence B4galt1 expression in NE4C cells using chemically synthesized siRNA, optimization experiments were first conducted in order to obtain good and stable silencing effect. The optimizations for the transfection efficiency include cell number, FBS concentration, transfection reagent type and amount, and incubation time. Firstly, parameters for seeding cells such as cell number, FBS concentration, and growth time to confluence in 6-well plate were optimized by triplicates experiment. It was found that 8×10^4 cells/well, growing in MEM with 5% FBS could get the most ideal results, 40%, 75%, 85% confluence seeding after 24 hours, 48 hours, and 72 hours. Higher cell numbers or FBS concentration led to over confluence, and cells

not grow well under less cell number and lower FBS concentration. Secondly, transfection reagent type, amount, and incubation time were optimized using positive control of silencing select GAPDH siRNA (Ambion, Inc. Cat No.4390850) and siNegtive control (Ambion, Inc. Cat No.4390844), both of which were from Ambion. We compared the use of transfection reagents SiportAmine (Ambion), Oligofactamine (Invitrogen) and DharmaFECT1 (Dharmacon). 5 µl of siPORTAmine can give a silencing efficiency of 40% with 10% cell death rate, while 20 µl of Oligofectamine can achieve 90% silencing efficiency with 20% cell death rate. Both of the two reagents were toxic and less effective for NE4C cells. In the end, 5 µl of transfection reagent of DharmaFECT1, 5 nM of siRNA, 24 hours of exposure time led to the highest and most stable transfection efficiency of 87.84% (**Fig. 3.9**) for GAPDH siRNA with the least cell death, and the cell morphology was not changed after transfection compared with normal cells (**Fig. 3.10**).

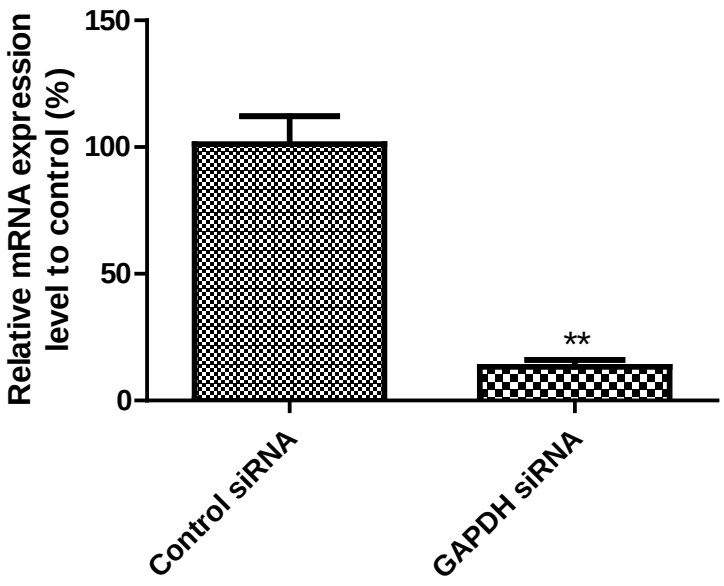

Fig. 3.9 Silence effect of positive siRNA targeting GAPDH mRNA in NE4C cells. Under optimized parameters, GAPDH mRNA expression was silenced more than 80% compare that in the non-targeting siRNA transfected group. The optimized parameters in the transfection: 8 x 10^4/well in 6-well plate with 5 µl DF1 and 5 µM siRNA. Data are expressed as mean ±SEM, n=3, unpaired student t-test, **P<0.01.

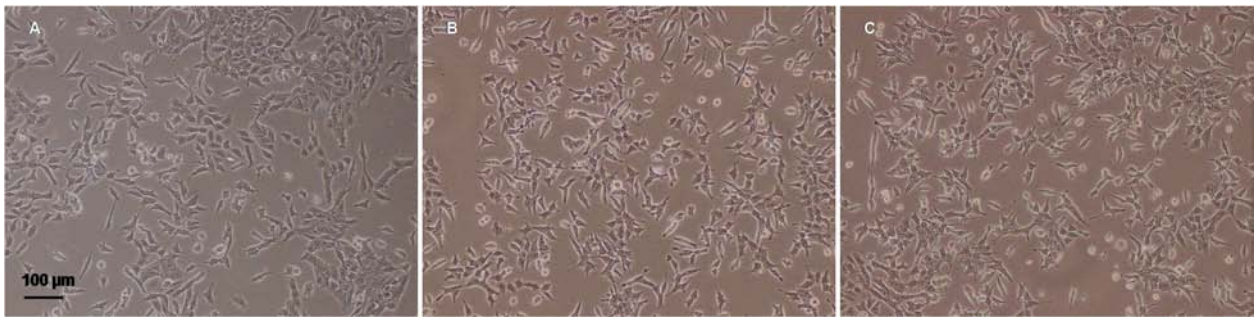

Fig. 3.10 Cell morphology after transfection. Under optimized transfection conditions DF1 transfection reagents did not adversely affect NE4C cell morphology at 48 hrs. (A) Normal cells under maintaining medium at 48 hrs. (B) Control non-targeting siRNA. (C) GAPDH siRNA. Cell pictures were taken under the same magnification, and scale bar in picture A designated as 100 µm.

3.7.2 Knockdown of B4galt1 mRNA expression by siRNA was gene-specific

To detect whether the expression of B4galt1 could be knockdown under the same transfection condition, 2 different siRNAs targeted to 2 different regions of B4galt1 mRNA were used for screening (**Fig. 3.11.A and Fig. 3.11.B**). Both sequences of the siRNA achieved the significant knockdown efficiency of more than 80%, and repeated triplicate experiment results showed that both of these two sequences could obtain an average of more than 70% knockdown efficiency at 48 hours (**Fig. 3.11.C**).

A

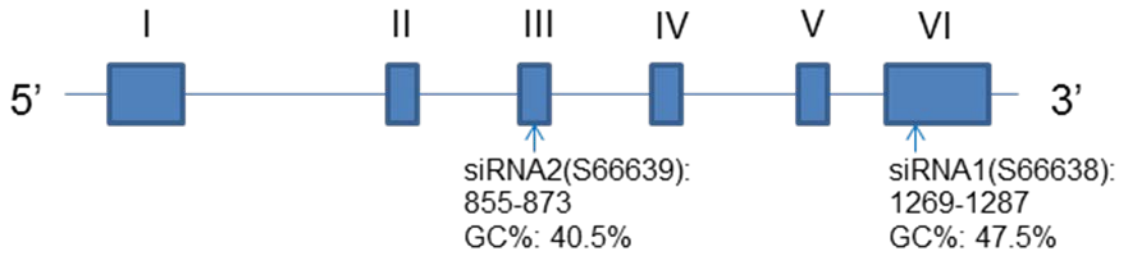

B

B4galt1 mRNA NM 022305.3

siRNA1 Ambion ID s66638
sense: 5'-GGAUCGCACAUACAAAGGAtt-3'
Antisense: 5'-UCCUUUGUAUGUGCGAUCCgg-3'
GC%: 47.5%
siRNA2 Ambion ID s66639

sense: 5'-CCAUGUUCAAUCGAGCUAAtt-3'
Antisense: 5'-UUAGCUCGAUUGAACAUGGtg-3'
GC%: 40.5%

C

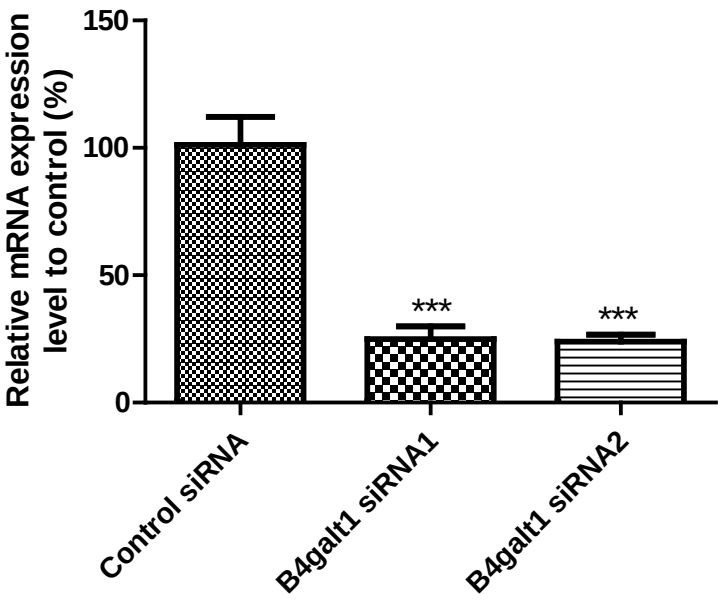

Fig. 3.11 Knockdown effects of two different siRNA sequences targeting B4galt1 mRNA in NE4C cells. (A) Design and synthesis of siRNAs against B4galt1. Schematic representation of the primary structure of mouse B4galt1 mRNA (gi: NM_022305.3) and two target sites of siRNAs. The blue boxes of I to VI represent six exons of B4galt1, and siRNA1 was on the VI exon while siRNA2 was on the III box. The sense chain of siRNA1 was from the 1269 to 1287bp, while the sense chain of siRNA2 was from the 855 to 873bp in the direction of 5' to 3'. (B) Sequence of siRNA duplexes. The two siRNA sequences were designed against B4galt1 in the modification of the nucleotide "T" substituted by "U" by Ambion, Inc. (C) Both two sequences achieved a silencing efficiency of more than 70%. From then on, both of them were used in the following experiments. Data were expressed as mean±SEM, n=3. One-way ANOVA, ***P<0.001; Turkey's Multiple Comparison test,***P<0.001, compared to control siRNA.

3.7.3 Reduction of B4galt1 expression by siRNA in the NE4C cells inhibited cell proliferation

B4galt1 has been shown to be involved in positive regulation of epithelial cell proliferation during wound healing. To investigate the effect of suppression of B4galt1 expression on NE4C cell proliferation, NE4C cells were transfected in triplicate with the two sequences of siRNA targeting B4galt1 gene or scrambled siRNA (control). 48 hours after transfection, cells were trypsinized and cell proliferation was measured by direct cell counting

using MTS method. **Fig. 3.12** shows the effect of silencing B4galt1 mRNA expression on NE4C cell proliferation. Both of the two sequences of siRNA targeting B4galt1 show significant inhibition on NE4C cell growth. Reduction of B4galt1 mRNA expression by siRNA inhibited NE4C cell growth by 7.996% (sequence 1, *P<0.05) and 20.81% (sequence 2, ***P<0.0001), respectively.

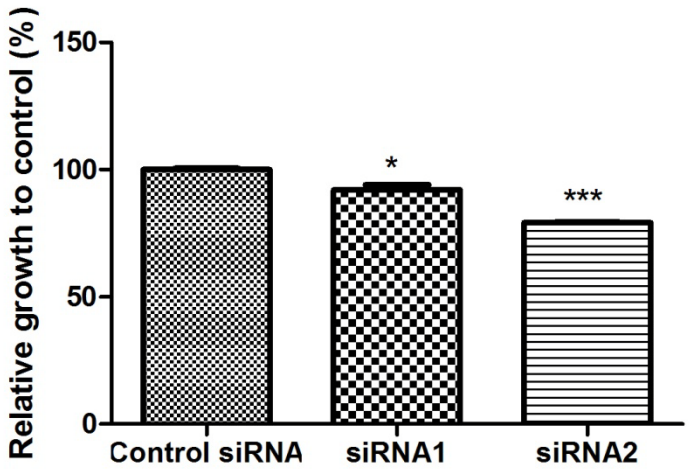

Fig. 3.12 Reduction of B4galt1 expression inhibited NE4C cell proliferation. Direct counting of viable cell number by MTS method 48 hours after transfection show that cell proliferation was significantly inhibited by 7.996% (sequence 1 in A, *P<0.05) and 20.81% (sequence 2 in B, ***P<0.0001), respectively. Experiments were performed in triplicate and results were expressed as mean ± SEM. One-way ANOVA, *P<0.05; Turkey's Multiple Comparison test, *P<0.05.

3.7.4 Knockdown of B4galt1 expression in NE4C cells inhibited cell adhesion to fibronectin and collagen I

Surface B4galt1 was known to be interacted with cell adhesion molecules such as E-cadherin or Collagen IV. To investigate the effect of suppression of B4galt1 expression on NE4C cell adhesion to fibronectin and collagen I, NE4C cells were transfected with two sequences of siRNA targeting B4galt1 gene or the control scrambled siRNA for 48 hours and the cells were re-seeded into the fibronectin- and collagen I-coated 96-well plates. The cells were allowed to

attach for 30 minutes and the adhesion ability were counted using MTS method. The adhesion ability was found significantly inhibited on both substrates by sequence 1. Sequence 2 has decreasing trends, but not significantly different, the p-values were slightly higher than 0.05, and the arrow bars were as similarly low as sequence 1 which imply it has inhibiting functions on adhesion. **Fig. 3.13** shows that NE4C cell adhesion to fibronectin were reduced by 12.09 (sequence 1, **P<0.01) and 1.478 (sequence 2, P=0.449), respectively. The adhesion ability of NE4C cells to Collagen I were reduced by 21.79 (sequence 1, *P<0.05) and 11.17 (sequence 2, P=0.065), respectively. These results demonstrate that silencing of B4galt1 inhibits the adhesion ability of NE4C cells.

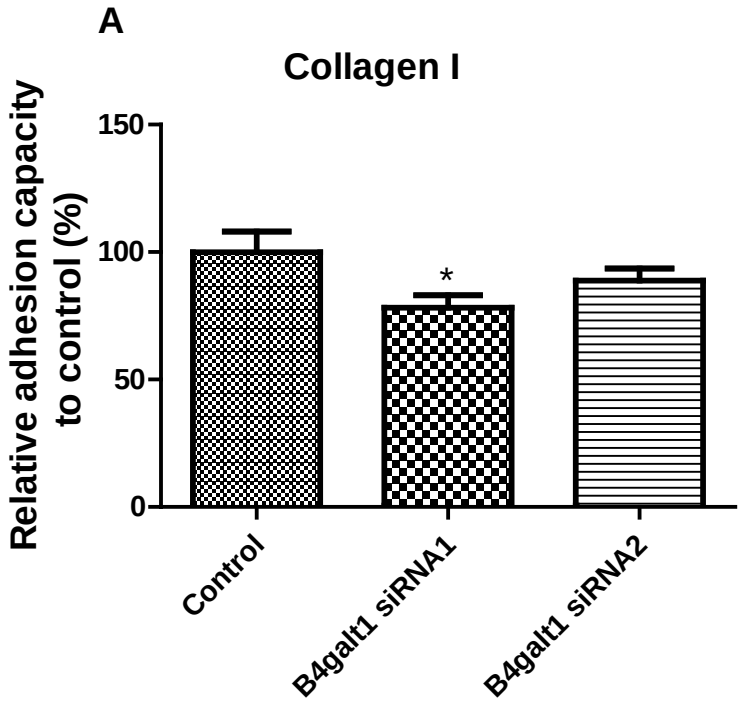

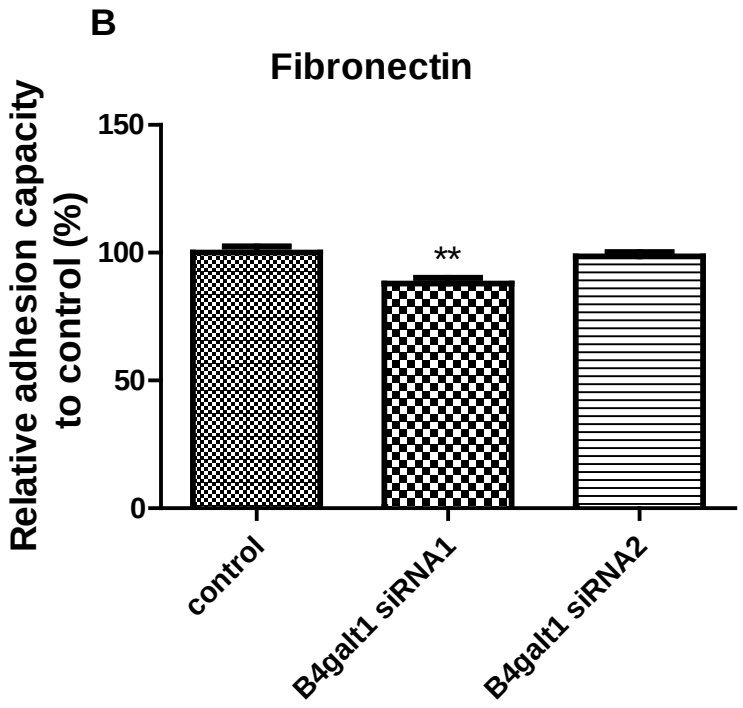

Fig. 3.13 Suppression of B4galt1 expression inhibited the adhesion ability of NE4C cells to fibronectin and Collagen I. NE4C cells were transfected with two sequences of siRNA targeting B4galt1 and the control scrambled siRNA. 48 hours after transfection, NE4C cells were trypsinized and resuspended in MEM without FBS and re-seeded into 96-well-plates pre-coated with fibronectin or collagen I. The cells were allowed to attach for 30 mins and MTS method was used to measure the number of attached cells. Data were expressed as mean ± SEM. One-way ANOVA, *P<0.05; Turkey's Multiple Comparison test, *P<0.05.

CHAPTER 4

DISCUSSION

4. Discussion

Neurulation is a complex process including several different but consecutive events. Its molecular mechanism was not comprehensible partly because of the finding of critical genes for this process was mainly by mutation studies. Associations among different genes are not very clear because different studies use different investigation conditions and platforms are not comparable. The purpose of this study was to set up a reliable framework in transcriptomic level at critical stages of neurulation, which was well studied and accepted by most investigators in this area. This framework of neurulation genes not only reflect the comprehensive feature of neurulation, but provide a basis for further investigating their regulation during normal and abnormal conditions.

4.1 A reliable transcriptomic profiling for mouse neurulation was generated by using laser capture microdissection (LCM) in combination with microarray

In order to increase the accuracy and reliability of the transcriptomic profiling of mouse neurulation, several strategies have been employed during the design and carrying out of the project. First, LCM technology was used to provide more homogenous tissues for microarray analysis, and the microdissected tissues were directly involved in neurulation; second, several technical methods were used to increase its reliability, so quality of RNA used on microarray was good; third, combined use of several software help to target genes with high possibility involving in neurulation; last but not least, gene expression pattern was consistent with reported according to literature research.

4.1.1 Gene expression in neurulation: microdissection versus whole mount tissue for microarray

Microarray is a good technology for monitoring the gene expression changes during biological process. The important thing is to afford the proper tissue samples. The more accurate the tissue samples, the more accurate the microarray results. El-Serag et al compared the gene expression of Barrett's esophagus using LCM microdissected glandular epithelium and biopsied whole tissues separately (El-Serag et al., 2009). They found that LCM sampling can not only meet the diagnostic purpose with 74% probe sets overlapped with whole mount biopsy samples, but also provide more information for investigating pathogenesis. A similar result was obtained by another independent investigation comparing gene expression in two adjacent tissues in prostate cancer using both whole mount and microdissected tissues (Sanati et al., 2009). Analysis using microdissected tissues can identify less transcripts but with more significant differences in expression.

In this current study, LCM was exploited to microdissect NT and MD from the whole mount embryo to increase the accuracy of tissue samples used for microarray analysis and with the hope to identify significant genes with more precision. The transcriptomic profiling with the expression of more than 39000 transcripts covering 34000 well known mouse genes provided a full view of neurulation spatially and temporally. More than thousands of differentially expressed genes between different stages by microarray analysis showed evidence for the successful use of LCM in microarray analysis. Moreover, around hundreds to thousands of MHP- and DLHP-related genes grant a precise and significant guide for further biological investigation in neurulation area.

4.1.2 A reliable protocol was established for transcriptomic analysis of laser microdissected mouse neural tissues with Affymetrix genechips

RNA quality is assurance for successful microarray analysis. A simple, low-cost and reliable protocol for RNA preservation by optimizing was developed by using three strategies for the LCM microdissected samples: mouse embryos were snap frozen immediately after dissection, RNAlater-ICE was applied directly on the cryosections, and a quick staining method.

Frozen method has the advantages of protecting histological details as well as yielding RNA of higher quality than paraffin-embedded sections or PF or ethanol fixed sections (Perlmutter et al., 2004). It has been used as a gold standard for gene expression analysis with laser microdissected samples (Espina et al., 2006; Stemmer et al., 2006). Stemmer K, *et al* fixed the kidney samples in RNAlater before cryosection and found its tissue morphology is damaged compared with snap-frozen with liquid nitrogen (Stemmer et al., 2006). During the preliminary experiment, the whole mount embryos were soaked in RNAlater before embedding and found the tissues could not freeze and attach on the slides well, the morphology of the tissue could not be well distinguished. Then RNAlater-ICE was applied directly on the cryosections. This novel usage of RNAlater-ICE protected the RNA quality without damaging the tissue morphology (**Fig.3.3** and **Fig.3.4**).

Haematoxylin (H) and eosin (E) staining has been a canonical staining methods for mouse embryo tissue sections, and this methods was also identified as an acceptable staining methods for frozen sections used for LCM (Espina et al., 2006). In the current experiment, the usage of haematoxylin only is enough for the staining effects and met the requirement of LCM work. Haematoxylin was found adequate for distinguishing the NT and MD easily under LCM and targeted cell populations can be microdissected without contamination from the adjacent

tissues. The optimized quick-staining method has the advantage of saving time and reduces the possibility of RNase contamination.

Using the optimized protocol, total RNA with good quality and quantity can be obtained from LCM microdissected mouse embryo tissues by two times microdissection from the same section (**Fig.3.4** and **Table 3.1**). A comprehensive transcriptomic profiling has also been obtained from these LCM RNA samples for analysis of gene expression during the closing process of neural tube.

4.1.3 Combined use of several software reduced the number of candidate genes by microarray analysis

Transcriptomic expression profiling with microarray analysis can explore differentially expressed genes during developmental process simultaneously in an abundance manner. In the current study, samples collected in triplicate for NT or MD at three stages were hybridized on Affymetrix Mouse Genome 2.0 2 GeneChip. The transcriptomic expression profiling was globally analyzed by different software for data normalization followed by identification and clustering of differentially expressed genes.

Microarray analysis is critical for arriving to the very similar true status of the biological process. GCOS, dChip, and GeneSpring are three well known software using different algorithms that are widely used for analyzing Affymetrix GeneChips. Differentially expressed genes between any two stages during neurulation were around or more than thousands (**Table 3.4**), which implies the difficulty for targeting critical genes. After intersection of differentially expressed genes in 7 datasets by Microsoft access, the common genes filtered by the three software were combined together, and the genes were narrowed down to around hundreds.

Further analysis was performed to reveal the MHP and DLHP related genes according to the growth features of neurulation. A total of 214 transcripts were revealed differentially expressed for MHP-NT related genes, and 219 for MHP-MD related genes, 95 for DLHP-NT related genes, and 56 for DLHP-MD related genes (Table 3.6). Detailed information of the genes regarding their spatial and temporal existing - whether they are up-regulated and down-regulated between different stages or where they present - in both NT and MD or NT only or MD only - were also revealed by analysis tools (**Fig.3.7**). The microarray data were further validated by real-time PCR. Functional analysis by the online software Gene Ontology of the MHP- and DLHP- related genes revealed numerous cellular biological functions, such as differentiation, proliferation, adhesion, migration, as well as multiple cellular pathways. Most of the genes are multifunctional and also involved in several pathways or cascades in different biological contexts. Each gene was specified a function according to combined knowledge from NetAffix and literature research as well.

Further analysis by GO revealed that these genes were more than enough for biological exploration. The combined usage of different software helps us to increase the accuracy, reliability and possibility to increase the accuracy of our downstream investigation. These genes are designated more reliable in that they are really differentially expressed during the neural tube formation and closure process.

4.2 Microarray findings: neurulation-associated genes setup a framework for future functional studies with multiple functions and pathways

4.2.1 Transcriptomic analysis of gene expression during critical stages of neurulation reveals associations to diverse biological processes

Previous studies found numerous genes with cell biological functions are essential for neural tube closure, and NTDs are found among mouse mutants of the proliferation, differentiation, cell cycle, cell viability regulation, cytoskeleton and signal transduction as well as transcription factors that affect chromatin structure. Analysis of differentially expressed genes with different functions may aid to provide critical candidate genes for investigating NTDs.

4.2.1.1 Cell proliferation and differentiation are essential functions for formation of MHP and DLHPs

Differentiation and proliferation are two facets of a coin for the development of neural tube. The neurulation stage embryo is a proliferating system. Neuroepithelial cells have a high proliferation rate before some of them exit the cell cycle and differentiate after the neural tube closure, indicating the essential role of the balance between proliferation and differentiation for successful neural tube closure (Copp and Greene, 2010b). Animal models displayed neural tube defects when the balance between neural proliferation and differentiation was disrupted (Lakkis et al., 1999; Smitherman et al., 2000; Takeuchi et al., 1995). The imbalance between neural proliferation and differentiation can destroy the consistent process of bending and apposition of the dorsolateral neural folds which were essential for closure of the neural tube.

There were many genes with functions related with proliferation and/or differentiation, as well as other cell-growth related functions such as cell cycle and apoptosis in the microarray results. They were differentially expressed during the neurulation process and distributed among almost all the MHP- and DLHP- related gene groups. From a global view, growth was active during the process of MHP- and DLHP- formation for the many genes with function of proliferation and differentiation differentially expressed and tightly regulated by the cell cycle and apoptosis genes.

During the neurulation process, proliferation and differentiation commences in different axial level at different timepoints and do not proliferate and differentiate in the same manner within each level and stage. Analysis of the spatial and temporal expression patterns along the different axial levels at different stages could reveal potential mechanisms that regulate when and where cell growth commence and exit. I discussed here several of the many genes whose biological functions have been studied and found related with neural tube development, leaving more to be explored in the future.

Epha7 is a member of the Eph family of tyrosine protein kinase receptors, mice with *Epha7* inactivation exhibit cranial NTDs (Holmberg et al., 2000), but the exact mechanism was not known. Ephrin tyrosine kinase receptors and their ligands ephrins have been proposed as Hox targets. A recent research showed that expression of *Epha7* was directly controlled by the expression of *Hoxa13* and *Hoxd13* in developing limbs (Salsi and Zappavigna, 2006). *Epha7* contains multiple *Hoxa13/Hoxd13* binding sites in the promoter region, mutation of any one was sufficient to abolish its transcription activation. Further investigation demonstrated that HOXD13 mutation in patients with brachydactyly-polydactyly syndrome fails to bind and transactivate *Epha7* promoter, which ascertained *Epha7* as a direct downstream target of *Hoxd13*

during limb development. Hox genes encode transcription factors and were first identified as providing positional information along the anterior-posterior body during embryonic development. In addition, they are proposed as regulators for cell division, cell adhesion, migration, and morphological differentiation (Ulijaszek *et al*, 1998). Hox-deficient mice display delayed closure of neural tube (Redline et al., 1992). *Hoxd13* and *Epha7* were presented in the MHP-NT-up-regulated group and their expression seems to have a negative correlation with MHP formation. *Hoxd13* was also presented in the DLHP-NT-up-regulated group, which means that its expression initiated at E9.0 when the DLHPs begin to form, and the expression increased dramatically at E9.5 during the existence of DLHPs, and at the same time, the expression of *Epha7* was induced to increase at E9.5. This expression pattern implies a possible hypothesis that *Epha7* may be a downstream target of *Hoxd13* during neurulation, and it may play a role in initiating the closure of neural tube as postulated (Holmberg et al., 2000).

FGFs are a class of diffusible glycoproteins with multiple functions during embryonic development. They are found related with neural induction, dorsoventral and antero-posterior patterning of the neural tube during neurulation. *Fgf9* was presented in MHP-MD-down-regulated group, consistent with previous study that *Fgf9* RNA was detected in intermediate mesoderm of late-stage gastrulation mouse embryos, as well as spinal cord motor neurons.

Fgf9 was shown to increase the expression of *Spry2* and *Spry4* in mouse embryo pancreas mesenchyme. *Spry2* was also found induced by Fgf signaling in limb embryogenesis which functions as FGF-induced feedback inhibitor. In situ hybridization showed that *Spry2* was highly expressed at PNP of mouse/chick embryo with an expression pattern similar to *Spry4*. Here in the same group presented *Spry2* gene with similar expression pattern as *Fgf9*, but its potential

function in neurulation was poorly known. If any, it was postulated that *Spry2* may be induced by Fgf signaling and play a role in regulating cell proliferation during neurulation.

Cutl1(**Table 3.9**), or *Cux1*, presented in both MHP-NT-up-regulated and MHP-MD-up-regulated groups, is a homeodomain transcription factor known to play multiple roles in development including cellular proliferation, differentiation, cell motility, and cell cycle progression. It is conserved among vertebrates and contains four DNA binding domains including three Cut repeats and one Cut homeodomain. The role of *Cutl1* in neurulation is not studied. Expression of Cutl1 at E9.5 NT and MD by microarray displays more than 2 fold higher than at E8.5 and E9.0. Phosphorylation of *Cutl1* by several kinases such as PKA or PKC has been shown to inhibit its DNA binding activity, and further affects *Cutl-1*-mediated proliferation and migration (Michl et al., 2006). It is known that targeted mutation of MARCKS (a substrate of PKC) results in exencephaly, and the PKA-deficient mouse model develops localized spinal NTDs displaying a dorsal expansion of *Shh* signal at the ventral tube (Huang et al., 2002). As a recent study found that *Cutl1* was a novel target of PKA that can be directly phosphorylated at serine 1215 in NIH3T3 fibroblasts, and the *Cutl1* target genes involved in proliferation and migration such as DNA polymerase A and *Dkk2* was also modulated by PKA-induced phosphorylation (Michl et al., 2006), it is postulated that PKA-down-regulation of *Shh* may be due to the down regulation of *Cutl1* and its target genes.

Cutl1 may participate in the formation of neural tube through a novel PARticular pathway (Wilson et al., 2009), a cascade of molecular interactions involving the protease-activated receptors (PARs) and their productive cleavage by cell-associated tissue proteases (Copp and Greene, 2010a). PARs belong to the G protein-coupled receptor (GPCR) family. Double mutant of PAR1 and PAR2 results in cranial neurulation defect (Camerer et al., 2010). A

number of serine proteases can activate PAR1 and PAR2 in the neurulation stage embryo with matriptase was one of them. Matriptase inhibitor HAI-2 knockout mice develop exencephaly and spina bifida, and these NTDs can be rescued by genetic depletion of matriptase (Szabo et al., 2009). The mechanism of neurulation defects led by PARs was not clear. A study reported that PAR2 can increase DNA binding activity of Cutl1 by regulating two DNA binding domains presented in all *cux-1* isoforms, the cut repeat 3 and the cut homeodomain (Wilson et al., 2009). In my microarray results, PARs inhibitor HAI-2 was down-regulated in both NT and MD, with high expression at E8.5 and E9.0 and decreased expression at E9.5 fish out by the GCOS software, while Cutl1, which can be increased by PARs was up-regulated in both MHP-NT and MHP-MD groups. These expression pattern were consistent with their reported functions and shed light on their potential role during neurulation by regulating the PAR or GPCR signaling, Though the probe sequence of Par1 (or its substitute name Pas5a) and Par2 were not included in the Affymetrix genechips, quite a number of GPCR signaling genes were found differentially expressed in the MHP- and DLHP- related gene groups, and further investigation are needed to unravel the mechanism.

Cutl1 was also found functioned at the G1/S transition and accelerating cell cycle progression into S phase in p110 CDP/Cux cells (Sansregret et al., 2006). This evident was confirmed by the mouse embryo fibroblasts obtained from *Cutl1* z/z mutant mice which displayed a longer G1 phase and slower proliferation rate than normal cells. This led to a possibility that *Cutl1* may be involved in the formation of hingepoint by regulating the number of S phase cells whose nucleus position will be at the bottom of the neuroepithelium.

Proliferation depends largely on the environment of cells as well as different kinds of growth factors. Regulation of proliferation may affect the tissue size and the responding of

progenitor cells to differentiation inducers. Proliferation during mammalian embryogenesis is regulated during the G1 phase of the cell cycle (Pardee, 1989).

D-type cyclins play a major role in positive regulation of G1 phase progression and S-phase entry (Baldin et al., 1993; Quelle et al., 1993; Lukas et al., 1994a,b; Musgrove et al., 1994;Resnitzky et al., 1994; Resnitzky and Reed, 1995). Cyclin Ds bind and activate cyclin-dependent kinases 4 and 6 (*CDK4* and *CDK6*) to phosphorylate and functionally inactivate the retinoblastoma protein (*pRb)*, thereby start a new round of DNA synthesis and promote cell cycle progression from mid to late G1 (Matsushime et al., 1992, 1994; Bates et al., 1994; Tamet al., 1994; Meyerson and Harlow, 1994; reviewed in Sherr, 1994; Weinberg, 1995). The *cyclin D-CDK4-pRB* interplay may be involved in multiple signaling cascades such as membrane tyrosine kinase receptors, and the cyclic AMP-dependent signaling pathway (Lukas et al., 1996; Peeper et al., 1997).

The neuroepithelium of neurulation stage has high proliferation rate with cell recycle times as short as 4-6 hours, thus the cell cycle activating gene *Ccnd2* and *CDK4* are expected to be highly expressed while the *Rb* gene is inhibited to some degree. In the current microarray exploring, many genes involved in regulation of proliferation and cell cycle have been found differentially expressed during the neural tube closure in the spinal region. The cell cycle initiation genes, both *Ccnd2* and *CDK4*, were found differentially expressed during spinal neurulation. The *Ccnd2* was up-regulated in mesenchymal gene list with a fold change of 2.3 at E9.5 compared with E9.0 and E8.5 (**Table 3.11**). It also displayed an increasing trend in neuroepithelium at E9.5 compared with E9.0. The expression pattern of *CDK4* in NT was up-regulated at E9.5 compared with E9.0 and E8.5 (**Table 3.9**). The expression intensity of *CDK4* in surrounding mesenchyme was high at all three stages but no obvious difference.

The gene *Rbbp4*, a histone binding protein that can bind *Rb* directly and regulate proliferation (Qian et al., 1993), was down-regulated in neuroepithelium, with a fold change similar to *Ccnd2* and *CDK4* (**Table 3.10**). This may be an indication that *Ccnd2/CDk4* complex is the main regulator of G1/S transition through regulating the binding of *Rbbp4* with *Rb* during spinal neurulation.

Ccnd2 was reported as developmental regulators and was first detected at the time of primitive streak formation and the expression domain expands gradually to the distal region of the embryo. The expression increases in posterior tissues such as ectoderm and mesoderm cells and coincide with the occurrence of a proliferation burst (Wianny et al., 1998). The expression of *Ccnd2* is also detected in the dorsal closing neural tube, and the main site is the neuroectoderm.

FGF signaling, *Shh* signaling as well as *Wnt* signaling pathways are known cell cycle regulators during the caudal neural plate (Lobjois et al., 2004). *FGF* signaling preserves the proliferative domain in the immature caudal neural plate by maintaining the *cyclin D2* expression and inhibiting *cyclin D1* expression which may be realized by down-regulation of *Shh*-signaling. Reduction of *FGF* signaling in the neural groove results in the decreasing of *Cyclin D2* and activation of *Cyclin D1*, which may depend on *Shh* signaling. *Wnt3a*, a gene mutation of which lead to NTD in mouse embryos, was also found expressed in the caudal region of the embryo and positively regulate the expression of *Cyclin D2* (Cauthen et al., 2001; Megason and McMahon, 2002). Ccnds are also transcriptional targets of the *Wnt-beta-catenin* signaling involved in regulation of cell proliferation by promoting the G1/S progression. After neural tube closure, the expression of both cyclins were constrained to the dorsal neural tube by the regulation of Wnt signaling. This restriction may contribute to the neuronal differentiation.

TGF-beta family members, including BMPs have been found expressed in the roof plate and the dorsal neural tube. They are supposed to induce the dorsal cell growth by anti-phosphorylation of *Rb* gene in growing cells (Laibo, et al, 1990; Basler et al, 1993; liem et al 1997). The increased expression of *TGFbr2* (**Table 3.9**) and the decreased expression of *Rbbp4* may indicate their involvement in the cell growth control in spinal neurulation.

Another cell growth regulator found in the gene lists are *REG-gama*, also known as *Psme3* (**Table 3.11**). It belongs to the REG family of proteasomal activators, mainly found in the nucleus, may play a role in chromosomal stability during mitosis and is implied to be a regulator of cell cycle transition and cell proliferation (Zhou, 2006). It was reported to facilitate the degradation of cyclin-dependent kinase inhibitor *p21* which is a cell cycle inhibitor preventing the G1/S transition. Mice deficient of *REG-gamma* were significantly reduced in body size while *REG-gamma* deficient embryonic fibroblasts have delayed entry from G1 to S phase in the cell cycle (Murata et al., 1999). So far there is no reported data regarding the role of *Regime* in neurulation. The *REGgama* displays a similar expression pattern as *Ccnd2* and *CDK4* in the microarray results, which indicate highly an involvement in the cell cycle regulation of spinal neurulation.

It was noticed that some of these genes also play important roles in cell cycle regulation and cell differentiation. This founding is consistent with reports that cell cycle parameters can affect the apico-basal position of nuclei within the NE. This affection of the cell shaping from rectangular to wedge shape may explain the obvious difference of cell shape between cells in hinge points and in non-bending regions. For example, cells become wider at the basal side and narrower at the apical side at the bending regions. Many other genes with function as cell cycle regulator were found differentially expressed, such as up-regulated genes *Tubb3* (**Table 3.9**), and

down-regulated genes *Seh1l* and *Ppp1cb* (**Table 3.10**). This finding indicates that genes regulating proliferation and differentiation are essential during the formation of MHP and DLHPs in neurulation and may have the potential possibility for further investigation in mammalian neurulation.

4.2.1.2 Cell structure and adhesion molecules changes at different stages during neurulation

Contracted actin microfilaments existed in the apical regions of neuroepithelial cells, especially within the closing neural tube, implying an embryonic morphogenesis model that bending of an epithelial sheet was induced by a "purse-string" contraction of actin microfilaments (Baker and Schroeder, 1967; Wessells et al., 1971; Burnside, 1973; Karfunkel, 1974; Nagele and Lee, 1980; Sadler et al., 1982). The molecular mechanism under the morphogenetic event known as apical constriction where columnar cells in the bending neural tube are converted into wedge-shaped cells is unclear, except that the known genes are actin-binding (*Shroom*) (Hildebrand and Soriano, 1999; Martin, 2004) and actin related (*p190RhpGap*, a negative regulator of Rho GTPase in the process of regulating actin dynamics) (Brouns et al., 2000).

Recent studies confirmed the importance of cytoskeleton in the neuroepithelium but question the role of cytoskeleton in the bending of the neural tube especially in the spinal region. Mutation of most of the cytoskeleton proteins can lead to NTDs which were mainly cranial NTDs. Only mutation of *Shrm* and *Mlp* (Wu et al., 1996) were found to result in spinal NTDs in addition to cranial NTDs. *Shrm* was found highly expressed in both neuroepithelium and the paraxial mesoderm with increasing expression pattern. In addition, there are many cytoskeleton

organization or regulation genes that have been presented in the spinal neurulation gene lists with a fold change more than 2. Among these genes, most of them are in the MHP-related gene lists with increasing expression pattern. Only few of them such as *Seh1l*, *Tmod3* (**Table 3.10**), *Cubn* (**Table 3.16**) displayed a decreasing expression pattern. Most of them have been reported to play important roles in nervous system development. For example, *Actc1* (**Table 3.11**) has been found differentially expressed during gastrulation by a microarray screening. The cell shape changing from columnar to wedge shape seems essential for the localized bending of the neuroepithelium at the midline and dorsolateral hinge points. This changing displays at least two features, the narrower of the cell apex and the broadening of the cell base. *Shrm* and *Mlp* have been related with the contraction of the cell apex. Whether there is any other cytoskeleton genes involved in this process remains unknown. Though no direct evidence showed their relationship with NTDs or neurulation process, there remains a gap for further investigation.

As for the basal expansion, it is thought to be related with the different nuclei positions at different phases of the cell cycle. Studies have demonstrated that the bending regions of the neuroepithelium contain more cells in S-phase than nonbending regions in either chick (Smith and Schoenwolf 1987) or mouse (Gerrelli and Copp, 1997). Since position of the nuclei during S-phase are mainly located in basal of the cells, the above results may support the hypothesis that local retardation of the cell cycle may result in a local accretion of S-phase cells, these cells adopting a wedge shape to form the bending of the hinge points. However, the molecular mechanism of how they know to modulate the cell cycle at the S-phase is not clear. There are many genes involved in the cell cycle regulation especially the G1/S phase transition have been discussed. Here, we also found some genes that play roles in both cytoskeleton regulation and cell cycle. For example, *Mtap2*, a microtubule cytoskeleton organization gene in the MHP-NT-

up group (**Table 3.9**), has been found as a regulator of GNP differentiation by inhibiting the cell cycle arrest protein *p27*. This may be an indication that some cytoskeleton proteins may be involved in the spinal neurulation by regulating cell cycle process.

The obvious importance of cell adhesion is in the contraction and fusion of the neural edges at the dorsal midline of embryos. Holmberg found expression of *Epha5* and *Epha7* in the cranial NT instead of spinal NT by *in situ* hybridization, and inactivation of *Epha5* or *Epha7* receptor results in NTDs (Holmberg et al., 2000). In my microarray data, *Epha7* was found 6 fold higher in expression at E9.5 than in E8.5 and E9.0 in NT (**Table 3.9**), though the expression signal intensity is relatively low, only just above average of 500. This finding indicates that *Epha7* may be important for the maintaining of DLHPs and its increasing trends of expression in NT may also support its role in closure and fusion of neural folds. It could not be detected by in situ hybridization at spinal region may be due to the high threshold of the ISH method, or its relatively lower expression itself (Brunskill et al., 2008). Expression signals of *Epha5* (**Table 3.10**) is lower and demonstrate a decreasing trends in the microarray data sets indicating that *Epha5* and *Epha7* played different roles in spinal neurulation though mutation of both of them can leads to NTDs. We also found many other adhesion molecules differentially expressed in the microarray analysis and have not been previously reported in relation with neurulation process, such as *Cdh11, Celsr2, Cldn5, Col2a1, Col3a1, Col9a1, Col11a1, Ncam1, Postn, Tgfbi, Alcam, Nrcam, Megf10, Nid1, Pkp2, Lgals1, Vwf*, et al. *Tgfbi* and *Epha7* were known molecules that involved in RTK signaling, in addition to many other RTK signaling molecules reported here, indicating an involvement of RTK pathway in neurulation. The expression pattern of *Ncam1* was found decreased in E9.5 NT compared with in E9.0 and E8.5 (**Table 3.10**) while N-cadherin *Cdh11* (**Table 3.9**) was increased in E9.5 NT compared with in E9.0 and E8.5 in the microarray

results. It is consistent with the report that *Ncam* and N-cadherin were produced in the neural tube and was implicated in fusion of the neural fold, though *Ncam*-mutation mice and N-cadherin mice do not produce NTD (Cremer et al., 1997; Radice et al., 1997b), a family based study discovered a significant association between human NTDs and single-nucleotide polymorphisms (SNPs) within the gene Ncam1 (Deak et al., 2005). This finding confirmed their presence in spinal neurulation and its potential role in neurulation may be speculated. Collagen molecules were found increasedly expressed in spinal neurulation with *Col3a1*, *Col9a1* in NT and *Col2a1*, *Col3a1* in MD, but their roles remains further investigated. The colocalization of *TGFbeta1* with collagen, fibronectin and proteoglycans has been reported in chick lung morphogenesis, it should not be surprising to find for the first time that the colocalization of them during the neural tube morphogenesis.

4.2.2 Expression profiling of NT and MD during critical stages of neurulation provided dynamic relationships to multiple signaling pathways

Among the 4 pathways revealed by GO biological process, Wnt signaling pathway is the most studied during neurulation, TGFbR signaling pathway is related with BMP signaling, which was found critical for MHP- and DLHP- formation, while TRPTK pathway has the most high number of genes involved, most of them were overlapped with ERP pathway. In addition, the pathway genes found by information from the NetAffyx center and literature research are also important and worth an investigation for their role in playing the harmonious of neurulation.

4.2.2.1 Wnt signaling

In addition to the 6 genes revealed by GO biological process as described in results 3.6.6.4, a further exploration in the original microarray data disclosed a total of 30 *Wnt* signaling pathway genes that were detected presenting in the microarray expression profiling, including *Wnt* ligands, receptors and regulators, 12 of them were differentially expressed during the spinal neurulation with a fold change of more than 2: *Wnt3a, Wnt5b, Sfrp1, Lrp1, Frzb, Frd2, Frd6, Dvl*, *Lrp2*, *Dkk1*, *Cer1* and *Celsr2*. These additional genes help us in elucidating the role played by Wnt signaling with the focus on the 6 genes that presented in the MHP- and DLHP- related groups.

Wnt signaling play multiple roles in neurulation, including PCP signaling in shaping the neural plate and the canonical Wnt signaling in neural tube progenitor proliferation, as well as in dorso-ventral patterning and antero-posterior patterning. *Wnt5a* and its cell surface receptor *Fzd5* were up-regulated in the MHP-NT and DLHP-NT groups, binding of these two proteins initiating signal transduction for proliferation neural precursors (Cayuso and Marti, 2005). As

Wnt receptor, *Fzd* has the seven-transmembrane-spanning segment with a Wnt-binding site in the form of a cystein-rich domain (CRD). Down-regulation of Wnt inhibitor *Wif1* and up-regulation of Wnt receptor *Fzd3* in MD groups confirmed the positive role of Wnt signaling during HP formation.

Several findings suggest a posteriorization pathway of Wnt-FGF-HOX genes ((Ding et al., 1998; Fekany-Lee et al., 2000; McGrew et al., 1997). The expression of proliferation genes *Fgf17* and *Hoxd13* in the same group as of *Wnt5a* in the DLHP-NT-up-regulated group may implicate potential interactions among these genes.

High expression of *Wnt5a* was observed in the tail bud, the PNP region and extending several somites cranially around the ventral curvature. In addition, expression of *Wnt5a* on the serially cut sections existed in all tissues adjacent to the tail bud but not the notochord. The signal is very strong in the recently closed neural tube and the dorsally open neural plate, but becomes confined to the apical region and is gradually decreased (Gofflot et al., 1997; Gofflot et al., 1998). There are no comparison sections from younger stages such as E9.0 and E8.5. But the relatively strong expression in the PNP region and the decreasing expression pattern cranially indicate a consistency with the microarray finding using three different stages. The expression pattern of *Wnt5a* and *Wnt5b* in E9.5 mouse embryos was reported in a study using in situ hybridization (Gofflot et al., 1998). The expression pattern of *Wnt5b* were similar as *Wnt5a* except the expression intensity is relatively lower, and expression in the tail bud mesenchyme increases than the caudal neuropore and recently closed neural tube. It is similar as in the microarray findings that caudal sections expressed more than cranial sections.

The process of convergence extension existed in both gastrulation and neurulation under the control of the noncanonical *Wnt/frizzled* pathway (PCP pathway). Blocking convergent

extension in gastrulation by mutation of the core PCP genes during gastrulation leads to neural tube defects such as Ct (*Fz*), Lp (*Vang*), Crash (*Celsr*), Circletail (*Scrbl*) and Craniorachischisis in *Dvl1/Dvl2* double mutant embryos. A hypothesis was postulated that disrupted mesodermal convergent extension suppressed the notochord development which induces a broadened MHP and lead to neurulation failure. Broaden of MHP may be the reason for failure of neural folds contraction regarding the NTDs induced (2003). Another model support a disorganized MHP yielded by an unusually wide zone of neuroepithelial cells due to convergence extension defect. There are not many data support the roles played by *Wnt* signaling during neurulation. A 2003 experiment provided data regarding the role of PCP signaling in the medial neural tissue for proper NT closure, but denied its requirement for formation of the hinge points, fusion of the neural folds or in the medially moving dorsal epidermis. The presence of so many *Wnt* signaling genes as well as the differential express of key genes such as *Wnt5a*, *Frd2*, *Sfrp1*, *Cer1* (**Table 3.14**), and *Celsr2* (**Table 3.15**) support their potential important roles in spinal neurulation.

Genes with function of neuron differentiation were also found strikingly different between E8.5 and E9.5 stage embryos. Though the role of cell differentiation in NTC has been rarely reported, this data may afford a platform for further studies. *Dkk1* was an interesting gene by playing as a negative regulator of *Wnt* and *BMP* pathways in addition to response to retinoic acid (*RA*) regulation (del, I et al., 2003; Glinka et al., 1998). This blocking activity of *Wnt* signaling may be due to its interaction with the *Wnt* co-receptor *LRP*, *Frizzled*, and *kremen* (Kong and Zhang, 2009). Though abundance expression of *Dkk1* was found in E6.5 and E7.5 mouse embryonic cells, *Dkk1* mutation mouse embryos were lethal at early stages (Grotewold et al., 1999). Kong X et al reported that overexpression of *Dkk1* promotes differentiation of ESCs (mouse embryonic stem cells) toward neuroectoderm. No expression pattern has been reported at

neurulation stage embryos so far. Herein, I reported for the first time of the expression pattern of *Dkk1* during neurulation stage mouse at the spinal region. It was found expressed lower in both NT and MD at E8.5, then expression level increased first at E9.0 MD, but expression not changed in NT at E9.0. While during the following stage of E9.5, expression level increased more than 2 fold at E9.5 NT, but decreased at the surrounding MD. This expression pattern is logically indicating the close relationship of *Dkk1* with DLHP formation. When the balance of regulating factors of MHP and DLHP changed, it was one of the factors that initiated expression in MD tissue when MHP was decreasing and then its signals was transducted into NT to give a hand in the formation of DLHP. The transcriptome study provided an important indication for future studies of the role of differentiation in DLHP formation.

Sostdc1, an ectodermal BMP inhibitor and Wnt signaling modulator, was up-regulated in the MHP-MD group. Several lines of evidence shows that it may play a role as cross linker among several pathways, for example, it was shown to integrate BMP, Shh and FGF signaling in tooth development (Ahn et al., 2010; Ding et al., 1998; Fekany-Lee et al., 2000; Laurikkala et al., 2003). Though its role in neurulation was seldom studied, the differential expression in the microarray result holds a promising interesting for further exploration.

4.2.2.2 TGFβ signaling

The transforming growth family beta (*TGFbeta*), including the *BMP* members and non-*BMP* members, are expressed in the dorsal-most surface ectoderm, the dorsal neural tube as well as the roof plate. Numerous studies support the requirement of *BMP* signaling in mouse neurulation (Sollowayand Robertson, 1999; Zhang and Bradley, 1996), but few reports regarding the function of non-BMP Tgf members in neurulation. In the 4 Tgf pathway genes revealed by

GO biological process, *Cer1* was presented in the DLHP-NT-down-regulated group (**Table 3.14**), while the other genes, *Onecut2, Thbs1* and *Prdm1b* were in the MHP-NT-up-regulated group (**Table 3.9**). *Cer1* was an antagonist of members of the TGF family. *Cer1* has been shown binding directly to *Nodal* and *BMP* proteins and behaves as antagonists during gastrulation in both mouse and Xenopus (Belo et al., 2000; Hsu et al., 1998; Jones et al., 1995). The role of *Cer1* may be compensated by another BMP antagonist *Noggin* for *Cer1*$^{-/-}$ mice embryos do not display any defects but *Cer1-/- Noggin-/-* double mutant mice display the same defects as Noggin-/- mice.

To know more about the role of TGF pathway in neurulation, the expression pattern of BMP members were searched among the original microarray data. *BMP* signaling, like *Shh*, is necessary to prevent DLHPs formation. They may play a role in cell proliferation during early stage of neurulation. Its antagonist, noggin, secreted from the tips of the neural folds, overcomes *BMP*-mediated inhibition and enables DLHPs formation. There are 8 *BMP* genes have been detected, but only 4 genes have obvious differentially expressed trends among the three stages in NT and/or MD: *BMP1*, *BMP2*, *Bmpr1a*, and *Msx1*.

BMP signaling is necessary and sufficient to inhibit DLHPs. *Bmp2* expression was correlated with upper spinal neurulation, and *Bmp2*-null embryos exhibited premature, exaggerated DLHPs, in addition, local release of *Bmp2* inhibits neural fold bending. In the microarray expression profiling, *Bmp2* was highly expressed in E8.5 and E9.0 NT and decreased in E9.5 NT. This differential expression was consistent with reported. The expression pattern of *Bmp1* was conversely different with *Bmp2*. It was consistently increased in NT at E9.0 and E9.5 compared with at E8.5, and the expression signal was also significantly increased in MD at E9.5 compared with at E9.0 and E8.5. This expression pattern was quite similar as *Msx1*, a *BMP*

mediated transcription factor. The role of *Bmp1* in neurulation is seldom investigated previously. The differentially expressed pattern indicated a potential role in neurulation which may be mediated by *Msx1*. Moreover, expression of *Bmpr1a* was also slightly increased at E9.5 compared with at E9.0 and E8.5 in either NT or MD. It is known that *caBMPRIa* can promote proliferation in dorsal neural patterning, and embryos lacking *Bmpr-lA* gene die at gastrulation without forming any mesoderm. It is postulated here that *Bmpr1a* may play a role in cell proliferation in either NT or MD, may by interacting with *Bmp2* signaling.

4.2.2.3 Shh signaling

The *Shh* signaling pathway has been deeply studied during neural tube closure. It was shown expressed ventrally and played roles in supporting MHP formation and preventing DLHP formation, while *BMP* and *Wnt* proteins expressed dorsally and play differing roles in supporting DLHP formation. Though there was no direct Shh signaling components detected in the MHP- and DLHP- related groups, the current microarray work successfully detected numerous of these genes and their family members or close partners in the original datasets, many of which were reported for the first time and hold a huge importance for future investigation. For example, there were 13 key components of known *Shh* signaling genes detected, including *Shh* ligands, *Shh* receptors, transcription factors, and regulated factors. 5 of these genes were differentially expressed at different stages during neurulation process: Patched related protein *TRC8*, Smoothened homologue of *Smoh*, *Sufu*, *Gas1*, and *Shroom* in *Shh* pathway.

Expression pattern of *Sufu* and *Smoh* in NT were greatly similar with increasing trend, E8.5<E9.0<E9.5. Though *Shh* was not detected, but its direct receptor, *patch2*, was detected, though its absolute intensity was lower than 500, its increasing expression pattern in NT, FC > 2

in E9.5 compared with E8.5. *Sufu* was known as a *Shh* signal transduction inhibitor, genetic knockout of *Sufu* lead to exencephaly and cardiac defects. Another two *Shh* negative regulators and also NTD genes, *Fkbp8* and *Prkaca*, displayed highly similar expression pattern during spinal neurulation with FC > 2 in E9.5 vs. E8.5 MD. The expression pattern of the above genes was consistent with the role of *Shh* pathway in neural tube defects. *Shh* play more important roles in MHP formation but inhibition of *Shh* signaling was important for the DLHP formation.

Gas1, a GPI-linked protein, was found to be a negative regulator of *Hh* signaling and has anti-proliferation effects (Allen et al., 2007; Stebel et al., 2000). A recent study found it function as a positive regulator of *Hh* signaling being expressed in many regions in mouse embryos before or after neurulation and may acts to help transform the *hh* protein gradient into the observed activity gradient (Martinelli and Fan, 2007). In the microarray results, *Gas1* was found highly expressed at E8.5 neuroepithelium, but down-regulated at E9.0 and E9.5 groups, indicating a role in the formation of DLHP. When Shh supports the MHP and inhibits the DLHP, Gas1 expressed highly to suppress the Shh function, while expression of Shh decreased, expression of *Gas1* reduced accordingly but still remains highly expressed at E9.0 and E9.5 NT, indicating it may also play a role in the sustaining of DLHPs during neural tube closure.

4.2.3 Expression profiling of GAG/PG genes implicate their essential roles in neural tube closure

GAGs have been found expressed in the sites of active neurulation (Copp and Bernfield, 1988b). Sulfated GAG and hyaluronate accumulated in the PNP and decreased progressively cranially. Newly synthesized glycoconjugates presented especially in the active neurulation sites such as the PNP region and the recently closed neural tube region, in the basement membrane, beneath the neuroepithelium and around the notochord. Different newly synthesized GAGs distributed in different axial levels during neurulation. In cranial neurulation, interstitial matrix hyaluronate may increase extracellular space within the mesenchyme of the neural folds. Decrease expression of hyaluronate in chick embryo produces spinal neural tube defects (Copp and Bernfield, 1988a).

4.2.3.1 GAG core proteins

The role of GAG core proteins in development have been investigated. *Sdc2* and *Sdc4* were found differentially expressed with reverse expression patterns in the MHP- and DLHP-gene lists. Expression of *Sdc2* increased gradually during neurulation while Sdc4 decreased profoundly by a FC of 5. Other GAG core proteins such as *Sdc1, Gpc1, Gpc4, Gpc3, HSPG2, Keratin* were highly expressed, while *Bgn, Sdc3, Gpc6,* and *Gpc2* were present but expression intensities were lower.

Sdc1 appears first during mouse embryogenesis, but *Sdc1* deficient mice show no defects in morphogenesis (Bellin et al., 2002). *Sdc3* deficient mice exhibits impaired neural migration in development, altered feeding behavior, and partial resistance to obesity. Both *Sdc1* and *Sdc3* were presented in the microarray screening but showed no obvious changes during the mouse

spinal neurulation. There is yet no *Sdc2*-deficient mice, however, Xenopus *Sdc2* has shown to be vital for left-right asymmetry in embryonic development (Chen et al., 2004; Kramer and Yost, 2002). Knockout of *Sdc4* in mice is vital and does not demonstrate macroscopic abnormalities (Ishiguro et al., 2000a; Ishiguro et al., 2000b). Down-regulation of *Sdc4* in zebra fish and Xenopus shows the necessity of this gene for normal neural crest migration and cell movement in convergent extension. In the above mentioned experiments, the scientists are able to show that *xSdc4* functions in the non-canonical Wnt pathway interacting with *xDsh* and synergizing with *xFz7* (Munoz et al., 2006). *Sdc4* activates *xDsh*, and the activation of *Sdc4* is regulated by fibronectin and *xFzd7* by Wnt ligands. This involvement of *Sdc4* in the non-canonical Wnt pathway may be conserved among vertebrates. Redundancy of *Sdc4* with other HSPGs or other components of the Wnt pathway may explain the *Sdc4*-deficient mice with no defects in gastrulation.

4.2.3.2 GAG synthesis enzymes

GAG synthesis enzymes were found in the microarray comparison, including the *B4galt1*, the chain elongation enzyme *Ext2*, and modification gene *Ndst1*. *B4galt1* is one of the GAG synthesis initiation enzyme and its expression during spinal neurulation decreased, while the other enzymes, the chain elongation enzyme *Ext2*, and modification gene *Ndst1* were expressed increasingly as neurulation processes. Genes from the same family demonstrate a similar expression trend, for example, expression of *B3galt6* decreased, while *Ext1*, *Ndst2*, *Hs6st1* demonstrate an increasing trend. In addition, numerous (around 13) GAG genes were found highly expressed during spinal neurulation but no obvious difference, whereas a lot of GAGs (around 20) were present with relatively lower intensities. *Ext* gene family were first found as

hereditary multiple exostoses (HME) (Solomon,L. 1964) and involved in HS biosynthesis by adding alternating GlcNAc and GlcA residues to HS chains (McCormick et al., 2000). *Ext1* and *Ext2* are type II transmembrane proteins comprising an N-terminal cytoplasmic tail, a transmembrane domain, a stalk, and a large globular domain that is likely to have enzymatic activity. *Ext1* and *Ext2* form a hetero-oligomeric complex in vivo and accumulate in the Golgi apparatus. *Ext2* in an *Ext1*-defect cell line do not have significant glycosyltransferase activity. The Drosophila homologue of this gene family *ttv* has been identified as an HS chain elongation enzyme (Bellaiche et al., 1998; Lin and Wells, 1997). *Hh* molecules can not move in the *ttv* mutants indicating the involvement of HSPG in an essential morphogenetic pathway, the *Hh* pathway. Further studies using *ttv* mutants found that only Hh signaling is affected but not Wingless and FGF signaling. *Ext1* is an ER-localized glycoprotein and its expression increases the synthesis of cell surface HS. The many highly presented HSs may be explained by the increased expression of *Ext1* and *Ext2*, both of which have the GlcNAc transferase and GlcA transferase activities that catalyze the elongation of HS chains. Ext1-deficient mice fail to gastrulates and result in embryonic lethality indicates the importance of HS in tissue morphogenesis (Yamaguchi et al., 2010). The potential specific roles of HS in spinal neurulation can be studied in specific neural cell types by conditional inactivation of Exts.

GlcNAc N-deacetylase/N-sulfotransferase (NDST) genes are the first HS modification enzymes when the HS chains are elongated to catalyze GlcNAc N-deacetylation/N-sulfation. Its expression level is affected by the level of *Ext1* and *Ext2*, which, thus, influence the HS structure (Presto et al., 2008). Overexpression of *Ext2* in HEk 293 cells improved expression and N-glycosylation of NDST1, and HS sulfation, whereas overexpression of EXT1 had differing effects. It is speculated that NDST1 competes with EXT1 for binding to EXT2 because an

immunoprecipitation experiment proposed an interaction between EXT2 and NDST1. NDST1 activity increased in EXT1 deficient fibroblast. In the microarray results, Ndst1 expression pattern is consistent with *Ext2* which support the above description about the interaction between *Ext2* and *Ndst1*. A previous experiment shows the affection of Ndst on both Wg and FGF receptor pathways (Pallerla et al., 2007), though no known human pathology is found related with this gene family. Studies through Ndst-knockout mice shows that Ndst genes are more likely to compensate each other which can explain why no human pathology were found related with this gene family.

B4galt1 belongs to the family of Golgi glycosyltransferase with a product to be a type II transmembrane protein (Amado et al., 1999). This family have 7 members, but *B4galt1* is shown to be the most efficient in galactosylating the structures of glycoproteins. It is also the only one that is found expressed in murine lactating mammary glands and function as a lactose synthase. Another experiment ensures that *B4galt1* is highly expressed in lactating mammary glands and ubiquitously expressed at lower levels in other adult and fetal human organs. However, the *B4galt* activity levels did not correlate with its mRNA levels measured in fetal and adult mouse brains. It's known that glycosyltransferase I and II are essential for initiation of the synthesis of proteoglycans by link the GAGs onto associated core proteins. In addition, the *b4GalT* gene family shows sequence similarity with UDP-GalNAc: polypeptide GalNAc-transferases in the putative catalytic sites, so they may also involved in the synthesis of GAGs by transferring GalNAc. In the microarray results, expression of *B4galt1* was high at E8.5, but decreased obviously in both NT and MD. It's observed that another three genes, *B3galt6, Krt2-8*, and *Kral-18* was decreased, too. The former one belongs to a similar glycosyltranserase family, while the later two were highly related with the *B4galt1* involved product, keratin.

It is a very complicated scenario that many GAG genes and their synthesis enzymes and binding proteins were highly expressed during the mouse spinal neurulation, but some of the synthesis enzymes increasingly expressed while other enzymes were decreasingly expressed. The level of GAGs as well as their binding proteins may affect the differential expression level of the GAG synthesis enzymes. But the specific mechanism remains to be further investigated.

B4galt1 is a type II membrane protein share common *B4galt* gene features as well as the first mammalian, UDP-Gal: bGlcNAc, b1,4-galactosyltransferase (*b4Gal-T*), was cloned by transfection cloning strategy in 1986, followed by the identification of 6 other members in the same galactosyltransferase family, *b4Gal-T2* to T7. They are type II transmembrane proteins with common domain structures. They have conserved sequence motifs in association with the putative catalytic region which give them genetic and functional redundancy in sharing specificity for donor nucleotide, reaction mechanism and often transferring to the same position of acceptor sugars. The *b4GalT* gene family shows sequence similarity with UDP-GalNAc: polypeptide GalNAc-transferases in the putative catalytic sites.

4.3 B4galt1 may be involved in neurulation by affecting cell proliferation and adhesion

The present study has shown that expression of *B4galt1* was significantly down-regulated in neuroepithelial cell lines. Knockdown of the expression of *B4galt1* by siRNA inhibited NE4C cell growth in culture, reduced its adhesion capacity in vitro, suggesting the possible functions of *B4galt1* in neuroepithelial growth and development.

Glycosaminoglycans (GAGs) are ubiquitously distributed on cell surface and in extracellular matrix. GAGs are participating in many biological processes such as tissue assembly, proliferation, differentiation, adhesion, motility, control of cell growth, and

morphogenesis by interacting with different proteins, growth factors, morphogens, or ligands, etc (Zhang, 2010b). Studies show that mutation in GAG core proteins or their biosynthetic enzymes in Drosophila, Xenopus or mouse influence the function of several growth factor pathways that are essential for growth and morphogenesis (Munoz et al., 2006; Princivalle and de, 2002; Yip et al., 2002). GAG synthesis is initiated by sequential addition of four monosaccharides (Xyl-Gal-Gal-GlcA) which links the sugar chains to core proteins. Galactosyltransferase play essential roles in GAG biosynthesis and extending of their sugar chains which determine the GAG heterogeneity and binding specificity and further their biological functions (Fransson et al., 2000; Silbert and Sugumaran, 2002; Zhang, 2010b). There are 7 members in the β4Gal-T family, they located at different chromosomal loci with exclusive specificity for the donor substrate UDP-Gal, and all transfers Gal in a β1,4-linkage to similar acceptor sugars: GlcNAc, Glc, and Xyl (Amado et al., 1999). Among these family members, *β4Galt1* is the most profoundly studied for its structure and expression.

4.3.1 B4galt1 affects NE4C cell proliferation

Surface GalTase has been suggested to function during cellular proliferation. In several studies, specifically perturbating GalTase could inhibit cell growth in vivo and in vitro. Further studies identified that surface GalTase and/or its galactosylated substrates controlling cell growth by delivering a growth inhibitory signal which may be epidermal growth factor (EGF) receptor (Hinton et al., 1995). There is so far no report regarding whether *B4galt1* expression has any effect on neuroepithelial cell proliferation. To answer this question, NE4C cells originating from the mouse neuroepithelial cell were transfected with two sequences of siRNA targeting *B4galt1* gene or scrambled siRNA (control). Decreased expression of *B4galt1* gene by silencing

both sequences was shown to significantly inhibit the NE4C cell growth, which is consistent with the reported studies. Both two sequences of siRNA were designed to target different residues of the catalytic domain of *B4galt1* which face the lumen side of the Golgi. The catalytic domain is the most important part for the functions of the gene *B4galt1*. It is responsible for recognizing the nucleotide donor by its N-terminal domain, and binding the acceptor substrate by its C-terminal domain. Mutation in catalytic domain may induce conformational change which may affect the bounding states of the enzyme, and further affect the binding specificity to different mental ions or sugar-nucleotides of the enzyme. This changing may result in cellular glycans with altered sugar residues and affect the normal cellular processes (Qasba et al., 2008). According to the results of this study, it is hypothesized that the silencing of B4galt1 may affect cell growth by two potential mechanisms: (1) The binding specificity was abrogated so that the expression of GAGs and their distribution in cells changed which may change the cell growth rate accordingly. (2) The conformational change in the catalytic domain of *B4galt1* affect the binding specificity of this gene to its ligands such as growth factors and further affect the cell proliferation as reported in other cell types. In a previous study, removing the terminal galactosyl residues in cytoplasmic domain by beta-galactosidase digestion will lose the growth inhibitory activity of isolated plasma membranes and specific glycoproteins (Wieser and Oesch, 1988). While in current study, perturbation of the catalytic domain of *B4galt1* by siRNA inhibited the cell proliferation.

4.3.2 B4galt1 affects NE4C cell adhesion

The GalTase was shown playing a role in cell adhesion in studies investigating primary spermatocytes. GalTase was shown to present on the surface of the mature sperm and mediating the sperm-egg reorganization and binding (Nixon et al., 2001). It was also expressed by spermatocytes and Sertoli cells and localized at the areas of putative germ cell-Sertoli cell contact region where it may mediate cell adhesion of the two cell types, while anti-GalTase antibodies inhibited the initial adhesion of spermatocytes to Sertoli cell monolayers (Miller et al., 1992; Shur, 1993). Most GalTase was found confined to the basal cell surface where it may mediate cell adhesion to the underlying basal lamina. The mechanism of GalTase to be an adhesion molecule was designated as the cytoplasmic extension of this molecule targeting its protein to the cell surface where it functions as a cell adhesion molecule.

As is well known, GAGs were involved in the critical process of neural tube closure (Copp and Bernfield, 1988b; Yip et al., 2002). In the current study, there were also many GAG genes as well as B4galt1 having been found differentially expressed in NT and MD during the critical stages of neural tube closure. What does it mean of the colocolization of GAG genes with adhesion genes for the neurulation process? What's the potential role of *B4galt1* during this process? Does it have any interaction with adhesion molecules during this process? To answer these questions, the expression of *B4galt1* was reduced by targeted silencing and its interaction with collagen and fibronectin was investigated in mouse neuroepithelial NE4C cells. Experiment results showed that reduced expression of *B4galt1* can significantly inhibit the adhesion ability of NE4C cells to collagen and fibronectin. Mutation in different residues on the catalytic domain of *B4galt1* got different results. As discussed above (in 4.3.1), this alteration in adhesion ability may be due to the conformational change in the catalytic domain of *B4galt1* gene which changed

its binding specificity to ligands. This mechanism may be different from the reported study that truncated dominant negative *B4galt1* without the catalytic domain can inhibit cell adhesion in both F9 embryonal carcinoma cells and Swiss 3T3 fibroblasts (Shur, 1983). It is hypothesized that both catalytic and cytoplasmic domains can be involved in the regulation of interaction to adhesion molecules, and they may function individually or in combination. Here we showed by targeted mutation at catalytic domain alone that catalytic domain can be involved in the regulation of interaction ability of *B4galts* to adhesion molecules individually. Another potential mechanism for the regulation of adhesion by *B4galt1* in the NE4C cell adhesion ability may be due to the expression and/or distribution of different proteoglycan molecules synthesized by *B4galt1*. A previous study reported that colocalization of collagen, fibronectin, and proteoglycan existed and functioned in chick lung morphogenesis, it should not excluded the possibility that the colocalization of collagen, fibronectin with different types of proteoglycans can also play roles in neural tube morphogenesis. Studies show that GalTase is preferentially localized on cell lamellipodia and filopodia by binding to its N-linked oligosaccharide substrate (Eckstein and Shur, 1989; Runyan et al., 1988), then it controls the lamellipodia formation by its cytoplasmic domains (Appeddu and Shur, 1994). As is known by an observation that directed lamelliform protrusions attaching to and crawl on adjacent cells during convergent extension (CE) and planar cell polarity (PCP) of the neural plate and the surrounding mesoderm (Keller, 2002), it is probable that GalTase may play a role during CE and PCP by binding to and regulating the formation of lamelliform protrusions. Though the above serial studies show no signs of interaction of GalTase to the fibronectin, which may not contain binding sites for surface GalTase (Appeddu and Shur, 1994), in the current study, reduction of *B4galt1* can affect the adhesion ability of NE4C cells to fibronectin by mutation on residues of the last exon in the

catalytic domain. The mechanism for the different results for mutation of different residues is exploratory. It may be change of three-dimensional structure of the gene which may affect the binding specificity or affinity of the gene.

Western blotting could be helpful to determine whether the function changes are due to changes in gene transcript levels or were accompanied by similar changes in protein level.

To further find out the mechanism by which suppression of *B4galt1* inhibits NE4C cell proliferation and adhesion ability, a systematic gene expression profiling analysis by microarray could be helpful. As *B4galt1* has been found to mediate Notch signaling in cultured mammalian cells (Chen et al., 2001) as well as affect Notch signaling in mammalian embryos during embryogenesis (Chen et al., 2006), and the Notch signaling has been revealed as essential for neural tube closure (Copp and Greene, 2010b), the study on gene expression profile after silencing *B4galt1* in NE4C cells could also reveal whether any pathways are deregulated by suppression of *B4galt1* in neural tube closure.

In summary, the present study has shown for the first time in mammalian cells that knockdown of the expression of *B4galt1* inhibited neuroepithelial cell growth and adhesion ability in vitro, suggesting the possibility that *B4galt1* involved in morphogenesis of neural epithelial cells.

CHAPTER 5

CONCLUSION AND FUTURE WORKS

5. Conclusion and future studies

This study investigated the genetic mechanism of mammalian spinal neurulation by high-density oligonucleotide microarray using laser capture microdissected tissues.

Firstly, a reliable and reproducible protocol was optimized to get total RNA with good quality and quantity from the LCM tissue samples. It was found that snap-freezing the mouse embryos by liquid nitrogen immediately after dissection protects RNA quality without damage to the morphology of the sections. This result is supported by other studies by Xiang, C.C. et al (Xiang et al., 2004).

To protect the RNA integrity during the microdissection processing time at room temperature, RNAlater-ICE was applied on the cryosections after cutting. The application of RNAlater-ICE helped protect the RNA quality especially for the MD tissues which were microdissected one hour later after the first microdissection of NT. The quality of the total RNA of the nine MD samples was found to be as good as the nine NT samples. This application is novel and can be taken as model for protecting RNA integrity in tissues processed at room temperature.

In the quickly stain method, sections were stained in Haematoxylin followed by dehydration in serial concentrations of ethanol. The length of time of staining and dehydration was reduced from several minutes of the classical method to several seconds. This method can save time and reduce the possibility of RNase contamination.

Total RNA was extracted from 18 microdissected samples. Concentrations of each sample were around 10 ng/µl of 11 µl, which were enough for amplification before hybridization on microarray chips. Quality of the total RNA was measured by Agilent 2100 bioanalyzer and RIN numbers of all RNA samples measured by the Analyzer were above 7.5 indicating good

quality of RNA for microarray analysis (Fleige and Pfaffl, 2006; Jones et al., 2006). The total RNA was amplified and labeled into Bio-cRNA by a two-step cDNA synthesis in combination with an IVT amplification. At least 27μg of Bio-cRNA was acquired from a starting 15ng total RNA, and these results show good quality of starting RNA and enough quantity of Bio-cRNA for microarray analysis (Dumur et al., 2004; Jones et al., 2006).

Secondly, the potential genetic mechanisms of spinal neurulation were studied by transcriptomic expression profiling analysis. One transcriptomic profiling was acquired for each array by single array analysis, and this profiling provided a snapshot for each stage during the neural tube closing process. Comparison of profiling between different stages revealed a variety of differentially expressed genes and these genes may account for morphology changing of the neuroepithelium, from formation of MHP to DLHP till closure of the PNP. Genes with functions of proliferation, differentiation, adhesion, migration and cell cycle were found in most of the gene lists, and genes with multiple other functions such as cell polarity, proteolysis, apoptosis, transport, metabolism, etc, were also found in the gene lists. These above mentioned functions were found to be important for neural tube closure in previous studies (Copp and Greene, 2010b), so the potential contributions of these genes are worth exploring in the future. Genes involved in several pathways and signaling cascades such as Wnt, Shh, RTK, GPCR, and MAkkk were found in the profiling analysis. A detailed investigation of genes involved in the diverse biological processes and multiple pathways revealed genes that directly or indirectly regulate neural tube closure by mechanism of inhibiting MHP and/or accelerating DLHP formation. The transcriptomic profiling analysis also revealed a group of GAG associated genes. Since GAG genes have been found involved in diverse biological processes and interacting with multiple pathways (Zhang, 2010b), they hold the possibility to be critical regulators during neurulation.

The GAG synthesizing initiating enzyme, B4galt1, was found differentially expressed in the microarray data. Knockdown of B4galt1 by siRNA in the mouse neuroepithelial cells inhibited cell proliferation and adhesion abilities. These results indicate that GAG genes found by microarray analysis are worth exploring further to find their specific roles in neurulation.

The transcriptomic profiling analysis in the current study provided a vivid description of the spatial and temporal expression of genes that were involved in the construction of neural tube during mouse neurulation, and offer a promising approach for finding the key players in specific events such as MHP and DLHP formation during neural tube closure. The present study provides a comprehensive framework for future investigations on the genetic mechanism of the spinal neurulation. This is the first time that a transcriptomic profiling was set up using LCM technology in neurulation stage mouse embryos. The selection of three critical stages with typical mode change increases the opportunity of picking up the most possible genes for the closing process of the neurulation. Based on the present findings, genes found differentially expressed between different developmental stages may play different roles according to their up-stream regulating genes or down-stream targeting genes. The same gene may be involved in different biological events and regulating different signaling pathways and cascades.

Further study by in situ hybridization to confine the cellular or tissue specific expression pattern of critical genes is therefore needed to confirm the microarray results and investigate the potential regulating genes. Over expression of down-regulated genes or knocking down of up-regulated genes in neuroepithelial cells are recommended in order to reveal the functions of these genes and their interacting partners. The findings from the mutation studies in cells need to be confirmed by animal models using mutation technology. In vitro and in ova electroporation could provide a novel approach for investigating gene expression and regulation on embryos,

especially for cell-specific expressed genes. The genes that are confirmed by mouse models can be used for screening susceptible population in human and/or design prevention methods and/or treatment for NTDs.

Reference List

Ahn,Y., Sanderson,B.W., Klein,O.D., and Krumlauf,R. (2010). Inhibition of Wnt signaling by Wise (Sostdc1) and negative feedback from Shh controls tooth number and patterning. *Development* **137,** 3221-3231.

Allen,B.L., Tenzen,T., and McMahon,A.P. (2007). The Hedgehog-binding proteins Gas1 and Cdo cooperate to positively regulate Shh signaling during mouse development. *Genes Dev.* **21,** 1244-1257.

Almeida,R., Levery,S.B., Mandel,U., Kresse,H., Schwientek,T., Bennett,E.P., and Clausen,H. (1999). Cloning and expression of a proteoglycan UDP-galactose:beta-xylose beta1,4-galactosyltransferase I. A seventh member of the human beta4-galactosyltransferase gene family. *J. Biol. Chem.* **274,** 26165-26171.

Altschul,S.F., Gish,W., Miller,W., Myers,E.W., and Lipman,D.J. (1990). Basic local alignment search tool. *J. Mol. Biol.* **215,** 403-410.

Amado,M., Almeida,R., Schwientek,T., and Clausen,H. (1999). Identification and characterization of large galactosyltransferase gene families: galactosyltransferases for all functions. *Biochim. Biophys. Acta* **1473,** 35-53.

Ang,S.L. and Rossant,J. (1994). HNF-3 beta is essential for node and notochord formation in mouse development. *Cell* **78,** 561-574.

Appeddu,P.A. and Shur,B.D. (1994). Control of stable lamellipodia formation by expression of cell surface beta 1,4-galactosyltransferase cytoplasmic domains. *J. Cell Sci.* **107 (Pt 9),** 2535-2545.

Asano,M., Furukawa,K., Kido,M., Matsumoto,S., Umesaki,Y., Kochibe,N., and Iwakura,Y. (1997). Growth retardation and early death of beta-1,4-galactosyltransferase knockout mice with augmented proliferation and abnormal differentiation of epithelial cells. *EMBO J.* **16,** 1850-1857.

Ashburner,M., Ball,C.A., Blake,J.A., Botstein,D., Butler,H., Cherry,J.M., Davis,A.P., Dolinski,K., Dwight,S.S., Eppig,J.T. et al. (2000). Gene ontology: tool for the unification of biology. The Gene Ontology Consortium. *Nat. Genet.* **25,** 25-29.

Auer,H., Newsom,D.L., and Kornacker,K. (2009). Expression Profiling Using Affymetrix GeneChip Microarrays. *Methods Mol. Biol.* **509,** 35-46.

Bai,X., Zhou,D., Brown,J.R., Crawford,B.E., Hennet,T., and Esko,J.D. (2001). Biosynthesis of the linkage region of glycosaminoglycans: cloning and activity of galactosyltransferase II, the sixth member of the beta 1,3-galactosyltransferase family (beta 3GalT6). *J. Biol. Chem.* **276,** 48189-48195.

Baker,J.C., Beddington,R.S., and Harland,R.M. (1999). Wnt signaling in Xenopus embryos inhibits bmp4 expression and activates neural development. *Genes Dev.* **13,** 3149-3159.

Bally-Cuif,L., Goridis,C., and Santoni,M.J. (1993). The mouse NCAM gene displays a biphasic expression pattern during neural tube development. *Development* **117,** 543-552.

Bellaiche,Y., The,I., and Perrimon,N. (1998). Tout-velu is a Drosophila homologue of the putative tumour suppressor EXT-1 and is needed for Hh diffusion. *Nature* **394,** 85-88.

Bellin,R., Capila,I., Lincecum,J., Park,P.W., Reizes,O., and Bernfield,M.R. (2002). Unlocking the secrets of syndecans: transgenic organisms as a potential key. *Glycoconj. J.* **19,** 295-304.

Belo,J.A., Bachiller,D., Agius,E., Kemp,C., Borges,A.C., Marques,S., Piccolo,S., and De Robertis,E.M. (2000). Cerberus-like is a secreted BMP and nodal antagonist not essential for mouse development. *Genesis.* **26,** 265-270.

Bertucci,F., Loriod,B., Tagett,R., Granjeaud,S., Birnbaum,D., Nguyen,C., and Houlgatte,R. (2001). [DNA arrays: technological aspects and applications.]. *Bull. Cancer* **88,** 243-252.

Boeggeman,E.E., Ramakrishnan,B., and Qasba,P.K. (2003). The N-terminal stem region of bovine and human beta1,4-galactosyltransferase I increases the in vitro folding efficiency of their catalytic domain from inclusion bodies. *Protein Expr. Purif.* **30,** 219-229.

Bonner,R.F., Emmert-Buck,M., Cole,K., Pohida,T., Chuaqui,R., Goldstein,S., and Liotta,L.A. (1997). Laser capture microdissection: molecular analysis of tissue. *Science* **278,** 1481,1483.

Botto,L.D., Moore,C.A., Khoury,M.J., and Erickson,J.D. (1999). Neural-tube defects. *N. Engl. J. Med.* **341,** 1509-1519.

Brouns,M.R., Matheson,S.F., Hu,K.Q., Delalle,I., Caviness,V.S., Silver,J., Bronson,R.T., and Settleman,J. (2000). The adhesion signaling molecule p190 RhoGAP is required for morphogenetic processes in neural development. *Development* **127,** 4891-4903.

Brunskill,E.W., Aronow,B.J., Georgas,K., Rumballe,B., Valerius,M.T., Aronow,J., Kaimal,V., Jegga,A.G., Yu,J., Grimmond,S. et al. (2008). Atlas of gene expression in the developing kidney at microanatomic resolution. *Dev. Cell* **15,** 781-791.

Burgemeister,R. (2005). New aspects of laser microdissection in research and routine. *J. Histochem. Cytochem.* **53,** 409-412.

Bustin,S.A. (2002). Quantification of mRNA using real-time reverse transcription PCR (RT-PCR): trends and problems. *J. Mol. Endocrinol.* **29,** 23-39.

Camerer,E., Barker,A., Duong,D.N., Ganesan,R., Kataoka,H., Cornelissen,I., Darragh,M.R., Hussain,A., Zheng,Y.W., Srinivasan,Y. et al. (2010). Local protease signaling contributes to neural tube closure in the mouse embryo. *Dev. Cell* **18,** 25-38.

Casu,B. and Lindahl,U. (2001). Structure and biological interactions of heparin and heparan sulfate. *Adv. Carbohydr. Chem. Biochem.* **57,** 159-206.

Catala,M. (2002). Genetic control of caudal development. *Clin. Genet.* **61,** 89-96.

Cauthen,C.A., Berdougo,E., Sandler,J., and Burrus,L.W. (2001). Comparative analysis of the expression patterns of Wnts and Frizzleds during early myogenesis in chick embryos. *Mech. Dev.* **104,** 133-138.

Cayuso,J. and Marti,E. (2005). Morphogens in motion: growth control of the neural tube. *J. Neurobiol.* **64,** 376-387.

Chen,E., Hermanson,S., and Ekker,S.C. (2004). Syndecan-2 is essential for angiogenic sprouting during zebrafish development. *Blood* **103,** 1710-1719.

Chen,J., Lu,L., Shi,S., and Stanley,P. (2006). Expression of Notch signaling pathway genes in mouse embryos lacking beta4galactosyltransferase-1. *Gene Expr. Patterns.* **6,** 376-382.

Chen,J., Moloney,D.J., and Stanley,P. (2001). Fringe modulation of Jagged1-induced Notch signaling requires the action of beta 4galactosyltransferase-1. *Proc. Natl. Acad. Sci. U. S. A* **98,** 13716-13721.

Chen,R.L. and Lander,A.D. (2001). Mechanisms underlying preferential assembly of heparan sulfate on glypican-1. *J. Biol. Chem.* **276,** 7507-7517.

Chiang,C., Litingtung,Y., Lee,E., Young,K.E., Corden,J.L., Westphal,H., and Beachy,P.A. (1996). Cyclopia and defective axial patterning in mice lacking Sonic hedgehog gene function. *Nature* **383,** 407-413.

Choudhuri,S. (2004). Microarrays in biology and medicine. *J. Biochem. Mol. Toxicol.* **18,** 171-179.

Colas,J.F. and Schoenwolf,G.C. (2001). Towards a cellular and molecular understanding of neurulation. *Dev. Dyn.* **221,** 117-145.

Conway,T. and Schoolnik,G.K. (2003). Microarray expression profiling: capturing a genome-wide portrait of the transcriptome. *Mol. Microbiol.* **47,** 879-889.

Cope,L., Hartman,S.M., Gohlmann,H.W., Tiesman,J.P., and Irizarry,R.A. (2006). Analysis of Affymetrix GeneChip data using amplified RNA. *Biotechniques* **40,** 165-6, 168, 170.

Copp,A.J. and Bernfield,M. (1988a). Accumulation of basement membrane-associated hyaluronate is reduced in the posterior neuropore region of mutant (curly tail) mouse embryos developing spinal neural tube defects. *Dev. Biol.* **130,** 583-590.

Copp,A.J. and Bernfield,M. (1988b). Glycosaminoglycans vary in accumulation along the neuraxis during spinal neurulation in the mouse embryo. *Dev. Biol.* **130,** 573-582.

Copp,A.J. and Greene,N.D. (2010a). Defining a PARticular pathway of neural tube closure. *Dev. Cell* **18,** 1-2.

Copp,A.J. and Greene,N.D. (2010b). Genetics and development of neural tube defects. *J. Pathol.* **220,** 217-230.

Copp,A.J., Greene,N.D., and Murdoch,J.N. (2003). The genetic basis of mammalian neurulation. *Nat. Rev. Genet.* **4,** 784-793.

Copp,A.J., Seller,M.J., and Polani,P.E. (1982). Neural tube development in mutant (curly tail) and normal mouse embryos: the timing of posterior neuropore closure in vivo and in vitro. *J. Embryol. Exp. Morphol.* **69,** 151-167.

Cremer,H., Chazal,G., Goridis,C., and Represa,A. (1997). NCAM is essential for axonal growth and fasciculation in the hippocampus. *Mol. Cell Neurosci.* **8,** 323-335.

Curtin,J.A., Quint,E., Tsipouri,V., Arkell,R.M., Cattanach,B., Copp,A.J., Henderson,D.J., Spurr,N., Stanier,P., Fisher,E.M. et al. (2003). Mutation of Celsr1 disrupts planar polarity of inner ear hair cells and causes severe neural tube defects in the mouse. *Curr. Biol.* **13,** 1129-1133.

Czeizel,A.E. and Dudas,I. (1992). Prevention of the first occurrence of neural-tube defects by periconceptional vitamin supplementation. *N. Engl. J. Med.* **327,** 1832-1835.

Dalma-Weiszhausz,D.D., Warrington,J., Tanimoto,E.Y., and Miyada,C.G. (2006). The affymetrix GeneChip platform: an overview. *Methods Enzymol.* **410,** 3-28.

Day,R.C., Herridge,R.P., Ambrose,B.A., and Macknight,R.C. (2008). Transcriptome analysis of proliferating Arabidopsis endosperm reveals biological implications for the control of syncytial division, cytokinin signaling, and gene expression regulation. *Plant Physiol* **148,** 1964-1984.

De Robertis,E.M. and Kuroda,H. (2004). Dorsal-ventral patterning and neural induction in Xenopus embryos. *Annu. Rev. Cell Dev. Biol.* **20,** 285-308.

De,M.P., Merello,E., Mascelli,S., and Capra,V. (2006). Current perspectives on the genetic causes of neural tube defects. *Neurogenetics.* **7,** 201-221.

Deak,K.L., Boyles,A.L., Etchevers,H.C., Melvin,E.C., Siegel,D.G., Graham,F.L., Slifer,S.H., Enterline,D.S., George,T.M., Vekemans,M. et al. (2005). SNPs in the neural cell adhesion molecule 1 gene (NCAM1) may be associated with human neural tube defects. *Hum. Genet.* **117,** 133-142.

del,B.B., I, Davidson,G., Grone,H.J., Westphal,H., and Niehrs,C. (2003). Dkk1 and noggin cooperate in mammalian head induction. *Genes Dev.* **17,** 2239-2244.

Detrick,R.J., Dickey,D., and Kintner,C.R. (1990). The effects of N-cadherin misexpression on morphogenesis in Xenopus embryos. *Neuron* **4,** 493-506.

Ding,Q., Motoyama,J., Gasca,S., Mo,R., Sasaki,H., Rossant,J., and Hui,C.C. (1998). Diminished Sonic hedgehog signaling and lack of floor plate differentiation in Gli2 mutant mice. *Development* **125,** 2533-2543.

Dumur,C.I., Garrett,C.T., Archer,K.J., Nasim,S., Wilkinson,D.S., and Ferreira-Gonzalez,A. (2004a). Evaluation of a linear amplification method for small samples used on high-density oligonucleotide microarray analysis. *Anal. Biochem.* **331,** 314-321.

Dumur,C.I., Nasim,S., Best,A.M., Archer,K.J., Ladd,A.C., Mas,V.R., Wilkinson,D.S., Garrett,C.T., and Ferreira-Gonzalez,A. (2004b). Evaluation of quality-control criteria for microarray gene expression analysis. *Clin. Chem.* **50,** 1994-2002.

Echelard,Y., Epstein,D.J., St-Jacques,B., Shen,L., Mohler,J., McMahon,J.A., and McMahon,A.P. (1993). Sonic hedgehog, a member of a family of putative signaling molecules, is implicated in the regulation of CNS polarity. *Cell* **75,** 1417-1430.

Eckstein,D.J. and Shur,B.D. (1989). Laminin induces the stable expression of surface galactosyltransferase on lamellipodia of migrating cells. *J. Cell Biol.* **108,** 2507-2517.

Eckstein,D.J. and Shur,B.D. (1992). Cell surface beta-1,4-galactosyltransferase is associated with the detergent-insoluble cytoskeleton on migrating mesenchymal cells. *Exp. Cell Res.* **201,** 83-90.

Eggenschwiler,J.T., Espinoza,E., and Anderson,K.V. (2001). Rab23 is an essential negative regulator of the mouse Sonic hedgehog signalling pathway. *Nature* **412,** 194-198.

El-Serag,H.B., Nurgalieva,Z.Z., Mistretta,T.A., Finegold,M.J., Souza,R., Hilsenbeck,S., Shaw,C., and Darlington,G. (2009). Gene expression in Barrett's esophagus: laser capture versus whole tissue. *Scand. J. Gastroenterol.* **44,** 787-795.

Elbashir,S.M., Harborth,J., Lendeckel,W., Yalcin,A., Weber,K., and Tuschl,T. (2001). Duplexes of 21-nucleotide RNAs mediate RNA interference in cultured mammalian cells. *Nature* **411,** 494-498.

Emmert-Buck,M.R., Bonner,R.F., Smith,P.D., Chuaqui,R.F., Zhuang,Z., Goldstein,S.R., Weiss,R.A., and Liotta,L.A. (1996). Laser capture microdissection. *Science* **274,** 998-1001.

Espina,V., Milia,J., Wu,G., Cowherd,S., and Liotta,L.A. (2006). Laser capture microdissection. *Methods Mol. Biol.* **319,** 213-229.

Evans,S.C., Lopez,L.C., and Shur,B.D. (1993). Dominant negative mutation in cell surface beta 1,4-galactosyltransferase inhibits cell-cell and cell-matrix interactions. *J. Cell Biol.* **120,** 1045-1057.

Fekany-Lee,K., Gonzalez,E., Miller-Bertoglio,V., and Solnica-Krezel,L. (2000). The homeobox gene bozozok promotes anterior neuroectoderm formation in zebrafish through negative regulation of BMP2/4 and Wnt pathways. *Development* **127,** 2333-2345.

Fend,F., Emmert-Buck,M.R., Chuaqui,R., Cole,K., Lee,J., Liotta,L.A., and Raffeld,M. (1999). Immuno-LCM: laser capture microdissection of immunostained frozen sections for mRNA analysis. *Am. J. Pathol.* **154,** 61-66.

Fire,A., Xu,S., Montgomery,M.K., Kostas,S.A., Driver,S.E., and Mello,C.C. (1998). Potent and specific genetic interference by double-stranded RNA in Caenorhabditis elegans. *Nature* **391,** 806-811.

Fleige,S. and Pfaffl,M.W. (2006). RNA integrity and the effect on the real-time qRT-PCR performance. *Mol. Aspects Med.* **27,** 126-139.

Fransson,L.A., Belting,M., Jonsson,M., Mani,K., Moses,J., and Oldberg,A. (2000). Biosynthesis of decorin and glypican. *Matrix Biol.* **19,** 367-376.

Gandhi,N.S. and Mancera,R.L. (2008). The structure of glycosaminoglycans and their interactions with proteins. *Chem. Biol. Drug Des* **72,** 455-482.

Geelen,J.A. and Langman,J. (1979). Ultrastructural observations on closure of the neural tube in the mouse. *Anat. Embryol. (Berl)* **156,** 73-88.

Ginsberg,S.D. (2005). RNA amplification strategies for small sample populations. *Methods* **37,** 229-237.

Glinka,A., Wu,W., Delius,H., Monaghan,A.P., Blumenstock,C., and Niehrs,C. (1998). Dickkopf-1 is a member of a new family of secreted proteins and functions in head induction. *Nature* **391,** 357-362.

Gofflot,F., Hall,M., and Morriss-Kay,G.M. (1997). Genetic patterning of the developing mouse tail at the time of posterior neuropore closure. *Dev. Dyn.* **210,** 431-445.

Gofflot,F., Hall,M., and Morriss-Kay,G.M. (1998). Genetic patterning of the posterior neuropore region of curly tail mouse embryos: deficiency of Wnt5a expression. *Int. J. Dev. Biol.* **42,** 637-644.

Goodrich,L.V., Milenkovic,L., Higgins,K.M., and Scott,M.P. (1997). Altered neural cell fates and medulloblastoma in mouse patched mutants. *Science* **277,** 1109-1113.

Greene,N.D. and Copp,A.J. (2009). Development of the vertebrate central nervous system: formation of the neural tube. *Prenat. Diagn.* **29,** 303-311.

Grotewold,L., Theil,T., and Ruther,U. (1999). Expression pattern of Dkk-1 during mouse limb development. *Mech. Dev.* **89,** 151-153.

Gustavsson,P., Copp,A.J., and Greene,N.D. (2008). Grainyhead genes and mammalian neural tube closure. *Birth Defects Res. A Clin. Mol. Teratol.* **82,** 728-735.

Habas,R., Dawid,I.B., and He,X. (2003). Coactivation of Rac and Rho by Wnt/Frizzled signaling is required for vertebrate gastrulation. *Genes Dev.* **17,** 295-309.

Habas,R., Kato,Y., and He,X. (2001). Wnt/Frizzled activation of Rho regulates vertebrate gastrulation and requires a novel Formin homology protein Daam1. *Cell* **107,** 843-854.

Hamatani,T., Carter,M.G., Sharov,A.A., and Ko,M.S. (2004). Dynamics of global gene expression changes during mouse preimplantation development. *Dev. Cell* **6,** 117-131.

Hamilton,A.J. and Baulcombe,D.C. (1999). A species of small antisense RNA in posttranscriptional gene silencing in plants. *Science* **286,** 950-952.

Hammond,S.M., Bernstein,E., Beach,D., and Hannon,G.J. (2000). An RNA-directed nuclease mediates post-transcriptional gene silencing in Drosophila cells. *Nature* **404,** 293-296.

Harris,M.J. and Juriloff,D.M. (2007). Mouse mutants with neural tube closure defects and their role in understanding human neural tube defects. *Birth Defects Res. A Clin. Mol. Teratol.* **79,** 187-210.

Hartmann,U. and Maurer,P. (2001). Proteoglycans in the nervous system--the quest for functional roles in vivo. *Matrix Biol.* **20,** 23-35.

Hathaway,H.J., Evans,S.C., Dubois,D.H., Foote,C.I., Elder,B.H., and Shur,B.D. (2003). Mutational analysis of the cytoplasmic domain of beta1,4-galactosyltransferase I: influence of phosphorylation on cell surface expression. *J. Cell Sci.* **116,** 4319-4330.

Hathaway,H.J. and Shur,B.D. (1992). Cell surface beta 1,4-galactosyltransferase functions during neural crest cell migration and neurulation in vivo. *J. Cell Biol.* **117,** 369-382.

Hildebrand,J.D. and Soriano,P. (1999). Shroom, a PDZ domain-containing actin-binding protein, is required for neural tube morphogenesis in mice. *Cell* **99,** 485-497.

Hinton,D.A., Evans,S.C., and Shur,B.D. (1995). Altering the expression of cell surface beta 1,4-galactosyltransferase modulates cell growth. *Exp. Cell Res.* **219,** 640-649.

Holmberg,J., Clarke,D.L., and Frisen,J. (2000). Regulation of repulsion versus adhesion by different splice forms of an Eph receptor. *Nature* **408,** 203-206.

Hsu,D.R., Economides,A.N., Wang,X., Eimon,P.M., and Harland,R.M. (1998). The Xenopus dorsalizing factor Gremlin identifies a novel family of secreted proteins that antagonize BMP activities. *Mol. Cell* **1,** 673-683.

Huang,Y., Roelink,H., and McKnight,G.S. (2002). Protein kinase A deficiency causes axially localized neural tube defects in mice. *J. Biol. Chem.* **277,** 19889-19896.

Hue,I., Degrelle,S.A., Campion,E., and Renard,J.P. (2007). Gene expression in elongating and gastrulating embryos from ruminants. *Soc. Reprod. Fertil. Suppl* **64,** 365-377.

Hui,C.C. and Joyner,A.L. (1993). A mouse model of greig cephalopolysyndactyly syndrome: the extra-toesJ mutation contains an intragenic deletion of the Gli3 gene. *Nat. Genet.* **3,** 241-246.

Irizarry,R.A., Hobbs,B., Collin,F., Beazer-Barclay,Y.D., Antonellis,K.J., Scherf,U., and Speed,T.P. (2003). Exploration, normalization, and summaries of high density oligonucleotide array probe level data. *Biostatistics.* **4,** 249-264.

Ishiguro,K., Kadomatsu,K., Kojima,T., Muramatsu,H., Nakamura,E., Ito,M., Nagasaka,T., Kobayashi,H., Kusugami,K., Saito,H. et al. (2000a). Syndecan-4 deficiency impairs the fetal vessels in the placental labyrinth. *Dev. Dyn.* **219,** 539-544.

Jackson,R.L., Busch,S.J., and Cardin,A.D. (1991). Glycosaminoglycans: molecular properties, protein interactions, and role in physiological processes. *Physiol Rev.* **71,** 481-539.

Jenny,A. and Mlodzik,M. (2006). Planar cell polarity signaling: a common mechanism for cellular polarization. *Mt. Sinai J. Med.* **73,** 738-750.

Jiang,B., Kumar,S.D., Loh,W.T., Manikandan,J., Ling,E.A., Tay,S.S., and Dheen,S.T. (2008). Global gene expression analysis of cranial neural tubes in embryos of diabetic mice. *J. Neurosci. Res.* **86,** 3481-3493.

Jones,C. and Chen,P. (2007). Planar cell polarity signaling in vertebrates. *Bioessays* **29,** 120-132.

Jones,C.M., Kuehn,M.R., Hogan,B.L., Smith,J.C., and Wright,C.V. (1995). Nodal-related signals induce axial mesoderm and dorsalize mesoderm during gastrulation. *Development* **121,** 3651-3662.

Jones,L., Goldstein,D.R., Hughes,G., Strand,A.D., Collin,F., Dunnett,S.B., Kooperberg,C., Aragaki,A., Olson,J.M., Augood,S.J. et al. (2006). Assessment of the relationship between pre-chip and post-chip quality measures for Affymetrix GeneChip expression data. *BMC. Bioinformatics.* **7,** 211.

Jorgensen,R. (1990). Altered gene expression in plants due to trans interactions between homologous genes. *Trends Biotechnol.* **8,** 340-344.

Kampke,T., Kieninger,M., and Mecklenburg,M. (2001). Efficient primer design algorithms. *Bioinformatics.* **17,** 214-225.

Keller,R. (2002). Shaping the vertebrate body plan by polarized embryonic cell movements. *Science* **298,** 1950-1954.

Keller,R., Shook,D., and Skoglund,P. (2008). The forces that shape embryos: physical aspects of convergent extension by cell intercalation. *Phys. Biol.* **5,** 015007.

Kibar,Z., Capra,V., and Gros,P. (2007). Toward understanding the genetic basis of neural tube defects. *Clin. Genet.* **71,** 295-310.

Kibar,Z., Vogan,K.J., Groulx,N., Justice,M.J., Underhill,D.A., and Gros,P. (2001). Ltap, a mammalian homolog of Drosophila Strabismus/Van Gogh, is altered in the mouse neural tube mutant Loop-tail. *Nat. Genet.* **28,** 251-255.

Klein,T.J. and Mlodzik,M. (2005). Planar cell polarization: an emerging model points in the right direction. *Annu. Rev. Cell Dev. Biol.* **21,** 155-176.

Klohs,W.D., Wilson,J.R., and Weiser,M.M. (1982). UDP-galactose inhibition of BALB/3T12-3 cell growth. Requirement for medium galactosyltransferase activity. *Exp. Cell Res.* **141,** 365-374.

Kong,X.B. and Zhang,C. (2009). Dickkopf (Dkk) 1 promotes the differentiation of mouse embryonic stem cells toward neuroectoderm. *In Vitro Cell Dev. Biol. Anim* **45,** 185-193.

Kramer,K.L. and Yost,H.J. (2002). Ectodermal syndecan-2 mediates left-right axis formation in migrating mesoderm as a cell-nonautonomous Vg1 cofactor. *Dev. Cell* **2,** 115-124.

Kuhn,D.E., Roy,S., Radtke,J., Khanna,S., and Sen,C.K. (2007). Laser microdissection and capture of pure cardiomyocytes and fibroblasts from infarcted heart regions: perceived hyperoxia induces p21 in peri-infarct myocytes. *Am. J. Physiol Heart Circ. Physiol* **292,** H1245-H1253.

Kultima,K., Nystrom,A.M., Scholz,B., Gustafson,A.L., Dencker,L., and Stigson,M. (2004). Valproic acid teratogenicity: a toxicogenomics approach. *Environ. Health Perspect.* **112,** 1225-1235.

Kuroda,H., Wessely,O., and De Robertis,E.M. (2004). Neural induction in Xenopus: requirement for ectodermal and endomesodermal signals via Chordin, Noggin, beta-Catenin, and Cerberus. *PLoS. Biol.* **2,** E92.

Lakkis,M.M., Golden,J.A., O'Shea,K.S., and Epstein,J.A. (1999). Neurofibromin deficiency in mice causes exencephaly and is a modifier for Splotch neural tube defects. *Dev. Biol.* **212,** 80-92.

Launay,C., Fromentoux,V., Shi,D.L., and Boucaut,J.C. (1996). A truncated FGF receptor blocks neural induction by endogenous Xenopus inducers. *Development* **122,** 869-880.

Laurikkala,J., Kassai,Y., Pakkasjarvi,L., Thesleff,I., and Itoh,N. (2003). Identification of a secreted BMP antagonist, ectodin, integrating BMP, FGF, and SHH signals from the tooth enamel knot. *Dev. Biol.* **264,** 91-105.

Lee,H.Y. and Nagele,R.G. (1985). Studies on the mechanisms of neurulation in the chick: interrelationship of contractile proteins, microfilaments, and the shape of neuroepithelial cells. *J. Exp. Zool.* **235,** 205-215.

Lin,X. and Wells,D. (1997). Isolation of the mouse cDNA homologous to the human EXT1 gene responsible for Hereditary Multiple Exostoses. *DNA Seq.* **7,** 199-202.

Lobjois,V., Benazeraf,B., Bertrand,N., Medevielle,F., and Pituello,F. (2004). Specific regulation of cyclins D1 and D2 by FGF and Shh signaling coordinates cell cycle progression, patterning, and differentiation during early steps of spinal cord development. *Dev. Biol.* **273,** 195-209.

Lopez,L.C., Youakim,A., Evans,S.C., and Shur,B.D. (1991). Evidence for a molecular distinction between Golgi and cell surface forms of beta 1,4-galactosyltransferase. *J. Biol. Chem.* **266,** 15984-15991.

Lu,X., Borchers,A.G., Jolicoeur,C., Rayburn,H., Baker,J.C., and Tessier-Lavigne,M. (2004). PTK7/CCK-4 is a novel regulator of planar cell polarity in vertebrates. *Nature* **430,** 93-98.

Luzzi,V., Mahadevappa,M., Raja,R., Warrington,J.A., and Watson,M.A. (2003). Accurate and reproducible gene expression profiles from laser capture microdissection, transcript amplification, and high density oligonucleotide microarray analysis. *J. Mol. Diagn.* **5,** 9-14.

Maillet,C.M. and Shur,B.D. (1994). Perturbing cell surface beta-(1,4)-galactosyltransferase on F9 embryonal carcinoma cells arrests cell growth and induces laminin synthesis. *J. Cell Sci.* **107 (Pt 6),** 1713-1724.

Manchester,K.L. (1996). Use of UV methods for measurement of protein and nucleic acid concentrations. *Biotechniques* **20,** 968-970.

Marchase,R.B., Kidd,V.J., Rivera,A.A., and Humphreys-Beher,M.G. (1988). Cell surface expression of 4 beta-galactosyltransferase accompanies rat parotid gland acinar cell transition to growth. *J. Cell Biochem.* **36,** 453-465.

Margolis,R.U. and Margolis,R.K. (1997). Chondroitin sulfate proteoglycans as mediators of axon growth and pathfinding. *Cell Tissue Res.* **290,** 343-348.

Marselli,L., Sgroi,D.C., Bonner-Weir,S., and Weir,G.C. (2009). Laser capture microdissection of human pancreatic beta-cells and RNA preparation for gene expression profiling. *Methods Mol. Biol.* **560,** 87-98.

Martin,P. (2004). Morphogenesis: shroom in to close the neural tube. *Curr. Biol.* **14,** R150-R151.

Martinelli,D.C. and Fan,C.M. (2007). Gas1 extends the range of Hedgehog action by facilitating its signaling. *Genes Dev.* **21,** 1231-1243.

Masibay,A.S., Balaji,P.V., Boeggeman,E.E., and Qasba,P.K. (1993). Mutational analysis of the Golgi retention signal of bovine beta-1,4-galactosyltransferase. *J. Biol. Chem.* **268,** 9908-9916.

Matise,M.P., Epstein,D.J., Park,H.L., Platt,K.A., and Joyner,A.L. (1998). Gli2 is required for induction of floor plate and adjacent cells, but not most ventral neurons in the mouse central nervous system. *Development* **125,** 2759-2770.

McCormick,C., Duncan,G., Goutsos,K.T., and Tufaro,F. (2000). The putative tumor suppressors EXT1 and EXT2 form a stable complex that accumulates in the Golgi apparatus and catalyzes the synthesis of heparan sulfate. *Proc. Natl. Acad. Sci. U. S. A* **97,** 668-673.

McDowell,L.M., Frazier,B.A., Studelska,D.R., Giljum,K., Chen,J., Liu,J., Yu,K., Ornitz,D.M., and Zhang,L. (2006). Inhibition or activation of Apert syndrome FGFR2 (S252W) signaling by specific glycosaminoglycans. *J. Biol. Chem.* **281,** 6924-6930.

McGrew,L.L., Hoppler,S., and Moon,R.T. (1997). Wnt and FGF pathways cooperatively pattern anteroposterior neural ectoderm in Xenopus. *Mech. Dev.* **69,** 105-114.

Megason,S.G. and McMahon,A.P. (2002). A mitogen gradient of dorsal midline Wnts organizes growth in the CNS. *Development* **129,** 2087-2098.

Michl,P., Knobel,B., and Downward,J. (2006). CUTL1 is phosphorylated by protein kinase A, modulating its effects on cell proliferation and motility. *J. Biol. Chem.* **281,** 15138-15144.

Millenaar,F.F., Okyere,J., May,S.T., van,Z.M., Voesenek,L.A., and Peeters,A.J. (2006). How to decide? Different methods of calculating gene expression from short oligonucleotide array data will give different results. *BMC. Bioinformatics.* **7,** 137.

Miller,D.J., Macek,M.B., and Shur,B.D. (1992). Complementarity between sperm surface beta-1,4-galactosyltransferase and egg-coat ZP3 mediates sperm-egg binding. *Nature* **357,** 589-593.

Mitchell,L.E. (2005). Epidemiology of neural tube defects. *Am. J. Med. Genet. C. Semin. Med. Genet.* **135C,** 88-94.

Mlodzik,M. (2002). Planar cell polarization: do the same mechanisms regulate Drosophila tissue polarity and vertebrate gastrulation? *Trends Genet.* **18,** 564-571.

Mocellin,S. and Rossi,C.R. (2007). Principles of gene microarray data analysis. *Adv. Exp. Med. Biol.* **593,** 19-30.

Mueller,O., Hahnenberger,K., Dittmann,M., Yee,H., Dubrow,R., Nagle,R., and Ilsley,D. (2000). A microfluidic system for high-speed reproducible DNA sizing and quantitation. *Electrophoresis* **21,** 128-134.

Muller,F. and O'Rahilly,R. (1987). The development of the human brain, the closure of the caudal neuropore, and the beginning of secondary neurulation at stage 12. *Anat. Embryol. (Berl)* **176,** 413-430.

Munoz,R., Moreno,M., Oliva,C., Orbenes,C., and Larrain,J. (2006). Syndecan-4 regulates non-canonical Wnt signalling and is essential for convergent and extension movements in Xenopus embryos. *Nat. Cell Biol.* **8,** 492-500.

Murata,S., Kawahara,H., Tohma,S., Yamamoto,K., Kasahara,M., Nabeshima,Y., Tanaka,K., and Chiba,T. (1999). Growth retardation in mice lacking the proteasome activator PA28gamma. *J. Biol. Chem.* **274,** 38211-38215.

Murdoch,J.N., Doudney,K., Paternotte,C., Copp,A.J., and Stanier,P. (2001). Severe neural tube defects in the loop-tail mouse result from mutation of Lpp1, a novel gene involved in floor plate specification. *Hum. Mol. Genet.* **10,** 2593-2601.

Murdoch,J.N., Henderson,D.J., Doudney,K., Gaston-Massuet,C., Phillips,H.M., Paternotte,C., Arkell,R., Stanier,P., and Copp,A.J. (2003). Disruption of scribble (Scrb1) causes severe neural tube defects in the circletail mouse. *Hum. Mol. Genet.* **12,** 87-98.

Nagai,T., Aruga,J., Minowa,O., Sugimoto,T., Ohno,Y., Noda,T., and Mikoshiba,K. (2000). Zic2 regulates the kinetics of neurulation. *Proc. Natl. Acad. Sci. U. S. A* **97,** 1618-1623.

Nagai,T., Aruga,J., Takada,S., Gunther,T., Sporle,R., Schughart,K., and Mikoshiba,K. (1997). The expression of the mouse Zic1, Zic2, and Zic3 gene suggests an essential role for Zic genes in body pattern formation. *Dev. Biol.* **182,** 299-313.

Niemann,H., Carnwath,J.W., and Kues,W. (2007). Application of DNA array technology to mammalian embryos. *Theriogenology* **68 Suppl 1,** S165-S177.

Nixon,B., Lu,Q., Wassler,M.J., Foote,C.I., Ensslin,M.A., and Shur,B.D. (2001). Galactosyltransferase function during mammalian fertilization. *Cells Tissues. Organs* **168,** 46-57.

Niyaz,Y., Stich,M., Sagmuller,B., Burgemeister,R., Friedemann,G., Sauer,U., Gangnus,R., and Schutze,K. (2005). Noncontact laser microdissection and pressure catapulting: sample preparation for genomic, transcriptomic, and proteomic analysis. *Methods Mol. Med.* **114,** 1-24.

Norman,R.X., Ko,H.W., Huang,V., Eun,C.M., Abler,L.L., Zhang,Z., Sun,X., and Eggenschwiler,J.T. (2009). Tubby-like protein 3 (TULP3) regulates patterning in the mouse embryo through inhibition of Hedgehog signaling. *Hum. Mol. Genet.* **18,** 1740-1754.

Nyholm,M.K., Abdelilah-Seyfried,S., and Grinblat,Y. (2009). A novel genetic mechanism regulates dorsolateral hinge-point formation during zebrafish cranial neurulation. *J. Cell Sci.* **122,** 2137-2148.

O'Rahilly,R. and Muller,F. (1989). Interpretation of some median anomalies as illustrated by cyclopia and symmelia. *Teratology* **40,** 409-421.

Okajima,T., Yoshida,K., Kondo,T., and Furukawa,K. (1999). Human homolog of Caenorhabditis elegans sqv-3 gene is galactosyltransferase I involved in the biosynthesis of the glycosaminoglycan-protein linkage region of proteoglycans. *J. Biol. Chem.* **274,** 22915-22918.

Padmanabhan,R. (2006). Etiology, pathogenesis and prevention of neural tube defects. *Congenit. Anom. (Kyoto)* **46,** 55-67.

Pallerla,S.R., Pan,Y., Zhang,X., Esko,J.D., and Grobe,K. (2007). Heparan sulfate Ndst1 gene function variably regulates multiple signaling pathways during mouse development. *Dev. Dyn.* **236,** 556-563.

Park,H.L., Bai,C., Platt,K.A., Matise,M.P., Beeghly,A., Hui,C.C., Nakashima,M., and Joyner,A.L. (2000). Mouse Gli1 mutants are viable but have defects in SHH signaling in combination with a Gli2 mutation. *Development* **127,** 1593-1605.

Paulson,J.C. and Colley,K.J. (1989). Glycosyltransferases. Structure, localization, and control of cell type-specific glycosylation. *J. Biol. Chem.* **264,** 17615-17618.

Pera,E.M., Ikeda,A., Eivers,E., and De Robertis,E.M. (2003). Integration of IGF, FGF, and anti-BMP signals via Smad1 phosphorylation in neural induction. *Genes Dev.* **17,** 3023-3028.

Pera,E.M., Wessely,O., Li,S.Y., and De Robertis,E.M. (2001). Neural and head induction by insulin-like growth factor signals. *Dev. Cell* **1,** 655-665.

Perlmutter,M.A., Best,C.J., Gillespie,J.W., Gathright,Y., Gonzalez,S., Velasco,A., Linehan,W.M., Emmert-Buck,M.R., and Chuaqui,R.F. (2004). Comparison of snap freezing versus ethanol fixation for gene expression profiling of tissue specimens. *J. Mol. Diagn.* **6,** 371-377.

Portillo,M., Lindsey,K., Casson,S., Garcia-Casado,G., Solano,R., Fenoll,C., and Escobar,C. (2009). Isolation of RNA from laser-capture-microdissected giant cells at early differentiation stages suitable for differential transcriptome analysis. *Mol. Plant Pathol.* **10,** 523-535.

Presto,J., Thuveson,M., Carlsson,P., Busse,M., Wilen,M., Eriksson,I., Kusche-Gullberg,M., and Kjellen,L. (2008). Heparan sulfate biosynthesis enzymes EXT1 and EXT2 affect NDST1 expression and heparan sulfate sulfation. *Proc. Natl. Acad. Sci. U. S. A* **105,** 4751-4756.

Princivalle,M. and de,A.A. (2002). Developmental roles of heparan sulfate proteoglycans: a comparative review in Drosophila, mouse and human. *Int. J. Dev. Biol.* **46,** 267-278.

Qasba,P.K., Ramakrishnan,B., and Boeggeman,E. (2008). Structure and function of beta -1,4-galactosyltransferase. *Curr. Drug Targets.* **9,** 292-309.

Qian,D., Jones,C., Rzadzinska,A., Mark,S., Zhang,X., Steel,K.P., Dai,X., and Chen,P. (2007). Wnt5a functions in planar cell polarity regulation in mice. *Dev. Biol.* **306,** 121-133.

Qian,Y.W., Wang,Y.C., Hollingsworth,R.E., Jr., Jones,D., Ling,N., and Lee,E.Y. (1993). A retinoblastoma-binding protein related to a negative regulator of Ras in yeast. *Nature* **364,** 648-652.

Radice,G.L., Ferreira-Cornwell,M.C., Robinson,S.D., Rayburn,H., Chodosh,L.A., Takeichi,M., and Hynes,R.O. (1997a). Precocious mammary gland development in P-cadherin-deficient mice. *J. Cell Biol.* **139,** 1025-1032.

Radice,G.L., Rayburn,H., Matsunami,H., Knudsen,K.A., Takeichi,M., and Hynes,R.O. (1997b). Developmental defects in mouse embryos lacking N-cadherin. *Dev. Biol.* **181,** 64-78.

Redline,R.W., Neish,A., Holmes,L.B., and Collins,T. (1992). Homeobox genes and congenital malformations. *Lab Invest* **66,** 659-670.

Rifat,Y., Parekh,V., Wilanowski,T., Hislop,N.R., Auden,A., Ting,S.B., Cunningham,J.M., and Jane,S.M. (2010). Regional neural tube closure defined by the Grainy head-like transcription factors. *Dev. Biol.* **345,** 237-245.

Rodeheffer,C. and Shur,B.D. (2002). Targeted mutations in beta1,4-galactosyltransferase I reveal its multiple cellular functions. *Biochim. Biophys. Acta* **1573,** 258-270.

Rolny,C., Spillmann,D., Lindahl,U., and Claesson-Welsh,L. (2002). Heparin amplifies platelet-derived growth factor (PDGF)- BB-induced PDGF alpha -receptor but not PDGF beta -receptor tyrosine phosphorylation in heparan sulfate-deficient cells. Effects on signal transduction and biological responses. *J. Biol. Chem.* **277,** 19315-19321.

Romano,N. and Macino,G. (1992). Quelling: transient inactivation of gene expression in Neurospora crassa by transformation with homologous sequences. *Mol. Microbiol.* **6,** 3343-3353.

Roseman,S. (1970). The synthesis of complex carbohydrates by multiglycosyltransferase systems and their potential function in intercellular adhesion. *Chem. Phys. Lipids* **5,** 270-297.

Roseman,S. (2001). Reflections on glycobiology. *J. Biol. Chem.* **276,** 41527-41542.

Rossi,A., Biancheri,R., Cama,A., Piatelli,G., Ravegnani,M., and Tortori-Donati,P. (2004). Imaging in spine and spinal cord malformations. *Eur. J. Radiol.* **50,** 177-200.

Roth,S., McGuire,E.J., and Roseman,S. (1971). Evidence for cell-surface glycosyltransferases. Their potential role in cellular recognition. *J. Cell Biol.* **51,** 536-547.

Roth,S. and White,D. (1972). Intercellular contact and cell-surface galactosyl transferase activity (cell culture-mouse-radioautography-contact inhibition-cis-and trans-galactosylation). *Proc. Natl. Acad. Sci. U. S. A* **69,** 485-489.

Rozen,S. and Skaletsky,H. (2000). Primer3 on the WWW for general users and for biologist programmers. *Methods Mol. Biol.* **132,** 365-386.

Rubin,J.B., Choi,Y., and Segal,R.A. (2002). Cerebellar proteoglycans regulate sonic hedgehog responses during development. *Development* **129,** 2223-2232.

Runyan,R.B., Maxwell,G.D., and Shur,B.D. (1986). Evidence for a novel enzymatic mechanism of neural crest cell migration on extracellular glycoconjugate matrices. *J. Cell Biol.* **102,** 432-441.

Runyan,R.B., Versalovic,J., and Shur,B.D. (1988). Functionally distinct laminin receptors mediate cell adhesion and spreading: the requirement for surface galactosyltransferase in cell spreading. *J. Cell Biol.* **107,** 1863-1871.

Ruppert,R., Hoffmann,E., and Sebald,W. (1996). Human bone morphogenetic protein 2 contains a heparin-binding site which modifies its biological activity. *Eur. J. Biochem.* **237,** 295-302.

Russo,R.N., Shaper,N.L., and Shaper,J.H. (1990). Bovine beta 1----4-galactosyltransferase: two sets of mRNA transcripts encode two forms of the protein with different amino-terminal domains. In vitro translation experiments demonstrate that both the short and the long forms of the enzyme are type II membrane-bound glycoproteins. *J. Biol. Chem.* **265,** 3324-3331.

Rutishauser,U. and Jessell,T.M. (1988). Cell adhesion molecules in vertebrate neural development. *Physiol Rev.* **68,** 819-857.

Sadler,T.W., Greenberg,D., Coughlin,P., and Lessard,J.L. (1982). Actin distribution patterns in the mouse neural tube during neurulation. *Science* **215,** 172-174.

Saito,A. and Munakata,H. (2004). Detection of chondroitin sulfate-binding proteins on the membrane. *Electrophoresis* **25,** 2452-2460.

Saito,A. and Munakata,H. (2007). Analysis of plasma proteins that bind to glycosaminoglycans. *Biochim. Biophys. Acta* **1770,** 241-246.

Saitsu,H., Yamada,S., Uwabe,C., Ishibashi,M., and Shiota,K. (2004). Development of the posterior neural tube in human embryos. *Anat. Embryol. (Berl)* **209,** 107-117.

Sakai,Y. (1989). Neurulation in the mouse: manner and timing of neural tube closure. *Anat. Rec.* **223,** 194-203.

Salsi,V. and Zappavigna,V. (2006). Hoxd13 and Hoxa13 directly control the expression of the EphA7 Ephrin tyrosine kinase receptor in developing limbs. *J. Biol. Chem.* **281,** 1992-1999.

Sanati,S., Watson,M.A., Salavaggione,A.L., and Humphrey,P.A. (2009). Gene expression profiles of ductal versus acinar adenocarcinoma of the prostate. *Mod. Pathol.* **22,** 1273-1279.

Sansregret,L., Goulet,B., Harada,R., Wilson,B., LeDuy,L., Bertoglio,J., and Nepveu,A. (2006). The p110 isoform of the CDP/Cux transcription factor accelerates entry into S phase. *Mol. Cell Biol.* **26,** 2441-2455.

Schadt,E.E., Li,C., Ellis,B., and Wong,W.H. (2001). Feature extraction and normalization algorithms for high-density oligonucleotide gene expression array data. *J. Cell Biochem. Suppl* **Suppl 37,** 120-125.

Schlessinger,K., Hall,A., and Tolwinski,N. (2009). Wnt signaling pathways meet Rho GTPases. *Genes Dev.* **23,** 265-277.

Schlett,K., Herberth,B., and Madarasz,E. (1997). In vitro pattern formation during neurogenesis in neuroectodermal progenitor cells immortalized by p53-deficiency. *Int. J. Dev. Neurosci.* **15,** 795-804.

Schlett,K. and Madarasz,E. (1997). Retinoic acid induced neural differentiation in a neuroectodermal cell line immortalized by p53 deficiency. *J. Neurosci. Res.* **47,** 405-415.

Schoenwolf,G.C. and Smith,J.L. (1990). Mechanisms of neurulation: traditional viewpoint and recent advances. *Development* **109,** 243-270.

Schroeder,A., Mueller,O., Stocker,S., Salowsky,R., Leiber,M., Gassmann,M., Lightfoot,S., Menzel,W., Granzow,M., and Ragg,T. (2006). The RIN: an RNA integrity number for assigning integrity values to RNA measurements. *BMC. Mol. Biol.* **7,** 3.

Scully,N.F., Shaper,J.H., and Shur,B.D. (1987). Spatial and temporal expression of cell surface galactosyltransferase during mouse spermatogenesis and epididymal maturation. *Dev. Biol.* **124,** 111-124.

Shalon,D., Smith,S.J., and Brown,P.O. (1996). A DNA microarray system for analyzing complex DNA samples using two-color fluorescent probe hybridization. *Genome Res.* **6,** 639-645.

Shaper,N.L., Hollis,G.F., Douglas,J.G., Kirsch,I.R., and Shaper,J.H. (1988). Characterization of the full length cDNA for murine beta-1,4-galactosyltransferase. Novel features at the 5'-end predict two translational start sites at two in-frame AUGs. *J. Biol. Chem.* **263,** 10420-10428.

Shaper,N.L., Shaper,J.H., Meuth,J.L., Fox,J.L., Chang,H., Kirsch,I.R., and Hollis,G.F. (1986). Bovine galactosyltransferase: identification of a clone by direct immunological screening of a cDNA expression library. *Proc. Natl. Acad. Sci. U. S. A* **83,** 1573-1577.

Shirane,M., Ogawa,M., Motoyama,J., and Nakayama,K.I. (2008). Regulation of apoptosis and neurite extension by FKBP38 is required for neural tube formation in the mouse. *Genes Cells* **13,** 635-651.

Shum,A.S. and Copp,A.J. (1996). Regional differences in morphogenesis of the neuroepithelium suggest multiple mechanisms of spinal neurulation in the mouse. *Anat. Embryol. (Berl)* **194,** 65-73.

Shur,B.D. (1977). Cell-surface glycosyltransferases in gastrulating chick embryos. I. Temporally and spatially specific patterns of four endogenous glycosyltransferase activities. *Dev. Biol.* **58,** 23-39.

Shur,B.D. (1983). Embryonal carcinoma cell adhesion: the role of surface galactosyltransferase and its 90K lactosaminoglycan substrate. *Dev. Biol.* **99,** 360-372.

Shur,B.D. (1993). Glycosyltransferases as cell adhesion molecules. *Curr. Opin. Cell Biol.* **5,** 854-863.

Silbert,J.E. and Sugumaran,G. (2002). Biosynthesis of chondroitin/dermatan sulfate. *IUBMB. Life* **54,** 177-186.

Smith,J.L. and Schoenwolf,G.C. (1988). Role of cell-cycle in regulating neuroepithelial cell shape during bending of the chick neural plate. *Cell Tissue Res.* **252,** 491-500.

Smith,J.L., Schoenwolf,G.C., and Quan,J. (1994). Quantitative analyses of neuroepithelial cell shapes during bending of the mouse neural plate. *J. Comp Neurol.* **342,** 144-151.

Smitherman,M., Lee,K., Swanger,J., Kapur,R., and Clurman,B.E. (2000). Characterization and targeted disruption of murine Nup50, a p27(Kip1)-interacting component of the nuclear pore complex. *Mol. Cell Biol.* **20,** 5631-5642.

Stebel,M., Vatta,P., Ruaro,M.E., Del,S.G., Parton,R.G., and Schneider,C. (2000). The growth suppressing gas1 product is a GPI-linked protein. *FEBS Lett.* **481,** 152-158.

Stemmer,K., Ellinger-Ziegelbauer,H., Lotz,K., Ahr,H.J., and Dietrich,D.R. (2006). Establishment of a protocol for the gene expression analysis of laser microdissected rat kidney samples with affymetrix genechips. *Toxicol. Appl. Pharmacol.* **217,** 134-142.

Stottmann,R.W., Berrong,M., Matta,K., Choi,M., and Klingensmith,J. (2006). The BMP antagonist Noggin promotes cranial and spinal neurulation by distinct mechanisms. *Dev. Biol.* **295,** 647-663.

Stoughton,R.B. (2005). Applications of DNA microarrays in biology. *Annu. Rev. Biochem.* **74,** 53-82.

Streit,A., Berliner,A.J., Papanayotou,C., Sirulnik,A., and Stern,C.D. (2000). Initiation of neural induction by FGF signalling before gastrulation. *Nature* **406,** 74-78.

Sugahara,K. and Kitagawa,H. (2002). Heparin and heparan sulfate biosynthesis. *IUBMB. Life* **54,** 163-175.

Szabo,R., Hobson,J.P., Christoph,K., Kosa,P., List,K., and Bugge,T.H. (2009). Regulation of cell surface protease matriptase by HAI2 is essential for placental development, neural tube closure and embryonic survival in mice. *Development* **136,** 2653-2663.

Takeuchi,T., Yamazaki,Y., Katoh-Fukui,Y., Tsuchiya,R., Kondo,S., Motoyama,J., and Higashinakagawa,T. (1995). Gene trap capture of a novel mouse gene, jumonji, required for neural tube formation. *Genes Dev.* **9,** 1211-1222.

Tan,K.B., Tan,S.H., Tan,K.H., and Yeo,G.S. (2007). Anencephaly in Singapore: a ten-year series 1993-2002. *Singapore Med. J.* **48,** 12-15.

Tomita,H., Vawter,M.P., Walsh,D.M., Evans,S.J., Choudary,P.V., Li,J., Overman,K.M., Atz,M.E., Myers,R.M., Jones,E.G. et al. (2004). Effect of agonal and postmortem factors on gene expression profile: quality control in microarray analyses of postmortem human brain. *Biol. Psychiatry* **55,** 346-352.

Tuschl,T., Zamore,P.D., Lehmann,R., Bartel,D.P., and Sharp,P.A. (1999). Targeted mRNA degradation by double-stranded RNA in vitro. *Genes Dev.* **13,** 3191-3197.

van Straaten,H.W., Hekking,J.W., Copp,A.J., and Bernfield,M. (1992). Deceleration and acceleration in the rate of posterior neuropore closure during neurulation in the curly tail (ct) mouse embryo. *Anat. Embryol. (Berl)* **185,** 169-174.

Veeman,M.T., Axelrod,J.D., and Moon,R.T. (2003). A second canon. Functions and mechanisms of beta-catenin-independent Wnt signaling. *Dev. Cell* **5,** 367-377.

Wallingford,J.B. (2005). Neural tube closure and neural tube defects: studies in animal models reveal known knowns and known unknowns. *Am. J. Med. Genet. C. Semin. Med. Genet.* **135C,** 59-68.

Wallingford,J.B., Fraser,S.E., and Harland,R.M. (2002). Convergent extension: the molecular control of polarized cell movement during embryonic development. *Dev. Cell* **2,** 695-706.

Wallingford,J.B. and Harland,R.M. (2001). Xenopus Dishevelled signaling regulates both neural and mesodermal convergent extension: parallel forces elongating the body axis. *Development* **128,** 2581-2592.

Wallingford,J.B. and Harland,R.M. (2002). Neural tube closure requires Dishevelled-dependent convergent extension of the midline. *Development* **129,** 5815-5825.

Wang,J. (2008). Computational biology of genome expression and regulation--a review of microarray bioinformatics. *J. Environ. Pathol. Toxicol. Oncol.* **27,** 157-179.

Wang,J., Hamblet,N.S., Mark,S., Dickinson,M.E., Brinkman,B.C., Segil,N., Fraser,S.E., Chen,P., Wallingford,J.B., and Wynshaw-Boris,A. (2006a). Dishevelled genes mediate a conserved mammalian PCP pathway to regulate convergent extension during neurulation. *Development* **133,** 1767-1778.

Wang,J., Mark,S., Zhang,X., Qian,D., Yoo,S.J., Radde-Gallwitz,K., Zhang,Y., Lin,X., Collazo,A., Wynshaw-Boris,A. et al. (2005). Regulation of polarized extension and planar cell polarity in the cochlea by the vertebrate PCP pathway. *Nat. Genet.* **37,** 980-985.

Wang,Y., Badea,T., and Nathans,J. (2006b). Order from disorder: Self-organization in mammalian hair patterning. *Proc. Natl. Acad. Sci. U. S. A* **103,** 19800-19805.

Wang,Y., Guo,N., and Nathans,J. (2006c). The role of Frizzled3 and Frizzled6 in neural tube closure and in the planar polarity of inner-ear sensory hair cells. *J. Neurosci.* **26,** 2147-2156.

Wang,Y. and Nathans,J. (2007). Tissue/planar cell polarity in vertebrates: new insights and new questions. *Development* **134,** 647-658.

Wassler,M.J. and Shur,B.D. (2000). Clustering of cell surface (beta)1,4-galactosyltransferase I induces transient tyrosine phosphorylation of focal adhesion kinase and loss of stress fibers. *J. Cell Sci.* **113 Pt 2,** 237-245.

Wei,G., Bai,X., Sarkar,A.K., and Esko,J.D. (1999). Formation of HNK-1 determinants and the glycosaminoglycan tetrasaccharide linkage region by UDP-GlcUA:Galactose beta1, 3-glucuronosyltransferases. *J. Biol. Chem.* **274,** 7857-7864.

Weinstein,D.C., Altaba,A., Chen,W.S., Hoodless,P., Prezioso,V.R., Jessell,T.M., and Darnell,J.E., Jr. (1994). The winged-helix transcription factor HNF-3 beta is required for notochord development in the mouse embryo. *Cell* **78,** 575-588.

Weinstein,D.C. and Hemmati-Brivanlou,A. (1999). Neural induction. *Annu. Rev. Cell Dev. Biol.* **15,** 411-433.

Wianny,F., Real,F.X., Mummery,C.L., Van,R.M., Lahti,J., Samarut,J., and Savatier,P. (1998). G1-phase regulators, cyclin D1, cyclin D2, and cyclin D3: up-regulation at gastrulation and dynamic expression during neurulation. *Dev. Dyn.* **212,** 49-62.

Wieser,R.J. and Oesch,F. (1988). Contact-dependent regulation of growth of diploid human fibroblasts is dependent upon the presence of terminal galactose residues on plasma membrane glycoproteins. *Exp. Cell Res.* **176,** 80-86.

Wilson,B.J., Harada,R., LeDuy,L., Hollenberg,M.D., and Nepveu,A. (2009). CUX1 transcription factor is a downstream effector of the proteinase-activated receptor 2 (PAR2). *J. Biol. Chem.* **284,** 36-45.

Wilson,S.I., Graziano,E., Harland,R., Jessell,T.M., and Edlund,T. (2000). An early requirement for FGF signalling in the acquisition of neural cell fate in the chick embryo. *Curr. Biol.* **10,** 421-429.

Woroniecki,R.P. and Bottinger,E.P. (2009). Laser capture microdissection of kidney tissue. *Methods Mol. Biol.* **466,** 73-82.

Wu,M., Chen,D.F., Sasaoka,T., and Tonegawa,S. (1996). Neural tube defects and abnormal brain development in F52-deficient mice. *Proc. Natl. Acad. Sci. U. S. A* **93,** 2110-2115.

Xiang,C.C., Mezey,E., Chen,M., Key,S., Ma,L., and Brownstein,M.J. (2004). Using DSP, a reversible cross-linker, to fix tissue sections for immunostaining, microdissection and expression profiling. *Nucleic Acids Res.* **32,** e185.

Yamaguchi,Y., Inatani,M., Matsumoto,Y., Ogawa,J., and Irie,F. (2010). Roles of heparan sulfate in mammalian brain development current views based on the findings from Ext1 conditional knockout studies. *Prog. Mol. Biol. Transl. Sci.* **93,** 133-152.

Ybot-Gonzalez,P., Cogram,P., Gerrelli,D., and Copp,A.J. (2002). Sonic hedgehog and the molecular regulation of mouse neural tube closure. *Development* **129,** 2507-2517.

Ybot-Gonzalez,P., Gaston-Massuet,C., Girdler,G., Klingensmith,J., Arkell,R., Greene,N.D., and Copp,A.J. (2007). Neural plate morphogenesis during mouse neurulation is regulated by antagonism of Bmp signalling. *Development* **134,** 3203-3211.

Yip,G.W., Ferretti,P., and Copp,A.J. (2002). Heparan sulphate proteoglycans and spinal neurulation in the mouse embryo. *Development* **129,** 2109-2119.

Zamore,P.D., Tuschl,T., Sharp,P.A., and Bartel,D.P. (2000). RNAi: double-stranded RNA directs the ATP-dependent cleavage of mRNA at 21 to 23 nucleotide intervals. *Cell* **101,** 25-33.

Zhang,L. (2010a). Glycosaminoglycan (GAG) biosynthesis and GAG-binding proteins. *Prog. Mol. Biol. Transl. Sci.* **93,** 1-17.

Zhang,L. (2010b). Glycosaminoglycans in development, health and disease. Preface. *Prog. Mol. Biol. Transl. Sci.* **93,** xvii-xviii.

Zhang,X.M., Ramalho-Santos,M., and McMahon,A.P. (2001). Smoothened mutants reveal redundant roles for Shh and Ihh signaling including regulation of L/R symmetry by the mouse node. *Cell* **106,** 781-792.

Zhou,P. (2006). REGgamma: a shortcut to destruction. *Cell* **124,** 256-257.

Zohn,I.E., Chesnutt,C.R., and Niswander,L. (2003). Cell polarity pathways converge and extend to regulate neural tube closure. *Trends Cell Biol.* **13,** 451-454.

Zolessi,F.R. and Arruti,C. (2001). Apical accumulation of MARCKS in neural plate cells during neurulation in the chick embryo. *BMC. Dev. Biol.* **1,** 7.